Insights into Cocrystal Bioavailability Through Analysis of *In Vitro* Dissolution Experiments

by

Nicholas M. Waltz

A dissertation submitted in partial fulfillment
of the requirements for the degree of
Doctor of Philosophy
(Pharmaceutical Sciences)
at the University of Michigan
2020

Doctoral Committee:

Research Professor Gregory E. Amidon, Co-Chair
Professor Naír Rodríguez-Hornedo, Co-Chair
Professor Mark A. Burns
Professor Duxin Sun

Nicholas Matthew Waltz

nmwaltz@umich.edu

ORCID: 0000-0002-1278-0935

ACKNOWLEDGEMENTS

There are many people that need to be acknowledged over the course of my graduate studies. I think it fitting that I thank the chairs of my committee Dr. Gregory Amidon and Dr. Naír Rodríguez first as they have imparted many lasting lessons to me. I am grateful to have had the chance to study with them for they are two of the most patient and caring advisors that a struggling student could ever ask for. I will always be thankful for the scientific conversations with Dr. Rodríguez as she has at times made me think harder than I thought I possibly could. Somehow, she could always find a way to bring the best out of me. I will always be thankful for the environment that Dr. Amidon created for me in his office. Countless meetings started with talking about Michigan Football or golf before turning to topics of research. One of the biggest life lessons I have learned from my co-chairs is that it is not about what you work on, it is about who you work with. To my committee members, Dr. Duxin Sun and Dr. Mark Burns, I have appreciated the guidance you have given me throughout the process. You have been instrumental in my growth as a scientist.

I would like to thank the faculty and staff in the College of Pharmacy that have given support throughout my time as a graduate student. I would not have gotten my start in grad school if it was not for Dr. Cherie Dotson helping place me in Dr. Amidon's lab. I appreciate the conversations that I had with Patrina Hardy when I came down to her office to ask her logistical questions. Most of all I would like to thank Dr. Karen Farris for being a great boss during the time I was her teaching assistant in addition to being a wonderful professional mentor. I have received plenty of great advice to prepare me for the real world.

Graduate school would have been much harder if not for the many graduate student friends that I was able to surround myself with. Much of the scientific and emotional support came from my student peers. I am thankful for those who I got to spend time with in the GEAmidon and Rodríguez labs. Dr. Lily Roy, Dr. Maya Lipert, Dr. Gislaine Kuminek, Katie Cavanagh, Dr. Deanna Mudie, Dr. Brian Krieg, Dr. Pat Sinko, Niloufar Salehi, and Nick Job. You were instrumental in surviving the ups and downs of research. I would like to thank Rachel Russ for the work she did as an undergrad to contribute to portions of this thesis. Many thanks to my AAPS student chapter mentor Max Mazzara and grandmentor Karthik Pisupati. We never did get that family picture for the holiday postcard. I miss the happy hour appetizers at the Blue Lep with my cohort Dr. Morgan Giles, Dr. Lukasz Ochyl and Dr. Mari Gasparyan back when we were naïve little first years. I enjoyed the visits from those in the neighboring labs: Brian Thompson, Jen Diaz Espinoza, Mery Vet George. Dr. Phil Rzeczycki, and Dr. Misha Murashov. You brought some cheer to the day. To Brain and Kathy, thanks for being close friends and confidants as well as wonderful godparents. I am grateful for the lifelong friends made in Grad School, especially Dr. Ryan Clauson. Our friendship was forged through some difficult times, but we made it through the fire and flames.

Lastly, I would like to thank my friends and family for their support. Mom and Dad, you laid the foundations to get me where I am today, and I am extremely grateful for that. Sorry, Grandma Waltz, I never got around to making you that new pain pill, but you did help motivate me to work hard and do my best. True friends that you can count on in the hour of need are hard to find and I am eternally grateful to have one of those. Stephen Graham, you are a gentleman and a scholar to offer to proofread a thesis on short notice. Most importantly, I would like to thank my

wife Nicole and little pup, Ned, for being there to help celebrate the highs and give emotional support through the lows of grad school.

TABLE OF CONTENTS

LIST OF FIGURES

LIST OF TABLES

ABSTRACT

Cocrystals are a promising strategy to improve the oral bioavailability of poorly soluble drugs by generating higher solubilities to create faster dissolution and supersaturation. Their solution behavior is complicated due to the numerous equilibria that determine the dissolution, supersaturation, and precipitation kinetics that control concentrations available for oral absorption. These variables can cause difficulties in the development of viable cocrystal products as supersaturation and precipitation can make experimental results unpredictable. A better understanding of cocrystal solution behavior, one with mechanistically based mathematical models, would take uncertainty and guess work out of cocrystal product development for promising new therapeutic agents. This dissertation links cocrystal thermodynamic solubility equations to aqueous kinetic dissolution, supersaturation, and precipitation behavior observed with *in vitro* dissolution experiments to gain knowledge of the variables responsible in controlling cocrystal oral absorption.

Mathematical expressions were developed and applied to describe three aspects of cocrystal solution behavior: 1) dissolution, 2) supersaturation, and 3) precipitation. Thermodynamic solubility equations and expressions for kinetic processes were combined to describe dissolution (rotating disk and particle) and precipitation for *in vitro* dissolution scenarios (biphasic and biorelevant). Knowledge gained from these analyses identify key parameters controlling cocrystal solution concentrations responsible for *in vivo* absorption.

Cocrystals of the basic drug Ketoconazole (KTZ) with the dicarboxylic acids adipic (ADP), fumaric (FUM), and succinic (SUC) were used as model compounds. Solubility

equations and intrinsic surface saturation theory for these cocrystals were applied to simulate dissolution rates for cocrystal in biphasic (octanol:water) rotating disk dissolution experiments. Measured drug and coformer partitioning rates into the organic phase revealed a 34% decrease in coformer mass transfer coefficient, when diffusing in the presence of the drug indicating a significant solution phase interaction.

Precipitation risk was assessed from bulk and interfacial supersaturation values determined for dissolution experiments in biorelevant media FeSSIF, FaSSIF, and blank equivalents. Under these conditions, KTZ cocrystals have bulk solubilities between 2- and 4500-times drug solubility (bulk solubility advantage or $SA_{bulk} = S_{cocrystal}/S_{drug}$). When dissolving in FaSSIF, KTZ cocrystals exhibited interfacial solubility advantages (SA_{int}) an order of magnitude lower than the associated SA_{bulk}, suggesting ranges of precipitation risk across dissolution media and between interfacial and bulk.

Cocrystal particle dissolution in FeSSIF and blank FeSSIF was simulated by combining established dissolution and cocrystal solubility theory. Cocrystal interfacial pH was estimated using mass transport theory and measured solubility experiment concentrations and final pH values. Nucleation and growth terms for bulk precipitation were added to particle dissolution equations to simulate *in vitro* experiments. The resulting equations fit observed results well and demonstrated that KTZ cocrystal bulk solution behavior is dominated by nucleation rate as nucleation rate constants varied over two orders of magnitude between the three KTZ cocrystals while growth constants varied by only 2- to 3-fold.

Simulations using dissolution theory with measured precipitation constants estimated the effect of cocrystal dissolution and precipitation on drug concentrations available to partition in a biphasic system. KTZ cocrystals were calculated to generate 2-fold increases in dose absorbed.

The absorption was predicted to increase with decreasing dissolution rate, decreasing nucleation rates or increasing permeability rates which reduces bulk supersaturation and precipitation. These analyses provide insight into how cocrystal dissolution and drug precipitation govern supersaturation and solution concentrations available for absorption *in vivo* and can serve as a guide for formulating cocrystal and related supersaturation generating therapeutics.

CHAPTER I

Introduction

There are many challenges associated with improving the bioavailability of orally dosed active pharmaceutical ingredients. For drugs that fall into the BCS class II and IV spectrum, increasing the solubility of the drug molecule can significantly increase the amount of drug absorbed. By cocrystallizing a poorly soluble drug with a more soluble coformer, the properties of the drug can be modified to get more desirable outcomes in terms of solubility, dissolution, or shelf life stability. The behaviors of cocrystal delivery systems *in vivo* are still not fully understood, however, as studies have shown that sometimes the more soluble cocrystal does not produce the higher blood levels. This is likely due, in part, to the very complicated nature of the chemical equilibria that control cocrystal solubility. Factors such as pH, micellar solubilization, and the ratio of drug to coformer all contribute to the solubility of a given cocrystal system. Dissolution rate also plays a large role in determining the amount of drug absorbed by the body and is driven by solubility. Modeling how cocrystal solubility and dissolution behaves in physiologically relevant conditions could give more insight into how cocrystal systems behave in the intestinal tract. Development of methods to simulate cocrystal dissolution, supersaturation, precipitation, and absorption could help predict the bioavailability of drugs in cocrystal systems and would further the knowledge of the cocrystal field, paving the way to advancing the understanding of cocrystal systems as a practical method of formulating poorly soluble pharmaceutical ingredients to improve oral bioavailability.

Background

Factors Affecting Drug Absorption

Solubility

Solubility and Dissolution Limited Drug Absorption

In order for orally dosed pharmaceutical agents to be absorbed across the intestinal membrane, they must first dissolve into solution. As diffusion across a membrane is driven by gradients of concentration, generally a solute that can achieve higher solution concentrations in the intestine will have higher amounts absorbed. Therefore, poorly soluble drugs which are limited by their dissolution rate have been correlated with less than ideal bioavailability[1]. Many different strategies at improving the solubility and dissolution rate of these poorly soluble drugs with the intention of increasing bioavailability have been documented in the literature and include using solid dispersions[2], lipid based formulations[3], amorphous solids and cocrystals[4] among others.

Supersaturation

Obtaining concentrations above drug solubility, or increasing dissolution rate, are two useful ways to improve the amount of a poorly soluble drug absorbed upon oral administration. The methods of improving drug solubility in the previous section allow for supersaturation with respect to drug in solution. Unfortunately, increasing drug concentration via supersaturation also increases its instability in solution and can cause precipitation to the more stable solid form[5]. The degree of supersaturation that is achieved also has an effect on the amount absorbed, as reports have shown the highest degree of supersaturation does not guarantee the highest transport across Caco-2 cells *in vitro*[6]. These findings suggest achieving and maintaining supersaturation are paramount to increasing drug absorption from the gastrointestinal tract.

Permeability

Passive Diffusion Through a Membrane

Small molecule drugs are able to passively diffuse through cellular membranes, but numerous variables control the ability of drugs to do so. Lipinski and his rule of five suggests properties of molecules are common among well absorbed drugs[7]. Molecular weight, lipid partition coefficient, and the number of hydrogen-bond donors and acceptors are important variables according to the rule of five. BCS class II drugs formulated into cocrystals typically have no problem passively diffusing through a membrane due to their high lipophilicity.

Transporter Mediated Absorption

Passive diffusion is not the only method molecules can use to pass across the intestinal membrane. Lipophilic molecules do not need much assistance crossing the intestinal cell membrane as they diffuse freely through, but hydrophilic molecules may have difficulty diffusing. Many species of active transport proteins have evolved to help solve this problem. Some very soluble molecules like glucose have transport proteins dedicated to helping increase transport across the intestinal epithelium regardless of luminal concentration[8]. Even molecules typically used as coformers in cocrystals, like salicylic acid, have been shown to be substrates for transport proteins[9].

Cocrystal Formulations and Their Implications for Improving Drug Absorption

Cocrystals, in the pharmaceutical world, are crystals made from molecules of drug and coformer which can interact in stoichiometric ratios via non-covalent bonding. These interactions can lead to a solid form with properties different than crystals of either pure parent compound. Typically a hydrophilic coformer is paired with a lipophilic drug to produce a new entity that can

be more soluble[10], dissolve faster[11], adsorb less water[12], and have more favorable chemical and solution stability than the drug alone[13,14].

Drug and coformers in cocrystalline systems interact through non-covalent bonds. Some of these include hydrogen bonding, pi-pi stacking, and Van der Waals forces[15]. For pharmaceutical cocrystals, the amino/carboxylic acid hydrogen bond is typically exploited in order to form a cocrystalline material[13]. Some examples are shown in (Figure 1.1).

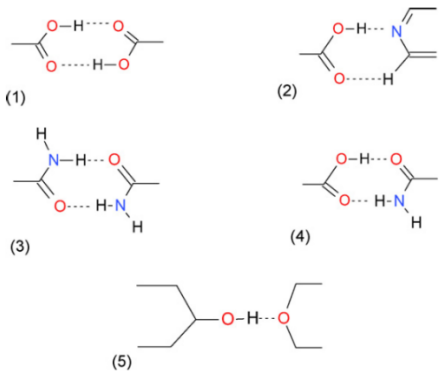

Figure 1.1: Common hydrogen bond synthons used for cocrystal formation[15].

There are multiple ways to produce cocrystalline material. Synthesizing cocrystals can be as simple as dissolving an equimolar stoichiometric ratio (i.e. 1:1) of drug and coformer into a solvent and allowing the solvent to evaporate[13]. This evaporation crystallization method, however, often fails because it does not generate congruent saturation of cocrystal components required for cocrystallization[16]. Grinding is another method to form cocrystals that can be done with or without solvent. Neat grinding (without solvent) is done by adding solid forms of drug and cocrystal together and grinding them manually with mortar and pestle or mechanically using a mill [17]. Grinding both drug and excess coformer together with a small volume of solvent is called the solvent-drop method[18]. The slurrying method involves placing equal molar amounts of drug and coformer into water and slurrying for 24 hours at room temperature[18]. Reaction crystallization is a method for creating cocrystals that uses unequal stoichiometric concentrations

of reactants. This is done by adding solid drug to a saturated solution of the coformer. Due to the nature of cocrystal equilibrium, the solution becomes supersaturated with respect to cocrystal and it precipitates[16]. These methods are a sampling of methods that have been shown to produce cocrystals in the literature. Depending on the cocrystal, synthesis via multiple methods can produce multiple polymorphs[18] and must be taken into account when designing synthesis experiments.

Completed Cocrystal Studies *In Vivo*

There have been a handful of scientific articles which have attempted to shed light on the question of cocrystal behavior in the body. Many different approaches have been used in the scientific literature for testing cocrystals *in vitro* to better understand bioavailability. Unfortunately, many of these approaches do not help fully elucidate the intricacies of cocrystal solution equilibria. The following sections will talk about the articles that have explored cocrystal absorption *in vivo* and discuss the findings.

Meloxicam

There are two articles found that have *in vivo* studies involving cocrystals of the drug Meloxicam, which is a zwitterionic, non-steroidal anti-inflammatory drug that is poorly soluble at low pH[19]. The first study chose to make meloxicam cocrystals with aspirin as the coformer[20]. Free drug and coformer solubility were tested *in vitro* before any pharmacokinetic studies were performed. These solubility studies used deionized water at 25^{o}C and pH 7.4 phosphate buffer at 37^{o}C in order to estimate the kinetic solubility in an environment reasonably comparable to that seen in the animal pharmacokinetic study. Kinetic solubility of the cocrystal was reported to be 0.22 mg/mL and Meloxicam being only 0.005 mg/mL[20], however, no dissolution profiles were reported in the article. Following the solubility study, the free drug and the cocrystal were both

dosed oral gavage into Sprauge-Dawley rats as suspensions in PEG400. The results of the pharmacokinetic study (Figure 1.2) show the cocrystal having an improved exposure as compared to the free drug.

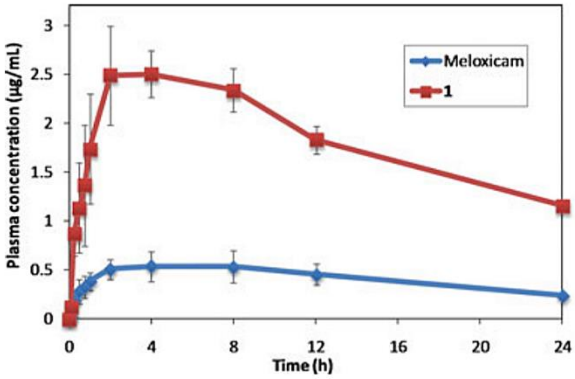

Figure 1.2: Pharmacokinetic profiles of meloxicam (♦) and meloxicam-aspirin cocrystal (■) over 24 hours in rat animal model[20].

More information could help give better insight into cocrystal equilibria *in vivo* as this study only looks at the kinetic solubility of the cocrystal in media that does not contain biorelevant surfactants. Reporting more pH dependent solubility values could also be very valuable as the Meloxicam has multiple solubilities depending on the pH due to its zwitterionic nature[19]. Knowledge of the dissolution characteristics of the cocrystal could also be beneficial before dosing *in vivo* to understand if dissolution rate has changed or if there is a precipitation event that may happen. Looking into these aspects of cocrystal equilibria would give better understanding of the solubility advantage or transformation kinetics the cocrystal may have over the course of the intestinal tract.

The second article exploring Meloxicam cocrystals takes a different approach than the previous work. Twelve different cocrystals were formed with meloxicam and all of them were tested *in vitro* to determine their powder dissolution characteristics. Powdered form of the cocrystals and solid drug were dissolved in pH 6.5 phosphate buffer at 37^{o}C and the concentration-

time profiles were recorded over 72 hours[21]. The maximum concentrations of drug over the 72 hours were recorded as S_{max}. Free drug and cocrystal were then dosed into Sprague-Dawley rats as a 10 mg/kg (meloxicam equivalent) suspension with PEG400. The route of administration was IV through implanted jugular catheter. The serum concentrations of meloxicam were recorded over a 4-hour period (Figure 1.3).

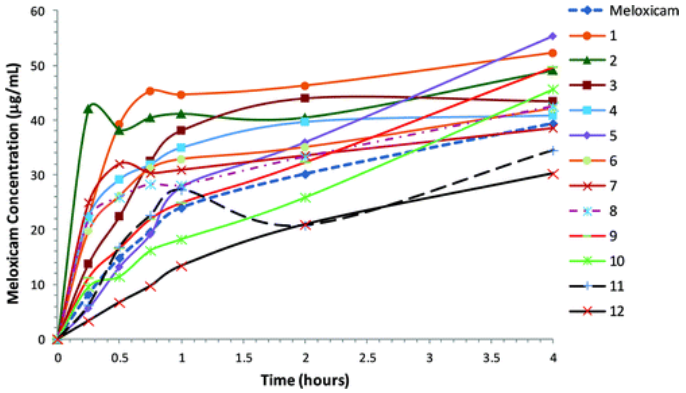

Figure 1.3: Pharmacokinetic profiles of meloxicam (-♦-) and 12 meloxicam cocrystals over four hours from *in vivo* rat model[21].

Most meloxicam cocrystals tested were reported to have an increased absorption rate compared to the free drug. Correlations between many of the recorded parameters were assessed, however, none could be drawn between parameters such as coformer and cocrystal solubility, cocrystal melting points, and S_{max}. *In vitro* dissolution rate and *in vivo* pharmacokinetic showed a correlation with $R^2 = 0.7067$[21]. Better correlations possibly could have been made if the *in vitro* dissolution studies had accounted for more, as in this case, the contributions of lipids and PEG 400 in were not accounted for *in vitro* as dissolution studies did not contain a polymer or biorelevant media.

Lamotrigine

Lamotrigine is a poorly soluble BCS class II drug that is used as an anti-convulsant drug used in treating epilepsy. With a pK_a of 5.7, Lamotrigine exhibits better solubility in 0.1 M HCl than in deionized water at 25°C[18]. The main objective for the study done by Cheney et al. was to

use crystal engineering to make the API more bioavailable. Lamotrigine salts, hydrates, and cocrystals were synthesized and tested both *in vitro* and *in vivo*. In this study, cocrystals were made from coformers methylparaben and nicotinamide by an assortment of methods including solvent-drop grinding, slurrying, and melting[18]. After thorough physicochemical characterization the cocrystals were tested *in vitro* with particle dissolution in the presence of excess solid. Deionized water at 25°C and aqueous 0.1M HCl solutions at 37°C were used as solvent systems for *in vitro* dissolution in volumes less than 100mL. Dissolution profiles were collected up to 240 minutes. Pharmacokinetic experiments were conducted over 24 hours in Sprague-Dawley rats. The HCl dissolution media chosen by the authors to give insight to the *in vivo* studies was not a good predictor of rat plasma values as shown when comparing the results (Figure 1.4). The cocrystals (2, 3, and 4) reached higher concentrations than free drug in the HCl dissolution media but when dosed in rats the free drug had higher serum concentrations. This lack of predictability may be due to the lack of biorelevant media used in the *in vitro* dissolution testing.

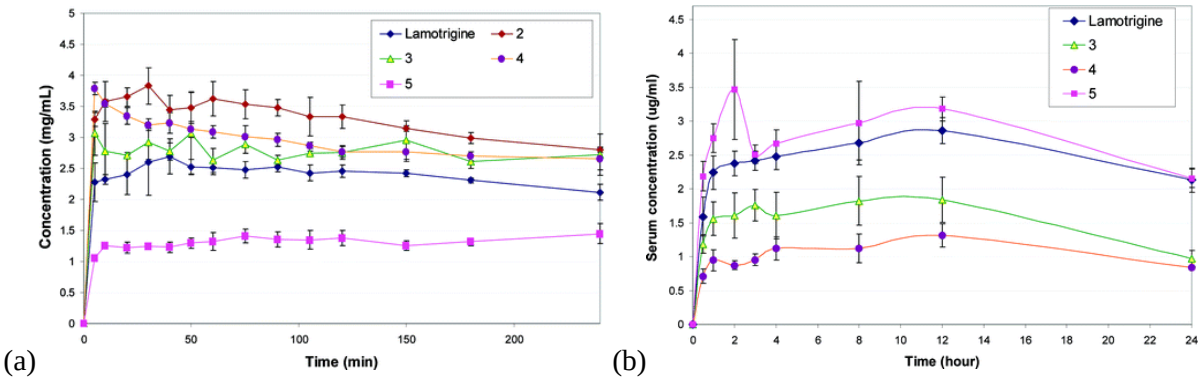

(a) (b)

Figure 1.4: (a) Lamotrigine free drug (♦) and cocrystal *in vitro* dissolution profiles in 0.1M HCl and (b) pharmacokinetic serum concentrations in rat animal model[18].

In order to fully understand the solubility behavior of salt and cocrystal forms due to pH, measurement of the thermodynamic solubility and obtainment of a K_{sp} for salt and cocrystal forms has been shown to be more accurate than using kinetic dissolution studies to assess solubility[22].

This study could have had more impact with the measurements of solubility products of the salt and cocrystal forms generated.

Carbamazepine

An *in vivo* study was completed with the objective of comparing the commercially available version of the poorly soluble, non-ionizable drug, carbamazepine (labeled as Tegretol), to a saccharin cocrystal[23]. *In vitro* dissolution studies used biorelevant conditions in simulated gastric fluid (SGF) at 37ºC. The author's intention was to determine the correlations between dissolution rate and particle size. For the *in vivo* portion of the study, cocrystal was loaded into HPMC capsules after being blended with lactose. The capsules containing cocrystal as well as the marketed product Tegretol were dosed to dogs and compared. The pharmacokinetic profiles (Figure 1.5) were assessed and showed the cocrystal had improved exposure compared to the free drug. This study does better to simulate intestinal conditions for the *in vitro* dissolution study, however, the dissolution study only looked at the effects of particle size.

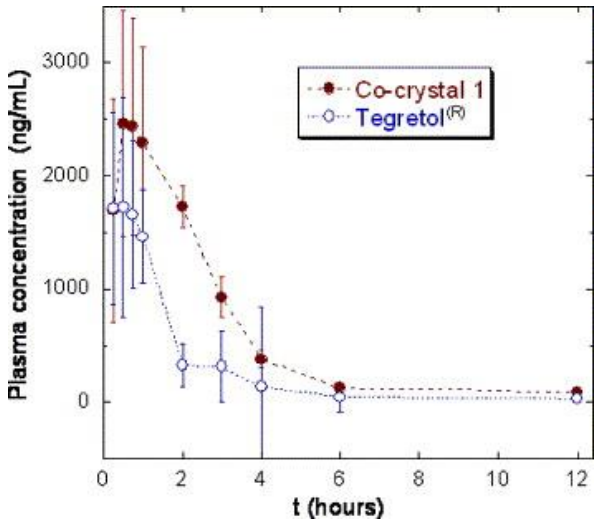

Figure 1.5: Plasma concentration-time profiles of carbamazepine (○) and carbamazepine-saccharin cocrystal (●) over 12 hours in dog animal model[23].

Data regarding important factors of cocrystal solubility advantage over drug, like degree of supersaturation and transformation kinetics of the cocrystal in biorelevant media, could have

supplemented the data gathered in this study. With this information, a more complete picture of *in vivo* cocrystal behavior could be drawn.

LCQ789

LCQ789 is a non-ionizable, poorly soluble, and highly permeable drug in the formulation stages of drug development during the early 2010s[24]. Due to low solubility, formulation strategies solid dispersions, microemulsions, and cocrystals were employed to improve oral absorption in the study[24]. The authors, however, did not fully explore cocrystal formulation, as measures to characterize any cocrystalline material were not reported other than a statement by the authors that the cocrystal did not show any advantage over drug in dissolution rate. A mesylate cocrystal was selected by the authors out of 27 different coformers due to good crystallinity and reproducibility. This lone cocrystal was then dosed, as a suspension, into both rat and dog. Cocrystal was compared to the parent drug and other formulation methods. Reported results are found in (Table 1.1). The cocrystal did not show any advantage over the free drug in rats but an advantage was seen in dogs. The cocrystal, however, was not able to facilitate drug exposure near the levels created by the microemulsion and solid dispersion forms tested.

Table 1.1: Pharmacokinetic data of LCQ789-mesylate cocrystal in rat (left) and dog (right) animal models[24].

Pharmacokinetic (PK) evaluation of LCQ789 formulation approaches in rat at 10 mg/kg.

Formulation	AUC/dose (ng·h/mL/mg/kg)	C_{max}/dose (ng/mL/mg/kg)	F%	T_{max} (hours)
Suspension	33.9±7.2	4.9±1.1	4.04	0.83
Co-crystal	50.1±16.2	5.8±2.7	5.91	0.83
ME	848.0±354	127.7±38	99.6	1.33
SD	629.5±126	84.7±1.7	74.0	1.33

(n=3).

Pharmacokinetic (PK) evaluation of LCQ789 formulation approaches in dog at 10 mg/kg.

Formulation	AUC/dose (ng·h/mL/mg/kg)	C_{max}/dose (ng/mL/mg/kg)	T_{max} (hours)
Suspension	4±1	1±0	0.5
Co-crystal	125±98.3	14±7	2
MEPC4	312±63.6	132±78	0.5
SD	210±30.4	58±17	1

(n=3).

This formulation study did not fully characterize cocrystals of this drug. With an understanding of the factors which control the *in vivo* absorption of drug in a cocrystalline material, a more thorough search could have potentially found a cocrystal to compete with the more favorable

exposure characteristics of both the microemulsions and solid dispersions that were characterized in more depth during this study.

Indomethacin

An *in vivo* study for an indomethacin-saccharin cocrystal was done with the goal of comparing it to the commercially available version of indomethacin (labeled as Indomec®). The article starts with an *in vitro* dissolution study that used USP recommendations for buffers of 0.1M HCl (pH 1.4) and pH 7.4 phosphate[25]. Surfactant was used in the HCl buffer but not in the phosphate. The dissolution study focused on dissolution rate and percent dissolved. Commercial drug, indomethacin-saccharin cocrystal, a physical mixture of drug and coformer, and free drug were all compared. The cocrystal achieved rates of dissolution that were faster than the free drug indomethacin and physical mix, but not significantly different than the commercial form[25]. The article also reported an *in vivo* study that involved the free drug, physical mixture, neat indomethacin-saccharin cocrystal, and Indomec® being dosed at equivalent drug amounts. The results (Table 1.2) depict that the pharmacokinetic profiles confirmed a bioavailability equivalence between cocrystal and Indomec® due to the similar parameters such as AUC, T_{max}, and C_{max}.

Table 1.2: Pharmacokinetic parameters of physical mix, indomethacin-saccharin (IND-SAC) cocrystals, and commercially available indomethacin in dog animal model[25].

	PhyMix	IND–SAC cocrystal (ground)	Indomee®
AUC0-∞ (μg h/ml)	7.58 ± 3.04	14.83 ± 7.46	16.46 ± 2.28
AUC_{0-24} (μg h/ml)	5.98 ± 2.74	14.52 ± 6.78	16.45 ± 3.41
C_{max} (μg/ml)	1.01 ± 0.40	6.31 ± 3.26	8.02 ± 4.22
T_{max} (h)	2.83 ± 1.03	1.00 ± 1.01	1.53 ± 1.34

Pharmacokinetic parameters were significantly different between ground IND–SAC and PhyMix; Indomee and PhyMix (ANOVA, $P < 0.05$). Whilst they were not significantly different between ground IND–SAC cocrystals and Indomee® (ANOVA, $P > 0.05$). The variation (±) indicates standard deviation in the value.

This study may not be a fair comparison as the formulated commercially available product was compared to an unformulated cocrystal. Cocrystal bioavailability could potentially be increased by formulation.

AMG-517

Two published studies describe the pharmacokinetics of AMG-517, a poorly soluble, basic drug from Amgen. The first article focuses on synthesizing and characterizing a sorbic acid cocrystal of AMG-517 before dosing it to rats[26]. After characterization by differential scanning calorimetry (DSC) and X-ray powder diffraction (XRPD), the cocrystal and free base form of the drug were solubility tested by slurrying the cocrystal in fasted state simulated intestinal fluid (FaSSIF). In this test, the authors reported supersaturation with respect to the drug was achieved, but the supersaturation caused precipitation within the 3-hour test (Figure 1.6). The cocrystal and drug were also later dosed into Sprague-Dawley rats at different doses, the highest being 500 mg/kg. According to the results in (Figure 1.6), the cocrystal did have an exposure advantage over the free drug[26].

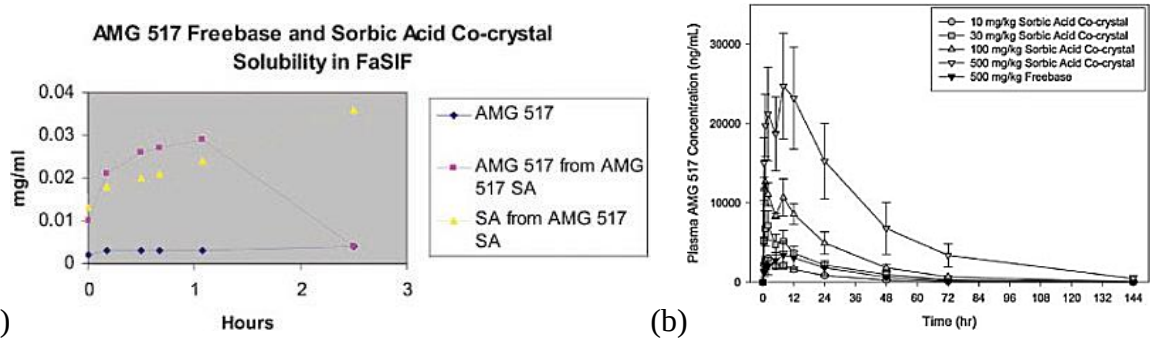

Figure 1.6: (a) FaSSIF *in vitro* solubility testing and (b) plasma concentration-time profiles of sorbic acid cocrystal of AMG-517 in rat animal model[26].

The second and more interesting article regarding AMG-517 contains a library of 12 cocrystals, all containing carboxylic acid coformers[27]. The 12 cocrystals and the free drug were tested *in vitro* with powder dissolution in FaSSIF and rotating disk dissolution at 37°C to determine the intrinsic dissolution rate. Both free drug and cocrystal were then dosed into Sprague-Dawley rats in a formulation suspended in 1% PVP K25. The polymer was not included in any of the *in vitro* dissolution studies which showed varying rates of dissolution and solution mediated phase transformation (Figure 1.7).

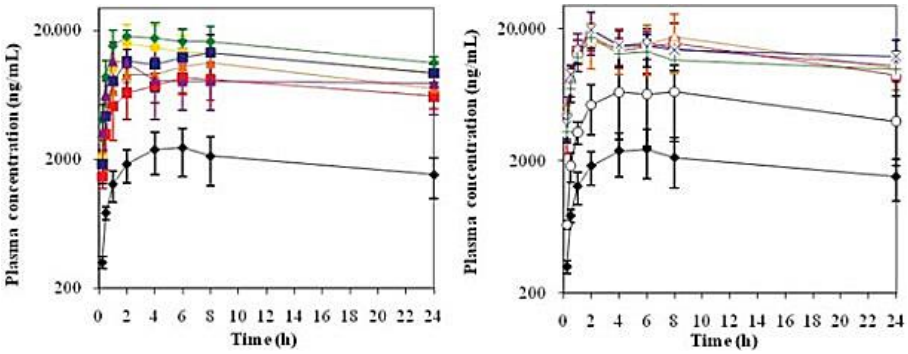

Figure 1.7: Powder dissolution profiles of AMG-517 (♦) and 12 of its cocrystals (colors) in FaSSIF over 240 minutes[27].

The results of the study show an interesting trend, or rather a lack thereof, where the solubility and intrinsic dissolution of the cocrystals do not necessarily correlate with the amount of drug that the animals are exposed to. The authors attempted to find correlations of *in vitro* intrinsic dissolution rates and concentrations of drug and cocrystal after 15 minutes to the *in vivo* absorption represented by the $AUC_{0\text{-}24h}$ (Figure 1.8). The results reveal no acceptable correlation.

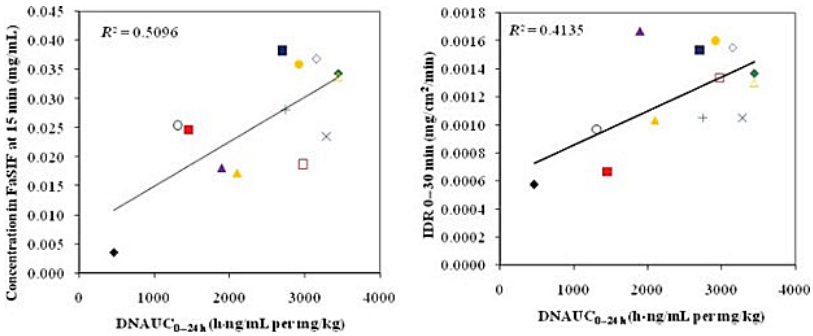

Figure 1.8: Correlations between *in vitro* cocrystal concentration at t = 15min (left), and intrinsic dissolution rate (right) to the $AUC_{0\text{-}24hr}$ of AMG-517 cocrystals in rat animal model[27].

Even though there is a degree of unpredictability in the results, likely due to poor fidelity to biorelevant conditions in testing, all cocrystals had better exposure *in vivo* than free drug and according to the authors could be moved forward for development. Better understanding of solution behavior and how it effects absorption might remove some uncertainties of this process.

Taken together, these studies show that there is a very complicated cocrystal equilibrium at play in the intestine with many variables affecting the transport of the drug into the body. To

improve predictions of absorption, more than just understanding the solubility and dissolution rate of the cocrystal is needed. Other factors such as differential absorption, solution stability, and conversion rate may be variables that control the absorption of the drug as these all affect how much and how long drug supersaturation can be maintained. What is clear from these studies is a more systematic approach to establishing the knowledge of how these variables change cocrystal equilibrium is needed to better predict how a cocrystalline product will behave in the human body. Knowing what to look for in a cocrystal will make it easier for predictions and selections of cocrystals, opening the possibilities for making successful products from drugs once thought impossible or impractical to formulate for oral delivery.

Factors Affecting Cocrystal Equilibrium

Solubility Product

When a cocrystal solid phase begins to dissolve into a solution, it dissociates into drug and coformer. The amounts of these components in solution are dictated by the equilibrium that is established between the solid phase and the drug and coformer in solution.

$$RA_s \rightleftharpoons R_{aq} + A_{aq} \tag{1.1}$$

In this case, (RA_s) is the solid cocrystal with 1:1 stoichiometry and drug (R_{aq}) and coformer (A_{aq}) are the non-ionized cocrystal components that are solubilized in the aqueous phase. As will be shown later, this basic expression for a cocrystal equilibrium can be modified to account for additional variables that can affect the cocrystal equilibrium.

Drug solubility in a cocrystal equilibrium is dictated by a solubility product much like salt ions and the common ion effect seen with those species[28]. This means that the amount of drug that can be maintained in solution at equilibrium decreases as the amount of coformer in solution

increases[29]. The mathematical expressions for a 1:1 stoichiometry of non-ionizable drug and coformer,

$$K_{sp} = [R_{aq}][A_{aq}] \tag{1.2}$$

$$S_R = [R_{aq}] = [A_{aq}] = \sqrt{K_{sp}} \tag{1.3}$$

where the K_{sp} is the equilibrium constant that is unique for each cocrystal and $[R_{aq}]$ and $[A_{aq}]$ are the concentrations of the drug and coformer, respectively. The solubility of the cocrystal (S_R) can be expressed in the form of equation (1.3) when the concentrations of $[R_{aq}]$ and $[A_{aq}]$are equal. These expressions show that in order to maintain the same K_{sp}, an increase in either drug or coformer concentration leads to a decrease in the concentration of the other. This is illustrated in (Figure 1.9).

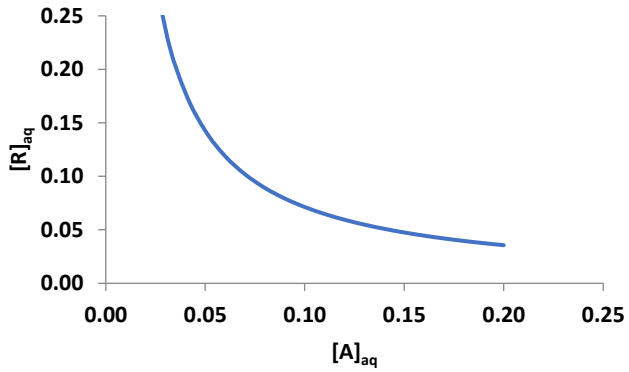

Figure 1.9: Cocrystal solubility (—) as a function of aqueous drug ($[R]_{aq}$) and coformer ($[A]_{aq}$) concentrations ($K_{sp} = 1.13x10^{-6}$).

pH Dependent Solubility

In many instances, coformers able to cocrystallize with drug are also ionizable species. This means that the pH of the solution modulates the equilibrium of the cocrystal. The equilibrium expression,

$$RHA_s \rightleftharpoons R_{aq} + HA_{aq} \tag{1.4}$$

$$K_{sp} = [R_{aq}][HA_{aq}] \tag{1.5}$$

$$HA_{aq} \rightleftharpoons H^{+}_{aq} + A^{-}_{aq} \tag{1.6}$$

$$K_a = \frac{[H^{+}_{aq}][A^{-}_{aq}]}{[HA_{aq}]} \tag{1.7}$$

has the non-ionizable drug (R_{aq}) and weak acid coformer (HA_{aq}). The acidic coformer can further dissociate to its negatively charged base ($A^{-}{}_{aq}$). The amounts of these ionized and non-ionized coformer components in solution are dictated by the coformer dissociation constant (K_a)[30].

Ionization of coformer will sequester the non-ionized species from its equilibrium with drug and, following Le Chatelier's principle, more of the cocrystal is drawn from the solid state into solution. This allows for a greater amount of drug that solubilizes and is described by

$$S_{RHA} = [R] = \sqrt{K_{sp}(1 + \frac{K_a}{[H^{+}]})} \tag{1.8}$$

which describes stoichiometric cocrystal solubility as a function of proton concentration ($[H^{+}]$).

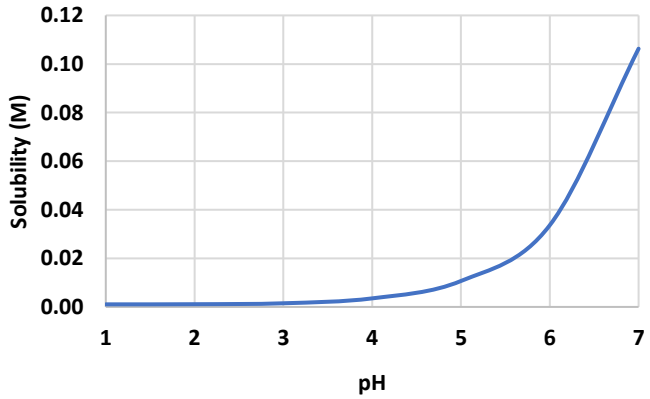

Figure 1.10: Carbamazepine-salicylic acid stoichiometric solubility (—) as a function of pH. Plot generated using equation (1.8). (K_{sp} = 1.13x10^{-6} M^2 pK_a = 3)

(Figure 1.10) shows that a cocrystal with an acidic coformer is least soluble at pH ranges lower than its pK_a. Once the pH rises above the pK_a of the coformer, the solubility of the cocrystal rises in a logarithmic fashion.

For some cocrystals, the increase in solubility caused by coformer ionization leads to a transition point. If the solubility product of the cocrystal dictates that the solubility of a cocrystal with an acidic coformer is less than that of the drug at low pH, then there is a point as pH increases where there is an intersection between the pH dependent solubility described by equation (1.8) and the intrinsic free drug solubility (Figure 1.11). This intersection happens at a certain pH, known as pH_{max}, and is the point where drug and cocrystal are at equal solubility. This phenomenon is also seen with salts[28]. For a cocrystal with an acidic coformer at a pH below the pH_{max}, the free drug is the less stable and more soluble form. At values of pH above the pH_{max}, the cocrystal becomes the more soluble form.

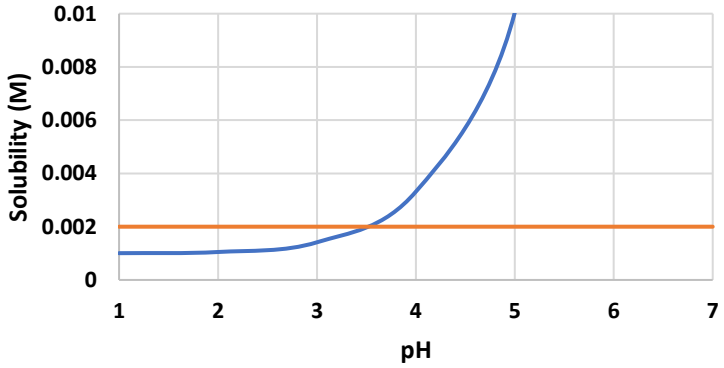

Figure 1.11: Cocrystal (—) and drug (—) solubilities as a function of pH show pH_{max} of cocrystal. Plots generated using equation (1.8) (K_{sp} = 1x10^{-6}. S_R = 0.002 M).

Micellar Solubilization

Cocrystal equilibrium is altered when the contributions of lipids and surfactants are added into consideration. When the concentration of lipid surpasses the critical micellar concentration (CMC), micelles are formed that both drug and coformer can solubilize into. Typically, the drug and coformer have different abilities to associate with micelles, and is apparent in equilibrium solubilization constants for drug(K_s^R), non-ionized coformer (K_s^{HA}), and ionized coformer ($K_s^{A^-}$) shown in the equilibrium expressions for a non-ionizable drug and acidic coformer[31],

$$RHA_s \rightleftharpoons R_{aq} + HA_{aq} \quad (1.9)$$

$$HA_{aq} \rightleftharpoons H^+_{aq} + A^-_{aq} \quad (1.10)$$

$$R_{aq} + M \rightleftharpoons R_{mic} \quad (1.11)$$

$$HA_{aq} + M \rightleftharpoons HA_{mic} \quad (1.12)$$

$$A^-_{aq} + M \rightleftharpoons A^-_{mic} \quad (1.13)$$

$$K_{sp} = [R]_{aq} + [HA]_{aq} \quad (1.14)$$

$$K_a = \frac{[H^+]_{aq}[A^-]_{aq}}{[HA]_{aq}} \quad (1.15)$$

$$K_s^R = \frac{[R]_{mic}}{[R]_{aq}[mic]} \quad (1.16)$$

$$K_s^{HA} = \frac{[HA]_{mic}}{[HA]_{aq}[mic]} \quad (1.17)$$

$$K_s^{A^-} = \frac{[A^-]_{mic}}{[A^-]_{aq}[mic]} \quad (1.18)$$

where subscripts denote the molecule is either in solid (*s*), aqueous (*aq*), or micellar (*mic*) phase and brackets denote concentrations. The concentration of micellar lipid or surfactant $[mic]$ is found by subtracting the value of the CMC from the total lipid or surfactant concentration.

The mathematical expressions for cocrystal solubility as a function of pH and micelle concentration have been previously derived[31]. The derivation starts by doing a total mass balance of the components of the cocrystal system in both aqueous and micellar phases.

$$S_{RHA,T} = [R]_{aq} + [R]_{mic} = [HA]_{aq} + [HA]_{mic} + [A^-]_{aq} + [A^-]_{mic} \quad (1.19)$$

With the mass balance accounted for and substituting the equations for equilibrium constants into the mass balance equations, the expression below is derived.

$$S_{RHA,T} = \sqrt{K_{sp}(1 + K_s^R[mic])(1 + \frac{K_a}{[H^+]} + K_s^{HA}[mic] + \frac{K_a}{[H^+]}K_s^{A-}[mic])} \quad (1.20)$$

This expression for the total stoichiometric solubility of a cocrystal ($S_{RHA,T}$) in equation (1.20) can be further simplified when it is assumed that the ability for ionized coformer to be solubilized into micelles is much less the ability of the non-ionized coformer (i.e. $K_s^{A-} \ll K_s^{HA}$).

$$S_{RHA,T} = \sqrt{K_{sp}(1 + K_s^R[mic])(1 + \frac{K_a}{[H^+]} + K_s^{HA}[mic])} \quad (1.21)$$

Equation (1.21) reveals the dependence of cocrystal solubility does not follow a linear relationship with increasing lipid or surfactant concentration. However, free drug solubilization has been shown to have a linear relationship with increasing surfactant concentration as shown by the equation below:

$$S_{R,T} = S_{R,aq}(1 + K_s^R[mic]) \quad (1.22)$$

Plotting equation (1.21) and equation (1.22) together as seen in (Figure 1.12), an intersection of the two curves appears. This point where the solubility of the drug and cocrystal meet is called the critical stabilization concentration (CSC). It is at this point that any increase in micellar concentration leads to the cocrystal being more stable than the drug and any decrease in micellar concentration leads to the cocrystal being the more soluble form. Above the CSC, the cocrystal no longer has a solubility advantage over the free drug. Below the CSC, the cocrystal is more soluble and supersaturation with respect to drug can be obtained.

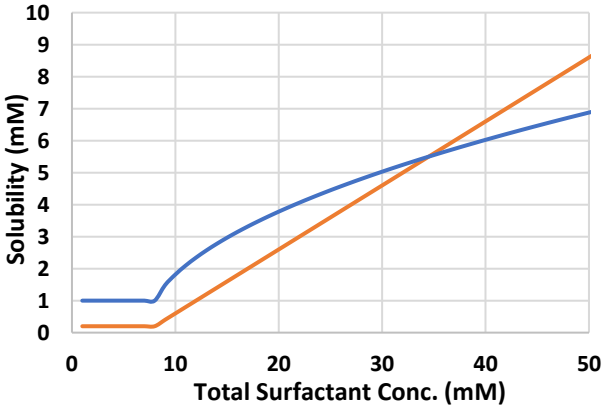

Figure 1.12: Cocrystal (—) and drug (—) solubility as a function of total surfactant concentration. Plots generated using equations (1.20-1.21). Parameters used: CMC = 8mM, K_{sp} = 1 mM^2, $S_{R,aq}$ = 0.2 mM, K_{sR} = 1 mM[31]

Cocrystals in Biorelevant Conditions

The gastrointestinal tract presents a complex set of conditions that affect the equilibrium of a cocrystalline material. The complexity at play in this environment can be better understood by first considering a simplified scenario before adding layers of intricacy at later steps. In terms of cocrystals, the most simplified gastrointestinal scenario would contain a non-ionizable drug paired with a non-ionizable coformer in a 1:1 stoichiometry allowing pH and micellar solubilization to be ignored. In this scenario, the K_{sp} is the main determinant of solubility. The system will try to saturate to a concentration equal to the square root of the K_{sp}, assuming the coformer and drug maintain equal 1:1 stoichiometric concentration and enough solid cocrystal is present.

Once a dose of cocrystal has been ingested, the cocrystal begins to dissolve in the stomach. The drug and coformer would enter solution in a fashion dictated by the 1:1 stoichiometry. This means that for each drug molecule entering solution, a coformer molecule also enters. Both drug and coformer would dissolve in a fashion to obtain steady state equilibrium concentrations defined by the K_{sp} of the cocrystal. For purposes of mass transport analyses, the ideal situation for an immediate release dosage form would have total dissolution of the cocrystal equal to its solubility within the residence time in the stomach. The cocrystal solubility would also ideally be able to generate a supersaturation with respect to drug. This supersaturated solution of drug would move into the intestine to be absorbed into the bloodstream.

The unique nature of the cocrystal system intuitively leads to a hypothesis that a difference in the absorption rate between cocrystal and drug would lead to a change in the solubility of the cocrystal so that the K_{sp} is not violated. Typically, with a coformer being more soluble than the drug, it is assumed that the drug will be absorbed across the membrane at a much faster rate than

its coformer, if the coformer is absorbed at all. The concentration of coformer in the intestinal lumen would begin to increase and no longer be at equal stoichiometric concentration with the drug. According to the current understanding of cocrystal solubility, this excess of coformer leads to two outcomes. The first being a decrease in the solubility of the cocrystal if undissolved cocrystal is present and the second being an increase in cocrystal stability in solution. This means that the cocrystal may lose its solubility advantage over the drug, however, it would also gain stability in solution that may delay the transformation from cocrystal to free drug and coformer. This increase in stability would only be advantageous to absorption if the cocrystal maintained supersaturation concentrations higher than the solubility of the free drug.

The previous ideal scenario is oversimplified as many cocrystals have some form of ionization. To add another degree of realism, the effects of pH on ionization would better simulate what happens in the intestine. The simplest pH scenario possible contains a cocrystal with non-ionizable drug and monoprotic acidic coformer. According to the previously mentioned equations for predicting pH dependent solubility, a cocrystal with acidic coformer is least soluble in the low pH range of the stomach as the pH of the gastric contents is typically lower than the pK_a of the coformer. This low pH also influences the dissolution rate of the cocrystal. In the small intestine, the pH changes from more acidic gastric to more neutral intestinal ranges cause a dramatic increase in the solubility of the cocrystal due an increase in ionization of the acidic coformer. Depending on the pK_a of the coformer, the level of cocrystal solubility may change drastically along its path from the acidic stomach to the more neutral environment of the intestine where absorption happens. This pH change may do two major things that could affect the absorption of the drug. First, the coformer becoming ionized may modify the absorption of the coformer since ionizing a molecule greatly reduces its ability to passively diffuse across a membrane[9]. Second, and maybe

a larger factor in absorption, ionization reduces the solution stability of the cocrystal as it becomes more soluble. If the drug can only hydrogen bond with the coformer when it is non-ionized, then the ionization of coformer upon entering the intestine causes a shortage of coformer that can associate with the drug and stabilize it in solution. Following Le Chatelier's principle, ionization will cause more cocrystal to dissolve to fill the reduced concentration of non-ionized coformer, but the increased amount of dissolved drug from coformer ionization cannot be sustained with the decreased amount of non-ionized coformer. A supersaturated solution with respect to the drug will provide an increased chance that the drug will precipitate out of solution as it wants to return to its least energetic form.

If ionization trades solubility for stability, theoretically, pH would then be a variable in the transformation kinetics of a cocrystal. If this is the case, it would be expected that the pH which causes a higher amount of ionized coformer would lead to a higher degree of supersaturation and much faster rate of conversion from cocrystal to free drug form. For a cocrystal to increase absorption from levels of free drug, the concentration of the drug in solution from a cocrystal system must be sustained at a supersaturated level for an extended period of time. Due to supersaturation induced by an ionized coformer or larger K_{sp}, an increased rate of solution mediated phase transformation may jeopardize the absorption advantage of cocrystal over free drug even if the cocrystal has a vast solubility advantage. Thus, a balance of cocrystal solubility and stability must be met in order to for the cocrystal to maintain advantage over the free drug for absorption.

These previous two ideal scenarios have neglected the contribution of intestinal lipids to the solubilization of the cocrystal in the lumen of the intestine. Upon entering the intestine, bile salts, phosphatidylcholine, and cholesterol are secreted into the intestine to aid in the digestion of

lipids in food[32]. These secretions help solubilize lipids in solution and can alter the solubility of the drug and cocrystal. Lipid solubilization can be advantageous to the cocrystal as it helps stabilize it, however, if the total concentration of lipids is above the CSC of the cocrystal, then there is no longer a solubility advantage of the cocrystal over the free drug. How cocrystal solubility will behave when cocrystal components associate with the different lipophilic species in the intestine is a major factor in understanding cocrystal absorption as the drug and coformer may be able to associate differently with bile salts than with cholesterol. Accurately mimicking biorelevant levels of intestinal secretions and describing how the cocrystal components behave with them *in vitro* may help bring more accuracy to *in vitro-in vivo* correlation.

In order to fully understand what happens when a cocrystal is placed into the gastrointestinal tract, all variables discussed in the previous scenarios need to be considered together. An understanding of how variables like pH, micellar solubilization, and absorption rate interplay with each other and affect the solubility and transformation kinetics of cocrystals is needed. With this knowledge, more accurate mass transport analyses and better predictions of absorption for poorly soluble drugs in cocrystal systems may be made possible.

Solubility

Lipid Solubilization and pH Dependent Solubility

To attempt to create a gastrointestinal tract environment in an *in vitro* setting, medium must be carefully selected to mimic conditions that are similar to the environment of the stomach and portions of the small intestine. These medium must contain relevant levels of lipid solubilizing agents[32], pH ranges, and buffer capacity[33] in order increase the ability of an *in vitro* study to correlate with any *in vivo* data for poorly soluble drugs.

Solution-Mediated Phase Transformation

Supersaturation of a poorly soluble drug is imperative to increasing absorption and the ability of cocrystals to achieve supersaturation is what makes them an attractive option for poorly soluble drugs. *In vitro* studies, however, confirmed when supersaturation is achieved there can be a solution-mediated phase transition of the cocrystal back to crystals of free drug and coformer[34-36]. Some cocrystals have been shown to transform very rapidly, almost instantaneously when dissolving in solution[37]. Other cocrystals have been shown to have small levels of transformation after 90 minutes, but completely transform within 24-hours[14]. Therefore, understanding the variables that cause precipitation of drug and coformer out of solution will help give a better understanding the absorption of a cocrystal in the gastrointestinal tract.

Some research has been done looking into inhibiting the precipitation of cocrystal components out of solution and studies have shown that many different conditions can affect the rate at which transformation can happen. The type of solution that a cocrystal dissolves in influences the transformation rate, as different buffer concentrations have been shown to have different cocrystal transformation rates[13]. Selection of appropriate excipients has also been shown to reduce the rates of transformation during dissolution[37]. In addition to excipients, lipids and surfactants have also been shown to stabilize cocrystals and can completely prevent transformation depending on their concentration in solution[38]. All of these factors must be taken into account when considering how each individual cocrystal may behave and control drug absorption in the intestinal tract.

Absorption

Absorption of a drug from a cocrystalline material in the intestinal tract creates some additional variables that need to be accounted for. The rates at which the drug and coformer are absorbed across the intestinal membrane, if significantly different, are expected to cause differing

concentrations in the intestinal lumen. The impact that this differential absorption has on the solubility and stability of the cocrystal in solution still needs to be fully understood. Considering extreme cases, if a cocrystalline material has a coformer that is unable to be absorbed across the intestinal membrane, there will be a greater amount of coformer than drug in solution. Depending on the cocrystal, this could advantageous or detrimental to cocrystal absorption as increasing the coformer concentration creates better stability but lessens solubility. If the increase in stability does not lead to the cocrystal losing its solubility advantage over the drug, an absorption advantage should still be possible.

Applying Mass Transport Analyses to Cocrystals

Dissolution

One of the first and most well-known mathematical models used to describe dissolution of a solid can be accredited to Noyes and Whitney[39]. Their first experimental setup used a spinning cylinder assuming a well-mixed bulk solution due to rotation and dissolution rate limited by the stagnant diffusion layer of saturated solution. The authors mathematically described the dissolution process as

$$\frac{dC}{dt} = K(C_s - C_b) \tag{1.23}$$

where the change in concentration over time is equal to a rate constant (K) multiplied by the difference between the solubility of the solid (C_s) and the concentration of the solid dissolved in the bulk (C_b).

Following the contribution of Noyes-Whitney, the group of Nernst and attempted to describe the rate constant (K) in equation (1.23). Applying Fick's law[40], Nernst and Brunner were able to account for the rate limiting stagnant diffusion layer. Their equation described change in mass over time, but can easily be re-written to describe change in concentration over time[41].

$$\frac{dM}{dt} = \frac{DS}{h}(C_s - C_b) \tag{1.24}$$

$$\frac{dC}{dt} = \frac{DS}{Vh}(C_s - C_b) \tag{1.25}$$

(M) is the mass of substance that dissolves over given time, (D) is the diffusion coefficient of the dissolving substance, (S) is the surface area of substance exposed to solution, (V) is the volume the substance dissolves in, (h) is the diffusion layer thickness, (C_s) is the solubility of the substance, and (C_b) is the concentration of substance in the bulk solution [41]. This model assumes that the diffusion layer is stagnant, and no mixing occurs in the region, whereas the bulk solution is assumed to be well mixed so that a homogenous concentration is created. A general schematic describing the different regions surrounding a dissolving solid that are accounted for by the Nernst-Brunner equation is shown below in Figure 1.13.

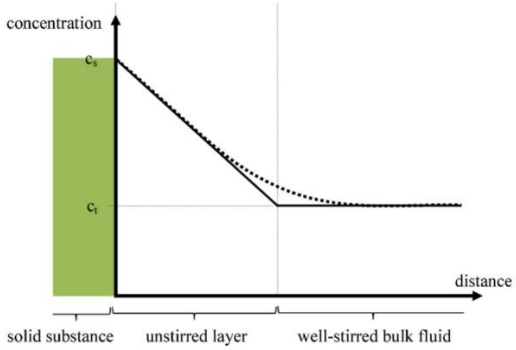

Figure 1.13: Schematic of stagnant diffusion layer at the interface of a dissolving substance as described by the Nernst-Brunner equation[42].

Intrinsic dissolution rate is generally expressed in terms of flux, as flux is the rate of solute passing through a given area [40]. By applying Fick's first law, assuming the concentration at the face of the dissolving solid is the solute's solubility and sink conditions at the edge of the diffusion layer, the diffusion equation can be written

$$J = -D_{eff}\frac{dC}{dx} = D_{eff}\frac{C_s}{h} \tag{1.26}$$

where (D_{eff}) is the effective diffusion coefficient of the solute, (C_s) is the saturating solubility of the solute, and (h) is the thickness of the diffusion layer.

Rotating disk, also known as the Wood apparatus, has hydrodynamics that are well defined and the diffusion thickness (h) has been solved by Levich[43]:

$$h = 1.612 D_{eff}^{1/3} \nu^{1/6} \omega^{-1/2} C_s \tag{1.27}$$

where (ν) is the kinematic viscosity and (ω) is the angular velocity. Substituting equation (1.27) into equation (1.26) gives the diffusive flux for rotating disk.

$$J = -D_{eff} \frac{dC}{dx} = 0.62 D_{eff}^{2/3} \nu^{-1/6} \omega^{1/2} C_s \tag{1.28}$$

The Noyes-Whitney and Nernst Brunner equations do not take into account changes in surface area. When particles dissolve, the surface area of solid exposed to solution decreases as a function of time. The authors Wang and Flanagan describe spherical particles whose radius shrinks as mass dissolves into the liquid phase. Intrinsic dissolution in terms of diffusional flux from spherical particles is shown in equation (1.29) and is dependent on the effective diffusion constant (D_{eff}), solute solubility (C_s), diffusion layer thickness (h), and radius of the particle (a).

$$J = -D_{eff} \frac{dC}{dx} = D_{eff} C_s \left(\frac{1}{h} + \frac{1}{a}\right) \tag{1.29}$$

The intrinsic dissolution in terms of diffusional flux can be easily modified to describe cocrystal dissolution by substituting the solubility of solute (C_s) with the already derived expressions for cocrystal solubility in different conditions. For non-ionizable cocrystals equation (1.3) can be substituted into equation (1.26) to give:

$$J = \frac{D_{eff}}{h} \sqrt{K_{sp}} \tag{1.30}$$

For cocrystals with an acidic coformer, equation (1.8) can be substituted into equation (1.26) to get:

$$J = \frac{D_{eff}}{h}\sqrt{K_{sp}(1 + \frac{K_a}{[H^+]_o})} \tag{1.31}$$

To account for micellar solubilization, equation (1.21) is substituted into equation (1.26).

$$J = \frac{D_{eff}}{h}\sqrt{K_{sp}(1 + K_s^R[mic])(1 + K_s^{HA}[mic] + \frac{K_a}{[H^+]_o})} \tag{1.32}$$

$[H^+]_o$ stands for the concentration of the H^+ ions at the face of the dissolving solid and has previously been solved for a non-ionizable drug with monoprotic acid

$$[H^+]_o = \frac{-(D_{H^+}[H^+]_h - D_{OH^-}[OH^-]_h - D_{A^-_{aq}}[A^-]_h) - \sqrt{(D_{H^+}[H^+]_h - D_{OH^-}[OH^-]_h - D_{A^-_{aq}}[A^-]_h)^2 + 4D_{H^+}K_w(D_{OH^-} + D_{A^-_{aq}}K_1\sqrt{K_{sp}})}}{-2 * D_{H^+}} \tag{1.33}$$

where the diffusion coefficients, equilibrium constants, and concentrations of the ionized components of water and acid are all included in determining interfacial pH. All these expressions for flux assume the dissolution occurs with sink conditions. The effective diffusion coefficient must account for the diffusion free drug as well as the drug within micelles.

Thinking intuitively about the manner in which the cocrystal would dissolve, stoichiometry should be paramount. For each molecule of drug entering solution, a molecule of coformer should also enter, and future dissolution contributions to mass transport analyses must account for this.

Permeation

Mathematically describing the process of absorption in the gastrointestinal tract is very difficult, as both active and passive diffusion across the intestinal membrane must be accounted for. Simplified *in vitro* models fall short in this respect, as active transport cannot be accurately described. The mathematics to describe *in vitro* model membrane diffusion is more simplified and easily solved for without the use of sophisticated computing software. For an artificial membrane or thin cell layers like those used in cell permeation studies, the simplest mathematical description

of mass transport deemed sufficient is a one-dimensional quasi-steady state approximation[44]. Diffusion in one-dimension through a membrane, is described by Fick's second law (1.34) and can be set equal to zero according to

$$\frac{\partial C_m}{\partial t} = D_{eff}\frac{\partial^2 C_m}{\partial x^2} = 0 \tag{1.34}$$

where (C_m) is the concentration of solute in the membrane and (D_{eff}) is the effective diffusion coefficient across the membrane[44]. Solving for the differential equation (1.34) and applying boundary condition gives equation (1.35),

$$C_m = K_m C_0 - K_m(C_0 - C_L)\frac{x}{L} \tag{1.35}$$

where (K_m) is the membrane partition coefficient, (C_0) is the concentration of solute at x=0, (C_L) is the concentration of solute at x=L, and (L) is the thickness of the membrane. (Figure 1.14) gives a diagram of the 1-D steady state diffusion model.

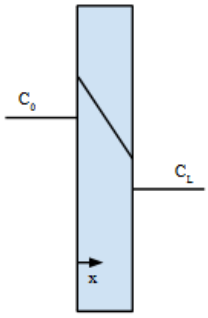

Figure 1.14: Schematic of solute concentration as a function of distance (x) across a membrane of thickness (L) for 1-dimensional diffusion (adapted from Truskey et al.[44]).

Applying Fick's First Law again and substituting the derivative of equation (1.35) with the term for $\frac{dC_m}{dt}$ leads to the steady state flux of solute across the membrane (J_m) where the coefficients for diffusion and partition, membrane thickness, and concentration gradient control the flux.

$$J_m = -D_{eff}\frac{dC_m}{dx} = \frac{D_{eff}K_m}{L}(C_0 - C_L) \tag{1.36}$$

This expression can be simplified even more as terms for diffusion coefficient, partition coefficient, and membrane thickness can be combined into the effective permeability constant (P_{eff}).

$$J_m = P_{eff}(C_0 - C_L) \tag{1.37}$$

$$P_{eff} = \frac{D_{eff}K_m}{L} \tag{1.38}$$

This expression holds true under non-sink conditions. For mass transport analyses describing the absorption across the intestinal membrane, blood flow maintains sink conditions on the basolateral side of the membrane. In this case (C_L) can be treated as zero and equation (1.37) simplifies to

$$J_m = P_{eff}C_0 \tag{1.39}$$

The previous method of describing membrane diffusion ignores stagnant diffusion layers on either side of the membrane. A schematic showing diffusion layers of equal thickness (h) adjacent to a membrane is shown in (Figure 1.15).

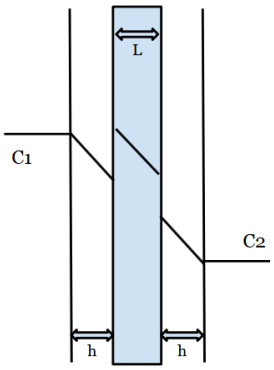

Figure 1.15: Schematic of solute concentration as a function of distance (x) across a membrane of thickness (L) for 1-dimensional diffusion with equal stagnant diffusion layers of length (h) adjacent to membrane. Concentration as a function of distance shown as sloped lines.

The diffusion layers can be easily incorporated into equation (1.37) by treating each of the diffusion layers like a membrane with its own permeability and, using a steady state assumption,

the flux through each diffusion layer and membrane are all equal. The permeability of each layer can be added together to make one total effective permeability coefficient (P_{eff}) expressed as[44]

$$\frac{1}{P_{eff}} = \frac{1}{P_1} + \frac{1}{P_m} + \frac{1}{P_2} = \frac{h}{DK} + \frac{L}{D_m K_m} + \frac{h}{DK} \tag{1.40}$$

which contain aqueous diffusion coefficient (D), membrane diffusion coefficient (D_m), aqueous partition coefficient (K), membrane partition coefficient (K_m) diffusion layer thickness (h), and membrane thickness (L).

Steady state membrane diffusion in the presence of surfactant is modified slightly from the previous form. Micelles diffuse slower than the free drug and this difference needs to be accounted for in the diffusive flux equations. This is done by adding the contributions of diffusion by free drug and micellar solubilized drug together in the aqueous stagnant diffusion layer[45]

$$J_1 = \frac{D}{h}\left(C_{1,b} - C_{1,s}\right) + \frac{D^*}{h}\left(C^*_{1,b} - C^*_{1,s}\right) \tag{1.41}$$

$$J_2 = \frac{D}{h}\left(C_{2,s} - C_{b,b}\right) + \frac{D^*}{h}\left(C^*_{2,s} - C^*_{2,b}\right) \tag{1.42}$$

where, (D) stands for the aqueous diffusion coefficient, (h) is layer thickness, (D*) is micellar diffusion coefficient and (C*) is the micellar concentration of drug Subscripts stand for bulk (b) and membrane surface (s) concentrations, and numbers represent the donor (1) or recipient (2) side of the membrane. The ratio of the concentration of drug in the micelle and the concentration of free drug multiplied by the micellar concentration describes the equilibrium distribution constant[45]:

$$k^* = \frac{C^*}{C[mic]} \tag{1.43}$$

This constant can be used to calculate the aqueous effective diffusion coefficient required for determining the permeability constant for the diffusion layer.

$$D_{eff} = \frac{D + k^*[mic]D^*}{1 + k^*[mic]} = fD + f^*D^* \tag{1.44}$$

The fraction of total solute of free and solubilized drug are (f) and (f^*), respectively. The expression for the steady state flux of solute through the membrane in the presence of surfactant is similar to equation (1.37) due to equal surfactant concentrations on both sides of the membrane. The permeability coefficient is slightly modified to

$$J_m = P_m(C_{1,m} - C_{2,m}) \tag{1.45}$$

$$P_m = \frac{D_m K_m}{L(1 + k^*[mic])} \tag{1.46}$$

and, assuming steady state, the flux through each layer can be set equal and the permeability of each layer can be summed up according to equation (1.30).

$$\frac{1}{P_{eff}} = \frac{1}{P_1} + \frac{1}{P_m} + \frac{1}{P_2} = \frac{h}{D_{eff}} + \frac{L}{D_m K_m} + \frac{h}{D_{eff}} \tag{1.47}$$

The effective permeability can be multiplied by the bulk concentration difference between donor and recipient compartments to get the total flux across the membrane.

$$J_m = P_{eff}(C_{1,b} - C_{2,b}) \tag{1.48}$$

Cocrystals, however, are made up of two components. It is not unlikely to think that the effective permeability coefficients of the drug and coformer through a membrane could be different, as these two types of molecules have different physicochemical properties. Most drugs in cocrystal systems are poorly soluble lipophilic BCS class II entities and are paired with a more soluble and hydrophilic coformer[15]. When describing the permeation of cocrystal through a membrane numerically, the concentrations of drug and coformer should be treated separately, assuming each cocrystal component does not affect the permeation of the other.

Precipitation

Transformation of cocrystal to free drug and coformer can only happen when the cocrystal solubility is greater than the free drug and supersaturation with respect to drug has been achieved. The scientific literature seems to lack articles pertaining to the mathematical description of solution transformation of cocrystals. Mass transport analyses may be formulated so that a term for transformation is incorporated to the simulation equations only when the drug concentration is above its solubility. The rate of transformation may or may not be different for each specific drug and coformer pairing. Crystallization of a drug, and the rates at which it happens in solution, can be influenced by many different factors. For the purposes of *in vitro* mass transport analyses, a simplified assumption with transformation kinetics rate constants derived from empirical data may be sufficient for ascertaining correlations between mass transport analyses, *in vitro*, and *in vivo* data.

Foundation for Cocrystal Mass Transport Analysis

A foundation to build upon future mass transport analyses of cocrystal should start with a simplified model with simplified assumptions before adding more intricacies. This was done by taking the Nernst-Brunner equation in combination with rotating disk hydrodynamics to describe dissolution and combining a steady state 1-dimensional membrane diffusion model with a receiver compartment under sink conditions. Carbamazepine (CBZ) and salicylic acid (SLC) were used as case study drug and coformer as physicochemical properties were readily available in the literature. To simplify the simulations and describe steady state concentrations, the assumptions of no precipitation and an infinite amount of drug were used.

Dissolution was first simulated using the Nernst-Brunner equation (1.25) with values for surface area and diffusion layer thickness from rotating disk dissolution found in literature[46].

Experimentally determined cocrystal solubility from literature was used[30]. The value for volume was arbitrarily assigned to 100 mL to simplify calculations. Results of the simulation are found in (Figure 1.16). Excess solid was assumed to allow for the simulation to saturate at the solubility of the cocrystal.

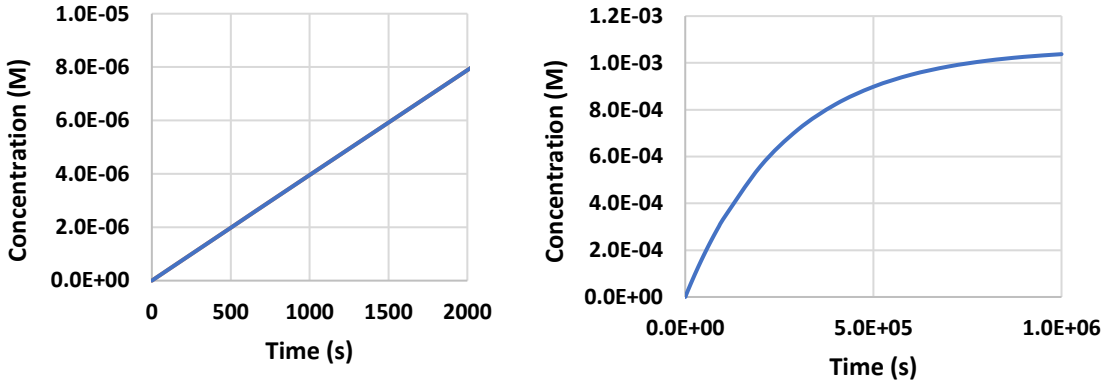

Figure 1.16: Simulated rotating disk dissolution profiles of carbamazepine-salicylic acid (—) from (a) 0 < t < 2000 seconds and (b) 0 < t < 1000000 seconds using equation (1.25).

To analyze differential absorption of CBZ and SLC, 1-D steady state membrane diffusion under sink conditions was used according to equation (1.39). Biorelevant permeability constants were pulled from literature as measured human intestinal permeability was found for CBZ[47] and Caco-2 cell line permeability for SLC [9] were found. Simulation was run from a concentration equal to the square root of the K_{sp} of CBZ-SLC cocrystal[30]. Contributions from pH or micellar solubilization were ignored. Results of the simulation (Figure 1.17) indicate a substantial difference in concentration are seen after only 30 minutes.

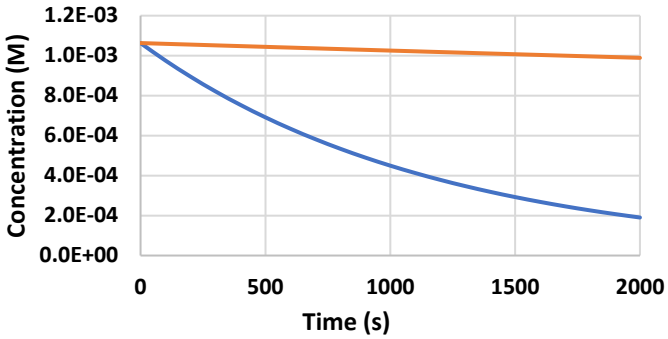

Figure 1.17: Donor phase simulation of differential absorption of carbamazepine (—) and salicylic acid (—) using 1-D steady state membrane diffusion mass transport analysis.

A simulation combining the Nernst-Brunner equation for dissolution and 1-D steady state absorption components together assumed that for each mole of cocrystal dissolved in stoichiometric (1:1) fashion. From there the separate concentrations of each cocrystal component was taken out of solution by their respective permeability constant. The solubility of the cocrystal in the bulk was calculated ignoring pH and micellar contributions using the concentrations of separate components according to equation (1.2). This changing solubility was then reciprocated back into the Nernst-Brunner equation. This changing solubility expression, however, may or may not accurately depict the concentrations of drug and coformer at the interface of the dissolving solid. Results of the simulation are found in Figure 1.18. According to the simulation, the drug concentration appears to reach steady state at approximately half the concentration of coformer in only 30 minutes.

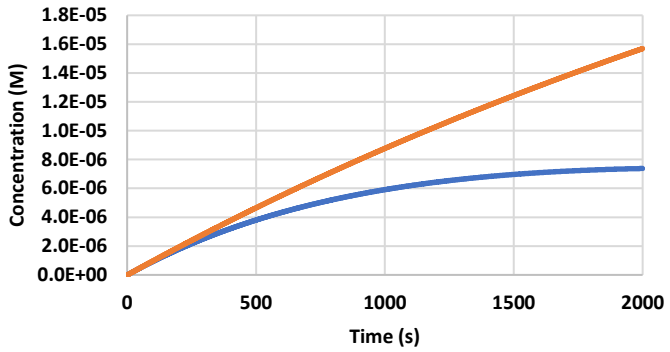

Figure 1.18: Donor phase simulations of simultaneous dissolution and absorption for carbamazepine (—) and salicylic acid (—) from 0 < t < 2000 seconds.

These approaches provide foundational work to build upon. More appropriate assumptions can be implemented to tailor mathematical expressions to more realistic scenarios of cocrystal dissolution and absorption.

References

1. Amidon, G.L., et al., *A Theoretical Basis for a Biopharmaceutic Drug Classification - the Correlation of in-Vitro Drug Product Dissolution and in-Vivo Bioavailability.* Pharmaceutical Research, 1995. **12**(3): p. 413-420.
2. Leuner, C. and J. Dressman, *Improving drug solubility for oral delivery using solid dispersions.* European Journal of Pharmaceutics and Biopharmaceutics, 2000. **50**(1): p. 47-60.
3. Pouton, C.W. and C.J. Porter, *Formulation of lipid-based delivery systems for oral administration: materials, methods and strategies.* Adv Drug Deliv Rev, 2008. **60**(6): p. 625-37.
4. Blagden, N., et al., *Crystal engineering of active pharmaceutical ingredients to improve solubility and dissolution rates.* Advanced Drug Delivery Reviews, 2007. **59**(7): p. 617-630.
5. Bevernage, J., et al., *Evaluation of gastrointestinal drug supersaturation and precipitation: Strategies and issues.* International Journal of Pharmaceutics, 2013. **453**(1): p. 25-35.
6. Bevernage, J., et al., *Supersaturation in human gastric fluids.* European Journal of Pharmaceutics and Biopharmaceutics, 2012. **81**(1): p. 184-189.
7. Lipinski, C.A., et al., *Experimental and computational approaches to estimate solubility and permeability in drug discovery and development settings.* Advanced Drug Delivery Reviews, 2001. **46**(1-3): p. 3-26.
8. Wood, I.S. and P. Trayhurn, *Glucose transporters (GLUT and SGLT): expanded families of sugar transport proteins.* British Journal of Nutrition, 2003. **89**(01): p. 3-9.
9. Takanaga, H., I. Tamai, and A. Tsuji, *Ph-Dependent and Carrier-Mediated Transport of Salicylic-Acid across Caco-2 Cells.* Journal of Pharmacy and Pharmacology, 1994. **46**(7): p. 567-570.
10. Good, D.J. and N. Rodriguez-Hornedo, *Solubility Advantage of Pharmaceutical Cocrystals.* Crystal Growth & Design, 2009. **9**(5): p. 2252-2264.
11. Lee, H.G., G.G.Z. Zhang, and D.R. Flanagan, *Cocrystal Intrinsic Dissolution Behavior Using a Rotating Disk.* Journal of Pharmaceutical Sciences, 2011. **100**(5): p. 1736-1744.
12. Chow, S.F., et al., *Simultaneously Improving the Mechanical Properties, Dissolution Performance, and Hygroscopicity of Ibuprofen and Flurbiprofen by Cocrystallization with Nicotinamide.* Pharmaceutical Research, 2012. **29**(7): p. 1854-1865.

13. Basavoju, S., D. Bostrom, and S.P. Velaga, *Indomethacin-saccharin cocrystal: Design, synthesis and preliminary pharmaceutical characterization.* Pharmaceutical Research, 2008. **25**(3): p. 530-541.

14. McNamara, D.P., et al., *Use of a glutaric acid cocrystal to improve oral bioavailability of a low solubility API.* Pharmaceutical Research, 2006. **23**(8): p. 1888-1897.

15. Qiao, N., et al., *Pharmaceutical cocrystals: An overview.* International Journal of Pharmaceutics, 2011. **419**(1-2): p. 1-11.

16. Childs, S.L., et al., *Screening strategies based on solubility and solution composition generate pharmaceutically acceptable cocrystals of carbamazepine.* Crystengcomm, 2008. **10**(7): p. 856-864.

17. Friscic, T. and W. Jones, *Recent Advances in Understanding the Mechanism of Cocrystal Formation via Grinding.* Crystal Growth & Design, 2009. **9**(3): p. 1621-1637.

18. Cheney, M.L., et al., *Effects of Crystal Form on Solubility and Pharmacokinetics: A Crystal Engineering Case Study of Lamotrigine.* Crystal Growth & Design, 2010. **10**(1): p. 394-405.

19. Luger, P., et al., *Structure and physicochemical properties of meloxicam, a new NSAID.* European Journal of Pharmaceutical Sciences, 1996. **4**(3): p. 175-187.

20. Cheney, M.L., et al., *Coformer Selection in Pharmaceutical Cocrystal Development: a Case Study of a Meloxicam Aspirin Cocrystal That Exhibits Enhanced Solubility and Pharmacokinetics.* Journal of Pharmaceutical Sciences, 2011. **100**(6): p. 2172-2181.

21. Weyna, D.R., et al., *Improving Solubility and Pharmacokinetics of Meloxicam via Multiple-Component Crystal Formation.* Molecular Pharmaceutics, 2012. **9**(7): p. 2094-2102.

22. Maheshwari, C., *Understanding the Solution Phase Chemistry and Solid State Thermodynamic Behavior of Pharmaceutical Cocrystals*. 2012.

23. Hickey, M.B., et al., *Performance comparison of a co-crystal of carbamazepine with marketed product.* European Journal of Pharmaceutics and Biopharmaceutics, 2007. **67**(1): p. 112-119.

24. Zheng, W.J., et al., *Selection of oral bioavailability enhancing formulations during drug discovery.* Drug Development and Industrial Pharmacy, 2012. **38**(2): p. 235-247.

25. Jung, M.S., et al., *Bioavailability of indomethacin-saccharin cocrystals.* Journal of Pharmacy and Pharmacology, 2010. **62**(11): p. 1560-1568.

26. Bak, A., et al., *The co-crystal approach to improve the exposure of a water-insoluble compound: AMG 517 sorbic acid co-crystal characterization and pharmacokinetics.* Journal of Pharmaceutical Sciences, 2008. **97**(9): p. 3942-3956.

27. Stanton, M.K., et al., *Improved Pharmacokinetics of AMG 517 Through Co-crystallization Part 2: Analysis of 12 Carboxylic Acid Co-crystals.* Journal of Pharmaceutical Sciences, 2011. **100**(7): p. 2734-2743.

28. Serajuddin, A.T.M., *Salt formation to improve drug solubility.* Advanced Drug Delivery Reviews, 2007. **59**(7): p. 603-616.

29. Nehm, S.J., B. Rodriguez-Spong, and N. Rodriguez-Hornedo, *Phase solubility diagrams of cocrystals are explained by solubility product and solution complexation.* Crystal Growth & Design, 2006. **6**(2): p. 592-600.

30. Bethune, S.J., et al., *Understanding and Predicting the Effect of Cocrystal Components and pH on Cocrystal Solubility.* Crystal Growth & Design, 2009. **9**(9): p. 3976-3988.

31. Huang, N. and N. Rodriguez-Hornedo, *Engineering Cocrystal Solubility, Stability, and pH(max) by Micellar Solubilization.* Journal of Pharmaceutical Sciences, 2011. **100**(12): p. 5219-5234.

32. Porter, C.J., et al., *Enhancing intestinal drug solubilisation using lipid-based delivery systems.* Adv Drug Deliv Rev, 2008. **60**(6): p. 673-91.

33. Kalantzi, L., et al., *Characterization of the Human Upper Gastrointestinal Contents Under Conditions Simulating Bioavailability/Bioequivalence Studies.* Pharmaceutical Research, 2006. **23**(1): p. 165-176.

34. Anquetil, P.A., et al., *Laser Raman spectroscopic analysis of polymorphic forms in microliter fluid volumes.* Journal of Pharmaceutical Sciences, 2003. **92**(1): p. 149-160.

35. Childs, S.L., et al., *Crystal engineering approach to forming cocrystals of amine hydrochlorides with organic acids. Molecular complexes of fluoxetine hydrochloride with benzoic, succinic, and fumaric acids.* Journal of the American Chemical Society, 2004. **126**(41): p. 13335-13342.

36. Shiraki, K., et al., *Dissolution improvement and the mechanism of the improvement from cocrystallization of poorly water-soluble compounds.* Pharmaceutical Research, 2008. **25**(11): p. 2581-2592.

37. Remenar, J.F., et al., *Celecoxib : Nicotinamide dissociation: Using excipients to capture the cocrystal's potential.* Molecular Pharmaceutics, 2007. **4**(3): p. 386-400.

38. Huang, N. and N. Rodriguez-Hornedo, *Effect of Micelliar Solubilization on Cocrystal Solubility and Stability.* Crystal Growth & Design, 2010. **10**(5): p. 2050-2053.

39. Noyes, A.A. and W.R. Whitney, *THE RATE OF SOLUTION OF SOLID SUBSTANCES IN THEIR OWN SOLUTIONS.* Journal of the American Chemical Society, 1897. **19**(12): p. 930-934.

40. Fick, A., *Ueber diffusion.* Annalen der Physik, 1855. **170**(1): p. 59-86.

41. Brunner, E., *Reaktionsgeschwindigkeit in heterogenen Systemen*. 1903: Georg-Augusts-Universitat, Gottingen.

42. Siepmann, J. and F. Siepmann, *Mathematical modeling of drug dissolution.* International Journal of Pharmaceutics, 2013. **453**(1): p. 12-24.

43. Levich, V.G. and S. Technica, *Physicochemical hydrodynamics*. Vol. 689. 1962: Prentice-hall Englewood Cliffs, NJ.

44. Truskey, G.A., F. Yuan, and D.F. Katz, *Transport phenomena in biological systems*. 2004: Pearson/Prentice Hall Upper Saddle River NJ:.

45. Amidon, G.E., W.I. Higuchi, and N.F. Ho, *Theoretical and experimental studies of transport of micelle-solubilized solutes.* J Pharm Sci, 1982. **71**(1): p. 77-84.

46. Tsinman, K., et al., *Powder Dissolution Method for Estimating Rotating Disk Intrinsic Dissolution Rates of Low Solubility Drugs.* Pharmaceutical Research, 2009. **26**(9): p. 2093-2100.

47. Lennernas, H., *Modeling Gastrointestinal Drug Absorption Requires More In Vivo Biopharmaceutical Data: Experience from In Vivo Dissolution and Permeability Studies in Humans.* Current Drug Metabolism, 2007. **8**(7): p. 645-657.

CHAPTER II

Mechanistic Analysis of Cocrystal Dissolution and Partitioning in Biphasic Media

Introduction

Poorly soluble active pharmaceutical ingredients (APIs) are often difficult to develop into a successful drug product due to slow dissolution rates and low solution concentrations causing problems for intestinal absorption[1]. As absorption is fundamentally a diffusion-controlled process, the amount of drug absorbed is a function of the concentration that a dissolving solid can generate within the lumen of the intestine. Cocrystals offer a potential solution to these problems as solubility and dissolution rates of a parent drug can be altered and higher intestinal absorption can potentially be achieved[2-6]. However, cocrystal dissolution is controlled by many variables and often leads to unexpected experimental outcomes when comparing *in vitro* and *in vivo* testing[7]. The ability to simulate solution concentrations from cocrystal dissolution and estimate amounts of absorption could help guide experiments during development stages and help save time and money in creating a viable cocrystal product.

Ketoconazole (KTZ) is a weak base and a member of the azole group of antifungal drugs used to treat fungal infections[8]. It is a Biopharmaceutics Classification System (BCS) class II drug that has high lipophilicity (logP = 4.35) and a poor intrinsic aqueous solubility at neutral pH[9]. Cocrystals of dibasic KTZ with diprotic carboxylic acids discovered have been shown to have faster dissolution and higher solubility than the drug alone under a variety of experimental

conditions[10]. A mechanistic analysis of the dissolution of these ketoconazole cocrystals was undertaken by Cao and coworkers and expressions developed to predict dissolution[11].

Because of the important interplay of dissolution and absorption *in vivo*, further mechanistic mass transport analysis is undertaken in this work utilizing a two-phase dissolution apparatus for testing simultaneous dissolution and absorption rates of ketoconazole cocrystals.[12, 13]. The system comprises of two immiscible liquids, one an aqueous buffer acting as a donor compartment and the other an organic (typically 1-Octanol) that acts as a receiver compartment[14]. *In vitro* biphasic dissolution and partitioning experiments of poorly soluble drugs have attempted to make *in vitro-in vivo* correlations (IVIVC)[12, 13, 15]. Rates of drug transport across this barrier have been studied in detail and are accompanied with mathematical expressions to describe them[16]. The purpose of this study is to develop and test a mechanistic mass transport analysis to explain the dissolution and mass transport of ketoconazole-fumaric acid cocrystal (KTZ-FUM) in a two-phase rotating disk dissolution apparatus as a proof of concept for simulating cocrystal dissolution in combination with absorption environments.

Materials and Methods

Materials

Ketoconazole (lot BS1200333121 purity 98%) was purchased from Bosche Scientific (New Brunswick, NJ) and used as received. Fumaric Acid (lot 09426EE purity 99+%) was purchased from Sigma-Aldrich (St. Louis, MO) and used as received.

High-performance liquid chromatography (HPLC) grade methanol and acetone were purchased from Fisher Chemical (Fair Lawn, NJ), phosphoric acid (lot B056524 purity 85+%) from Acros Organics (NJ), sodium hydroxide (lot 280988 purity 98.6%) from J.T. Baker

(Phillipsburg, NJ), and 1-octanol (Lot K46372891 605 purity 99%) was purchased from EMD Millipore (Billerica, MA) and used as received.

Cocrystal Synthesis

Reaction crystallization was used to synthesize cocrystals at room temperature. Equimolar ratios (1:1) of ketoconazole (KTZ) and fumaric acid (FUM) were added to a vial containing acetone. The suspension was placed in a temperature-controlled bath at 25^{o}C and magnetically stirred for 24 hours. Vacuum filtration was used to recover the solid phase and X-ray powder diffraction (XRPD) and differential scanning calorimetry (DSC) were used to determine solid phases.

Dissolution Media Preparation

Dissolution buffer (50 mM) was prepared by dissolving phosphoric acid into Milli-Q filtered water. The pH of the solution was then adjusted to pH 3 using sodium hydroxide. For both the single aqueous phase and two phase aqueous/organic experiments, the dissolution buffer and 1-octanol were equilibrated for 24 hours to allow each phase to become saturated.

Rotating Disk Dissolution Experiments

One hundred twenty-five mL of aqueous dissolution buffer saturated with octanol was placed in a water jacketed vessel at 25^{o}C and allowed equilibrate. A pellet of compressed solid material was created in the rotating disk apparatus by placing 100 mg of KTZ-FUM cocrystal into a 0.5 cm radius die and compacted using a hydraulic press using a force of 6.67 kN. Compression force was held for 1 min before decompressing at a steady rate for 30 seconds. The rotating disk assembly was placed in an overhead electric motor and a rotation speed of 50±1 RPM was used for all experiments. Agitation of the aqueous phase was accomplished by the rotating disk

apparatus. Time points were then taken at 15-minute intervals for 75 minutes. Sample concentrations were evaluated using HPLC.

Two-Phase Mass Transfer Coefficient Measurement Experiments

To determine the mass transfer rate of KTZ, FUM, and KTZ together with FUM, into the octanol phase, they were pre-dissolved in aqueous 50 mM phosphate buffer pH 3 at concentrations just below KTZ solubility to eliminate any chance of precipitation. The buffer solution containing solute of interest was placed into the dissolution vessel and the experiment started as soon 70 mL of 1-octanol was slowly poured into the dissolution vessel. Care was taken to ensure there was not excessive agitation of the aqueous/organic interface. Agitation of the aqueous phase was accomplished by the empty rotating disk (no solid) while the octanol phase agitation was accomplished by incorporating a paddle on the rotating shaft located in the middle of the octanol phase. A 0.5 mL sample was drawn through a cannula inserted in the aqueous phase and 0.15 mL from the octanol at 15-minute intervals and the final pH of the aqueous phase was measured. A schematic of the dissolution apparatus is shown in (Figure 2.1).

Two-Phase Rotating Disk Dissolution Experiments

Aqueous dissolution buffer (50 mM phosphate buffer pH 3) was equilibrated at room temperature with 1-octanol 24 hours prior to experiment to saturate both phases, and 125 mL of 1-octanol saturated dissolution buffer was placed in a water jacketed dissolution vessel and set to 25^{o}C and allowed to come to temperature. The compressed disk assembly was placed in an overhead electric motor and rotated of 50±1 RPM and then the dissolution vessel was raised to submerge the disk in the dissolution medium. Upon submersion of the disk, the experiment was started, and 70 mL of dissolution saturated 1-octanol was slowly poured into the vessel. Samples

were drawn in the same manner as the mass transfer coefficient experiments. A schematic of the dissolution apparatus is shown in (Figure 2.1).

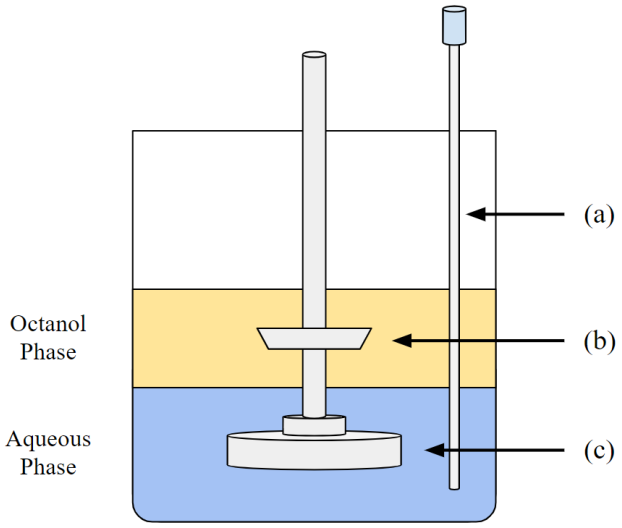

Figure 2.1: Schematic of the biphasic rotating disk dissolution apparatus with (a) cannula for sampling, (b) octanol impeller, and (c) rotating disk.

High Performance Liquid Chromatography (HPLC)

Experimental solution concentrations of KTZ and FUM were measured with a Waters 2950 HPLC with UV spectrometer detector and a Waters Atlantis C18 column (dimensions). The mobile phase used was a 60:40 ratio of Methanol and Milli-Q filtered water containing 0.1% trifluoroacetic acid (TFA). Peak absorbance wavelengths for KTZ (230 nm) and FUM (220 nm) were used.

Dissolution and Partitioning Simulations

The dependent differential equations used to simulate the dissolution and partitioning in two-phase experiments were numerically solved using the Runge-Kutta 4^{th} order method in Berkeley Madonna Software version [9.1.18]. Time steps were 10 minutes to coincide with the experimental time points and the simulations were run from 0 to 75 minutes (simulations with

smaller Δt did not change results). Differential equations with appropriate initial conditions and parameters to describe the conditions of the experiments can be found in Appendix 2A.

Theoretical

Rotating Disk Dissolution

The most fundamental dissolution theory based upon Fick's first law of diffusion states diffusion flux (J)

$$J = D_{aq}\frac{dC}{dx} \tag{2.1}$$

is a function of the aqueous diffusion coefficient (D_{aq}) and concentration gradient of the solute ($\frac{dC}{dx}$)[17]. Applying this concept to the surface of dissolving solid under steady state, equation (2.1) can be re-written

$$J = \frac{D_{aq}}{h}\Delta C \tag{2.2}$$

in terms of the concentration gradient (ΔC) and diffusion layer thickness (h). The organic phase in a biphasic system creates an absorption sink and dissolution experiments duration is kept short to justify the assumption that dissolution is occurring under sink conditions. This means that the concentration gradient is equal to the solute concentration at the dissolving interface,

$$J = \frac{D_{aq}}{h}C_s \tag{2.3}$$

defined here as the solute solubility (C_s). For rotating disk dissolution, the hydrodynamics near the surface of the dissolving solid are well defined. The Levich equation

$$h = 1.612 D_{aq}^{1/3} \nu^{1/6} \omega^{-1/2} \tag{2.4}$$

was used to calculate the effective diffusion layer thickness as a function of the kinematic viscosity (ν) and the rotational speed (ω)[18]. Substituting equation (2.4) into equation (2.3) leads to the following expression

$$J = 0.62 D_{aq}^{2/3} \nu^{-1/6} \omega^{1/2} C_s \tag{2.5}$$

to which surface saturation theory for cocrystals dissolution can be applied. The first assumption is the liquid phase at the solid-liquid interface is saturated according to the stoichiometric solubility of the cocrystal[19]. The stoichiometric cocrystal solubility (S_{cc}) can be substituted for the solubility of the dissolving solid and equation (2.5) becomes

$$J = 0.62 D_{aq}^{2/3} \nu^{-1/6} \omega^{1/2} S_{cc} \tag{2.6}$$

For the specific case of a cocrystal with dibasic drug (B) and diprotic acidic coformer (H_2A), the cocrystal stoichiometric solubility equation is[11]

$$S_{cc} = \sqrt{K_{sp}\left(1 + \frac{[H^+]_0}{K_{a2}^B} + \frac{[H^+]_0^2}{K_{a1}^B K_{a2}^B}\right)\left(1 + \frac{K_{a1}^{H_2A}}{[H^+]_0} + \frac{K_{a1}^{H_2A} K_{a2}^{H_2A}}{[H^+]_0^2}\right)} \tag{2.7}$$

and the variables controlling cocrystal solubility at the solid-liquid interface in equation (2.7) are the solubility product (K_{sp}), the dissociation constants for both drug (K_{a1}^B, K_{a2}^B) and coformer ($K_{a1}^{H_2A}$, $K_{a2}^{H_2A}$), and the interfacial pH ($[H_0^+]$). The second assumption of the surface saturation theory for cocrystal dissolution is that the total fluxes of drug (J_B) and coformer (J_{H_2A}) are equal under steady state sink conditions.

$$J_B = \frac{D_{R,aq}[B]_0}{h} = J_{H_2A} = \frac{D_{H_2A,aq}[H_2A]_0}{h} \tag{2.8}$$

Interfacial concentrations of drug ($[B]_0$) and coformer ($[H_2A]_0$) constitute the diffusion gradient as sink conditions are assumed. Equation (2.7) can be combine with equation (2.6) to derive

$$J_B = J_{H_2A} = 0.62 D_{aq}^{2/3} \nu^{-1/6} \omega^{1/2} \sqrt{K_{sp}(1 + \frac{[H^+]_0}{K_{a2}^B} + \frac{[H^+]_0^2}{K_{a1}^B K_{a2}^B})(1 + \frac{K_{a1}^{H_2A}}{[H^+]_0} + \frac{K_{a1}^{H_2A} K_{a2}^{H_2A}}{[H^+]_0^2})} \quad (2.9)$$

the final form flux equation used to estimate the concentrations of the cocrystal components as a function of time by applying it to the rotating disk surface area (S) available for dissolution and dividing by the volume of the aqueous dissolution compartment (V_{aq}) according to

$$\frac{dC_B}{dt} = \frac{dC_{H_2A}}{dt} = \frac{S}{V_{aq}} 0.62 D_{aq}^{2/3} \nu^{-1/6} \omega^{1/2} \sqrt{K_{sp}(1 + \frac{[H^+]_0}{K_{a2}^B} + \frac{[H^+]_0^2}{K_{a1}^B K_{a2}^B})(1 + \frac{K_{a1}^{H_2A}}{[H^+]_0} + \frac{K_{a1}^{H_2A} K_{a2}^{H_2A}}{[H^+]_0^2})} \quad (2.10)$$

simulate the changes in concentration due to rotating disk dissolution. This expression assumes the absence of precipitation and experiments were done at pH 3 where the cocrystal is less soluble than drug to accommodate this assumption.

Two-Phase Partitioning Mass Transport

The partitioning of drug from aqueous to octanol phases is assumed to be driven by concentration gradient and diffusion across the diffusion layers on each side of the aqueous-octanol interface according to Fick's first law in equation (2.1). A partition mass transfer coefficient ($k_{B,P}$) can be used to simplify the expression and combine the effective diffusion coefficients and thicknesses of the aqueous and organic diffusion layers at the interface

$$J_{B,P} = -k_{B,P}(C_{B,aq} - \frac{C_{B,oct}}{K_{ap}}) \quad (2.11)$$

where the flux of the drug ($J_{B,P}$) into the octanol phase is a function of the aqueous ($C_{B,aq}$) and octanol ($C_{B,oct}$) drug concentrations and the apparent octanol/water partition coefficient (K_{ap}). This equation can be rearranged to express the change in aqueous donor and octanol receiver compartment concentrations

$$\frac{dC_{B,aq}}{dt} = -\frac{A}{V_{aq}} k_{B,P}(C_{B,aq} - \frac{C_{B,oct}}{K_{ap}}) \quad (2.12)$$

$$\frac{dC_{B,oct}}{dt} = \frac{A}{V_{oct}} k_{B,P}(C_{B,aq} - \frac{C_{B,oct}}{K_{ap}}) \tag{2.13}$$

in terms of the aqueous/organic interfacial area (A) and aqueous (V_{aq}) and octanol (V_{oct}) compartment volumes. Solving the resulting differential equation and applying the appropriate initial conditions leads to the final equation expressing the concentration of drug in the donor compartment as a function of time (t)

$$C_{B,aq}(t) = \frac{\frac{V_{aq}}{V_{oct}K_{ap}} C_{B,aq,0} - C_{B,aq,0} e^{\frac{-Ak_{B,P}\left(1+\frac{V_{aq}}{V_{oct}K_{ap}}\right)}{V_{aq}}t}}{(1 + \frac{V_{aq}}{V_{oct}K_{ap}})} \tag{2.14}$$

where (A) is the area of the aqueous/organic interface, (V_{aq}) and (V_{oct}) the donor and receiver compartment volumes, respectively, (K_{ap}) is the octanol/water partition coefficient, and ($C_{B,aq,0}$) is the initial concentration of drug in the donor compartment. The equation can be rearranged to

$$k_{B,P} = -\frac{V_{aq}}{A\left(1 + \frac{V_{aq}}{V_{oct}K_{ap}}\right)t} \ln[\frac{\frac{V_{aq}}{V_{oct}K_{ap}} C_{B,aq,0} - C_{B,aq}(t)\left(1 + \frac{V_{aq}}{V_{oct}K_{ap}}\right)}{C_{B,aq,0}}] \tag{2.15}$$

which permits concentration data to be used to obtain the mass transfer coefficient from experimental concentrations of KTZ and FUM. The equations (2.11-2.15) were also used to obtain the mass transfer coefficient for the coformer.

Cocrystal Rotating Disk Dissolution in Biphasic Media

Equations describing changes in concentration over time from the aqueous rotating disk dissolution equation (2.10) and partition equation (2.12) were combined to obtain

$$\frac{dC_B}{dt} = \frac{S}{V_{aq}} 0.62 D_{aq}^{2/3} \nu^{-1/6} \omega^{1/2} \sqrt{K_{sp}(1 + \frac{[H^+]_0}{K_{a2}^B} + \frac{[H^+]_0^2}{K_{a1}^B K_{a2}^B})(1 + \frac{K_{a1}^{H_2A}}{[H^+]_0} + \frac{K_{a1}^{H_2A} K_{a2}^{H_2A}}{[H^+]_0^2})} - \frac{A}{V_{aq}} k_{B,P}(C_{B,aq} - \frac{C_{B,oct}}{K_{ap}}) \tag{2.16}$$

that describes cocrystal rotating disk dissolution and precipitation behavior in the aqueous phase of a biphasic experiment. This expression will hold if the aqueous and organic phases do not reach saturation. Experimental duration was short enough to maintain concentrations well below saturation in either phase since single phase rotating disk dissolution experiment confirms this with a linear dissolution profile for duration of experiment.

Results

Aqueous Rotating Disk Dissolution

Since KTZ-FUM cocrystal dissolution is pH dependent, the dissolution rate is determined by the pH at the dissolving cocrystal surface and may be significantly different from bulk pH (pH_b) due to KTZ and/or FUM pKa ionization as described in the work of Cao and coworkers[11]. Estimates for Ketoconazole cocrystal interfacial pH (pH_o) in unbuffered conditions were shown by Cao to be approximately equal to the bulk pH when the bulk pH is less than 4. Thus, the bulk pH value may be used as the interfacial pH to simulate rotating disk dissolution in pH 3 phosphate buffer. The estimated dissolution rate based on equation (2.10) was found to be in close agreement (~0.1 uM/min) with the experimental data (Figure 2.2).

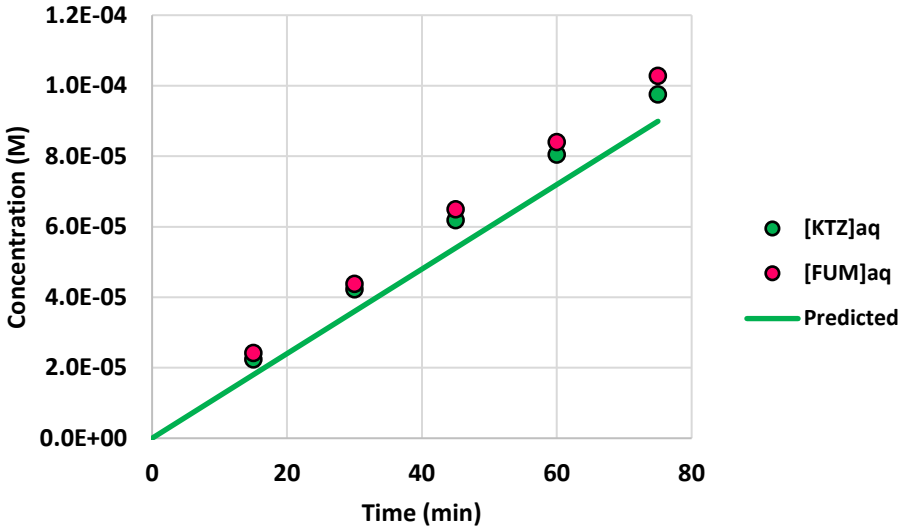

Figure 2.2: Measured concentrations of KTZ (●) and FUM (●) from a single cocrystal rotating disk dissolution experiment in pH 3 phosphate buffer (50 mM). Error bars plotted but within symbols. Dissolution of KTZ-FUM (—) was simulated using equation (2.10) and $pH_o = 3$.

A better appreciation of the accuracy of the dissolution prediction can be gathered by examining the sensitivity of changes to interfacial pH. A ΔpH_o of 0.1 at the interface causes a change in the predicted dissolution rate by ~0.15 uM/min as seen in (Figure 2.3).

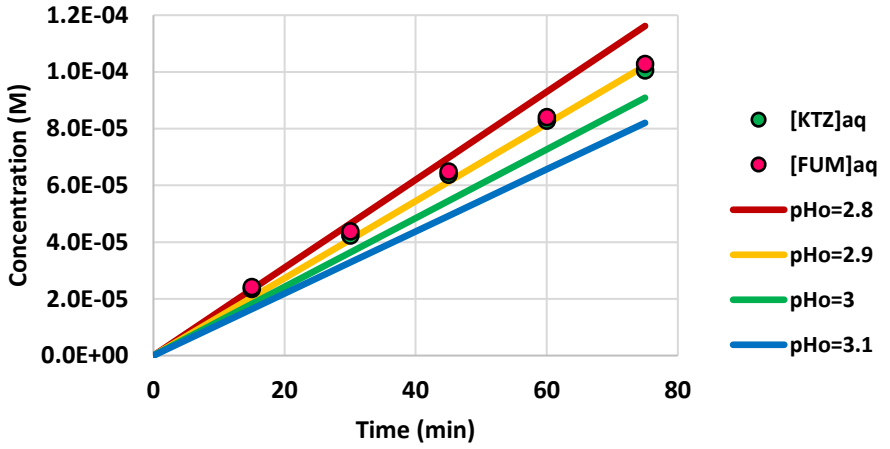

Figure 2.3: Simulations of KTZ-FUM rotating disk dissolution in pH 3 phosphate buffer (50 mM) with pH_o values of 2.8 (—), 2.9 (—), 3 (—), and 3.1 (—). Measured concentrations of KTZ (●) and FUM (●) from single rotating disk experiment for reference. Error bars plotted but within symbols.

Solute Diffusion Transport between Aqueous and Organic Phases

Drug and coformer diffusion rates were estimated according to Othmer-Thaker theory[20], however, the hydrodynamics of the aqueous/organic interface in the dissolution vessel are not well defined and appropriate diffusion layer thicknesses cannot be determined readily. Therefore, drug and coformer mass transfer coefficients were obtained by fitting experimental data.

Pre-dissolved aqueous solutions of drug, coformer, and cocrystal were prepared at concentrations just below drug solubility. A two-compartment diffusion model was fitted to the data generated using equation (2.14) to obtain mass transfer coefficients (Figure 2.4). The mass transfer coefficient obtained for FUM was approximately 30 percent higher than that of KTZ (Figure 2.5) when measured independently. This is reasonable as FUM is has a smaller molecular weight than KTZ and therefore would be expected to have a larger diffusion coefficient in both aqueous and octanol phases.

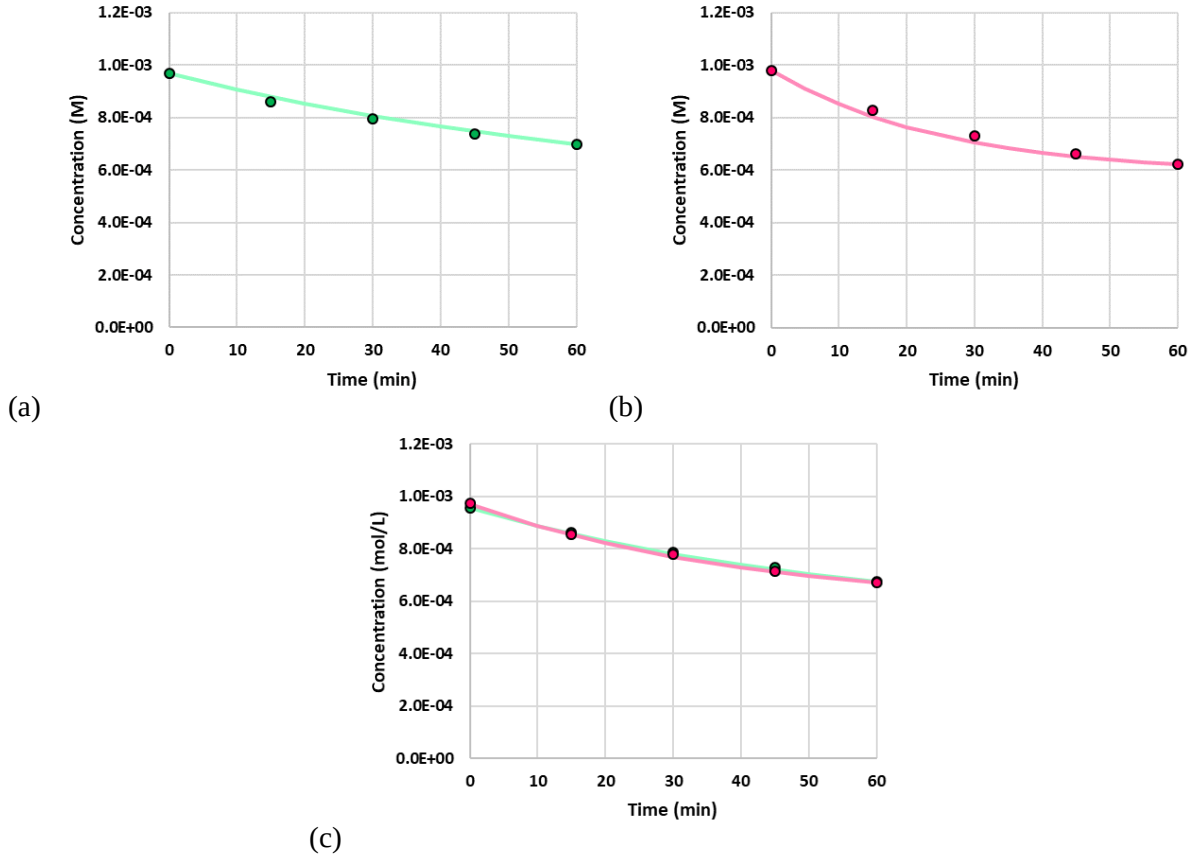

Figure 2.4: Measured aqueous donor concentrations of KTZ (●) and FUM (●) from mass transfer partitioning experiments for (a,b) separate and (c) simultaneous diffusion. Equation (2.13) is plotted with fit values of mass transfer coefficients for KTZ (—) and FUM (—).

When the two molecules diffused in the presence of each other, the coformer mass transfer coefficient was significantly ($p<0.05$) smaller compared to its independent mass transfer coefficient (Figure 2.5). This suggest interaction in solution reducing the mass transfer rate across the aqueous/organic interface and associated diffusion layers. The drug mass transfer coefficient did not significantly change suggesting that the interaction which the much smaller coformer does not substantially slow the diffusion rate of the drug.

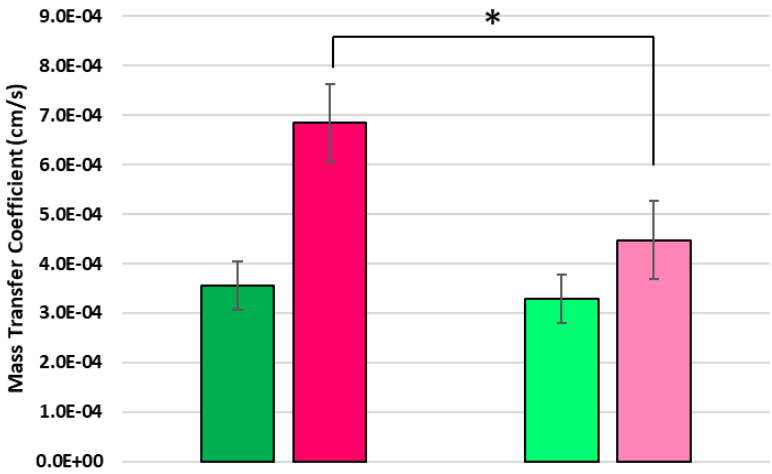

Figure 2.5: Obtained mass transfer coefficients for separately diffusing KTZ (■) and FUM (■) and simultaneously diffusing KTZ (■) and FUM (■). (* $p < 0.05$)

Cocrystal Rotating Disk Dissolution in Biphasic Media

The independently estimated dissolution and measured partitioning components were combined and applied using equation (2.16) and equation (2.13) to predict the aqueous and octanol phase drug concentrations, respectively, in a rotating disk dissolution two-phase experiment. Conditions, including hydrodynamics, were kept consistent with the previous independent experiments. (Figure 2.6) shows the concentration time profiles for the aqueous and organic phases. The use of the mass transfer coefficients of KTZ and FUM obtained when they diffused together allows for a more accurate simulation of the concentration profiles as a function of time as evidenced by the R-squared values reported in (Table 2.1).

Discussion

The ability to estimate the dissolution rate of a cocrystal containing a weakly basic drug and acidic coformer was previously shown in solution without buffer species[11]. What has been shown in (Figure 2.1) is that the dissolution rate of KTZ-FUM cocrystal can be simulated in 50 mM phosphate buffer using the interfacial pH estimated in an unbuffered system. This gives

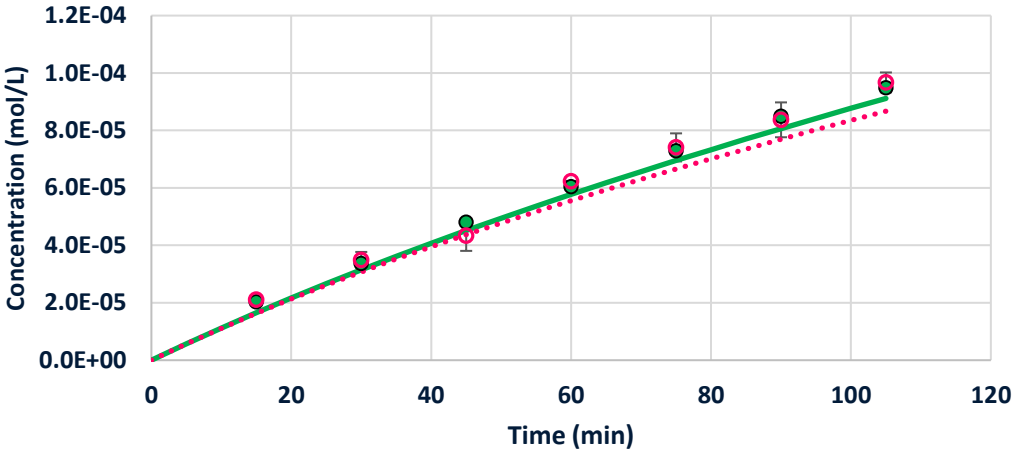

(a)

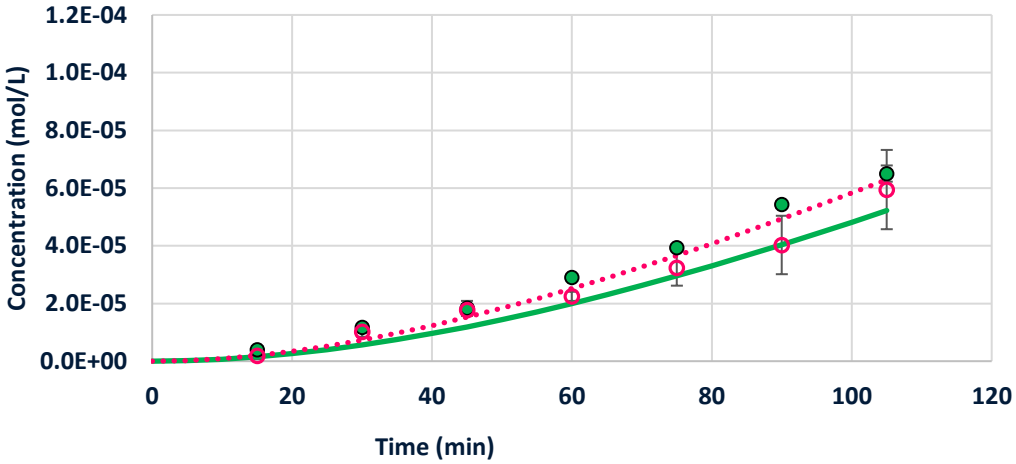

(b)

Figure 2.6: Measured concentrations of KTZ (●) and FUM (○) in biphasic rotating disk dissolution experiments for (a) aqueous donor (pH 3 phosphate buffer) and (b) octanol receiver phases. Dissolution and partitioning simulations of KTZ (—) and FUM (…) generated according to equation (2.16) for donor and equation (2.13) for receiver phases.

Table 2.1: Coefficients of determination between measured and simulated concentrations of KTZ and FUM in the biphasic cocrystal rotating disk dissolution experiments for simultaneous and separate mass transfer coefficients.

	R^2 Values	
	Simultaneous	Separate
KTZ Aqueous	0.989	0.982
KTZ Octanol	0.763	0.839
FUM Aqueous	0.929	0.759
FUM Octanol	0.956	0.786

confidence that the theory can be used to simulate the dissolution rates in a two-phase rotating disk experiment.

When cocrystal components dissociate from the solid cocrystal, there are two assumptions that could be made for the diffusion of these species through stagnant diffusion layers. The drug and coformer either diffuse independently without affecting each other or interact in a manner that causes diffusion rates to differ. The results of this study suggest that there is some ability of the drug and coformer to influence the rate of diffusion of the other (Figure 2.5).

The mathematical expressions derived in this study demonstrate the ability to estimate the kinetics of cocrystal dissolution and absorption in a two-phase experimental system (Figure 2.6). Predicting the solution kinetics of a drug from a cocrystal and the amount absorbed into an organic absorption compartment serves as a foundation for more complex models to simulate the dissolution and *in vivo* absorption. Estimating particle dissolution rates and substituting human intestinal permeability for octanol mass transfer coefficients are examples of future steps to utilizing mass transfer analysis to estimate the potential exposure of a patient to a drug from a cocrystal system.

Conclusions

This study presents an approach to simulating the dissolution of a weakly basic cocrystal in the presence of an *in vitro* absorption compartment. Interfacial pH of the dissolving cocrystal in buffer was approximately equal to unbuffered calculations for bulk pH values below the acidic coformer pK_a. Cocrystal components interact in the solution phase to the extent that the diffusion coefficients are altered across a stagnant diffusion layer. The solution interaction of drug and coformer could be an important variable to consider when simulating the absorption associated with cocrystal dissolution. This ability to simulate cocrystal dissolution in an *in vitro* absorption

environment may give insight into cocrystal performance *in vivo* and help guide experiments to select the most appropriate cocrystal for further development.

Acknowledgements

The authors acknowledge the financial support from the University of Michigan College of Pharmacy.

References

1. Amidon, G.L., et al., *A Theoretical Basis for a Biopharmaceutic Drug Classification - the Correlation of in-Vitro Drug Product Dissolution and in-Vivo Bioavailability.* Pharmaceutical Research, 1995. **12**(3): p. 413-420.
2. McNamara, D.P., et al., *Use of a glutaric acid cocrystal to improve oral bioavailability of a low solubility API.* Pharmaceutical Research, 2006. **23**(8): p. 1888-1897.
3. Childs, S.L., P. Kandi, and S.R. Lingireddy, *Formulation of a Danazol Cocrystal with Controlled Supersaturation Plays an Essential Role in Improving Bioavailability.* Molecular Pharmaceutics, 2013. **10**(8): p. 3112-3127.
4. Jung, M.S., et al., *Bioavailability of indomethacin-saccharin cocrystals.* Journal of Pharmacy and Pharmacology, 2010. **62**(11): p. 1560-1568.
5. Smith, A.J., et al., *Cocrystals of Quercetin with Improved Solubility and Oral Bioavailability.* Molecular Pharmaceutics, 2011. **8**(5): p. 1867-1876.
6. Weyna, D.R., et al., *Improving Solubility and Pharmacokinetics of Meloxicam via Multiple-Component Crystal Formation.* Molecular Pharmaceutics, 2012. **9**(7): p. 2094-2102.
7. Stanton, M.K. and A. Bak, *Physicochemical properties of pharmaceutical co-crystals: A case study of ten AMG 517 co-crystals.* Crystal Growth & Design, 2008. **8**(10): p. 3856-3862.
8. Blum, R.A., et al., *Increased gastric pH and the bioavailability of fluconazole and ketoconazole.* Ann Intern Med, 1991. **114**(9): p. 755-7.
9. Sangster, J., *LOGKOW Databank. A databank of evaluated octanol-water partition coefficients (Log P) on microcomputer diskette*. 1993, Montreal, Quebec, Canada: Sangster Research Laboratories.
10. Martin, F.A., et al., *Ketoconazole Salt and Co-crystals with Enhanced Aqueous Solubility.* Crystal Growth & Design, 2013. **13**(10): p. 4295-4304.
11. Cao, F.J., N. Rodriguez-Hornedo, and G.E. Amidon, *Mechanistic Analysis of Cocrystal Dissolution, Surface pH, and Dissolution Advantage as a Guide for Rational Selection.* Journal of Pharmaceutical Sciences, 2019. **108**(1): p. 243-251.
12. Shi, Y., et al., *Application of a biphasic test for characterization of in vitro drug release of immediate release formulations of celecoxib and its relevance to in vivo absorption.* Mol Pharm, 2010. **7**(5): p. 1458-65.
13. Grundy, J.S., et al., *Studies on dissolution testing of the nifedipine gastrointestinal therapeutic system. I. Description of a two-phase in vitro dissolution test.* Journal of Controlled Release, 1997. **48**(1): p. 1-8.

14. Phillips, D.J., et al., *Overcoming sink limitations in dissolution testing: a review of traditional methods and the potential utility of biphasic systems.* Journal of Pharmacy and Pharmacology, 2012. **64**(11): p. 1549-1559.

15. Vangani, S., et al., *Dissolution of poorly water-soluble drugs in biphasic media using USP 4 and fiber optic system.* Clinical Research and Regulatory Affairs, 2009. **26**(1-2): p. 8-19.

16. Mudie, D.M., et al., *Mechanistic analysis of solute transport in an in vitro physiological two-phase dissolution apparatus.* Biopharmaceutics & Drug Disposition, 2012. **33**(7): p. 378-402.

17. Fick, A., *Ueber diffusion.* Annalen der Physik, 1855. **170**(1): p. 59-86.

18. Levich, V.G. and S. Technica, *Physicochemical hydrodynamics*. Vol. 689. 1962: Prentice-hall Englewood Cliffs, NJ.

19. Cao, F.J., et al., *Mechanistic Analysis of Cocrystal Dissolution as a Function of pH and Micellar Solubilization.* Molecular Pharmaceutics, 2016. **13**(3): p. 1030-1046.

20. Othmer, D.F. and M.S. Thakar, *Correlating diffusion coefficient in liquids.* Industrial & Engineering Chemistry, 1953. **45**(3): p. 589-593.

Appendix 2A

KTZ-FUM Rotating Disk Dissolution Simulations pH 3.01

METHOD RK4

STARTTIME = 0

STOPTIME=4500

DT = 900

;dissolved compound

d/dt(C1) = (S / V) * 0.62 * (DaqB)^(2/3) * (Omg)^(1/2) * (Nu)^(-1/6) * Scc

;initial conditions

init(C1) = 0; cmpddissolved mM

;cocrystal solubility

Scc = (Ksp * (1 + (Ka1A / H0) + (Ka1A * Ka2A / (H0)^2)) * (1 + (H0 / Ka2B) + ((H0)^2 / Ka1B / Ka2B)))^(1 / 2)

;parameters

Ksp = 1.5e-3; mM^2

Ka1A = 9.33e-4

Ka2A = 4.17e-5

Ka1B = 1.15e-3

Ka2B = 3.09e-7

H0 = 9.77237e-4

DaqA = 9.95e-6; cm^2/s

DaqB = 3.81e-6; cm^2/s

S = 0.785398; cm^2

V = 125; mL

Omg = 5.2359877; rad/s

Nu = .008926; cm^2/s

KTZ-FUM Biphasic Rotating Disk Dissolution Simulations

METHOD RK4

STARTTIME = 0

STOPTIME = 6300

DT = 300

;dissolved compound

d/dt(C1) = (S / V1) * 0.62 * DaqB^(2/3) * Omg^(1/2) * Nu^(-1/6) * Scc - (A / V1)* k1 * (C1 - (C2/KapB))

d/dt(C2) = (A / V2)* k1 * (C1 - (C2/KapB))

d/dt(C3) = (S / V1) * 0.62 * DaqB^(2/3) * Omg^(1/2) * Nu^(-1/6) * Scc - (A / V1)* k2 * (C3 - (C4/KapB))

d/dt(C4) = (A / V2)* k2 * (C3 - (C4/KapB))

;initial conditions

init(C1) = 0; cmpddissolved mM

init(C2) = 0; cmpddissolved mM

init(C3) = 0; cmpddissolved mM

init(C4) = 0; cmpddissolved mM

;cocrystal solubility

Scc = (Ksp * (1 + (Ka1A / H0) + (Ka1A * Ka2A / H0^2)) * (1 + (H0 / Ka2B) + (H0^2 / Ka1B / Ka2B)))^(1 / 2)

;partition coefficients

KapB = 10.215 *pHb - 29.892

;parameters

Ksp = 1.5e-3; mM^2

Ka1A = 9.33e-4

Ka2A = 4.17e-5

Ka1B = 1.15e-3

Ka2B = 3.09e-7

pHb = 3.13

H0 = .000912

DaqA = 9.95e-6; cm^2/s

DaqB = 3.81e-6; cm^2/s

S = 0.785398; cm^2

V1 =125; mL

V2 = 70; mL

A = 43.00840343; cm^2

Omg = 5.23598776; rad/s

Nu = .008926; cm^2/s

k1 = 0.00032867; cm*s-1

k2 = 0.00044753; cm*s-1*

KapA = 1.2

CHAPTER III

Assessing Cocrystal Thermodynamic Solubility Equations to Determine Potential Precipitation Risks in *In Vitro* Dissolution Experiments

Introduction

A common problem in drug product development is poor aqueous solubility. In simple terms, oral bioavailability is a factor of solubility and permeability,[1] and improving the aqueous solubility can increase drug exposure[2-6]. Cocrystallization is one strategy that has the potential for improving the aqueous solubility of a drug. A current hotbed of research is assessing the ability of cocrystals to generate supersaturation and improve the oral bioavailability of their poorly soluble drugs. Studies have confirmed that there is merit to this idea, however, a wide range of variability in cocrystal behavior exists leading to *in vitro* and *in vivo* data that appear to contradict[2, 7, 8]. The ability to efficiently estimate and assess the potential supersaturation of a cocrystal in a given dissolution system could help guide experiments in cocrystal product development and save time and resources in the process.

Ketoconazole (KTZ) is a weakly dibasic antifungal drug of the azole family that struggles with absorption due to poor aqueous solubility at intestinal pH. Cocrystals of KTZ with diprotic carboxylic adipic (ADP), fumaric (FUM), and succinic (SUC) acids have been discovered and shown to increase the solubility and dissolution rates under intestinally relevant conditions[9]. These properties lead the generation of supersaturation and precipitation from solution that has been studied[10].

Cocrystal thermodynamic solubility equations have been developed for these dibasic cocrystals and the goal of this study is to apply these cocrystal solubility equations to estimate the potential supersaturation values in the context of a biorelevant experimental system and gain knowledge of potential precipitation risks.

Methods

Cocrystal Solubility Estimations

Drug and cocrystal solubilities were calculated using equations 3.7 and 3.22, respectively. Parameters were sourced from literature and have been compiled in Tables 3.1-3.3. Bulk pH values of 5.0 and 6.5 were used to calculate solubilities for Fed State Simulated Intestinal Fluid (FeSSIF)/blank FeSSIF and Fasted State Simulated Intestinal Fluid (FaSSIF)/blank FaSSIF, respectively. Interfacial pH values to estimate solubilities in unbuffered conditions were taken from Cao et al[11].

Interfacial pH Estimations in Buffered conditions

Approach taken from Mooney et al.[12] was adapted for cocrystals. Main assumptions for the estimation of interfacial pH are 1) diffusion according to Fick's second law, 2) sink conditions, 3) mass and proton balance within the diffusion layer, 4) sum of flux for buffer species is zero, 5) flux of acid reacting species is equal to base reacting species, and 6) concentrations of drug and coformer to cocrystal solubility equations according to the surface saturation theory proposed by Cao et al[13]. A summary of the derivation can be found in Appendix 3A. Interfacial pH estimates for KTZ cocrystals were made for acetate (FeSSIF/blank FeSSIF) and phosphate (FaSSIF/blank FaSSIF) buffers.

Theoretical

Drug and Cocrystal Solubility

The aqueous solubility of the dibasic drug ketoconazole (B_{aq}) as a function of hydrogen ion ($[H^+_{aq}]$) and micelle ($[mic]$) concentrations is determined by the equilibria:

$$BH^{2+}_{2\,aq} \rightleftharpoons H^+_{aq} + BH^+_{aq} \tag{3.1}$$

$$K^B_{a1} = \frac{[H^+_{aq}][BH^+_{aq}]}{[BH^{2+}_{2\,aq}]} \tag{3.2}$$

$$BH^+_{aq} \rightleftharpoons H^+_{aq} + B_{aq} \tag{3.3}$$

$$K^B_{a2} = \frac{[H^+_{aq}][B_{aq}]}{[BH^+_{aq}]} \tag{3.4}$$

$$B_{aq} + mic \rightleftharpoons B_{mic} \tag{3.5}$$

$$K^B_s = \frac{[B_{mic}]}{[B_{aq}][mic]} \tag{3.6}$$

The total drug solubility can then be expressed in the terms of the ionization (K^B_{a1}, K^B_{a2}) and solubilization (K^B_s) constants of the drug and written as

$$S_{drug} = S_o(1 + K^B_s[mic] + \frac{[H^+_{aq}]}{K^B_{a2}} + \frac{[H^+_{aq}]^2}{K^B_{a1}K^B_{a2}}) \tag{3.7}$$

where (S_o) is the intrinsic unionized solubility of the drug. Cocrystal solubility is driven by the solubility product (K_{sp}) in addition to the drug (B_{aq}) and coformer (H_2A_{aq}) ionization and solubilization equilibria[14]:

$$(BH_2A)_s \rightleftharpoons B_{aq} + H_2A_{aq} \tag{3.8}$$

$$K_{sp} = [B_{aq}][H_2A_{aq}] \tag{3.9}$$

$$BH_{2\,aq}^{2+} \rightleftharpoons H_{aq}^{+} + BH_{aq}^{+} \tag{3.10}$$

$$K_{a1}^{B} = \frac{[H_{aq}^{+}][BH_{aq}^{+}]}{[BH_{2\,aq}^{2+}]} \tag{3.11}$$

$$BH_{aq}^{+} \rightleftharpoons H_{aq}^{+} + B_{aq} \tag{3.12}$$

$$K_{a2}^{B} = \frac{[H_{aq}^{+}][B_{aq}]}{[BH_{aq}^{+}]} \tag{3.13}$$

$$B_{aq} + mic \rightleftharpoons B_{mic} \tag{3.14}$$

$$K_{s}^{B} = \frac{[B_{m}]}{[B_{aq}][mic]} \tag{3.15}$$

$$H_2A \rightleftharpoons H_{aq}^{+} + HA_{aq}^{-} \tag{3.16}$$

$$K_{a1}^{H_2A} = \frac{[H_{aq}^{+}][HA_{aq}^{-}]}{[H_2A_{aq}]} \tag{3.17}$$

$$HA_{aq}^{-} \rightleftharpoons H_{aq}^{+} + A_{aq}^{2-} \tag{3.18}$$

$$K_{a2}^{H_2A} = \frac{[H_{aq}^{+}][A_{aq}^{2-}]}{[HA_{aq}^{-}]} \tag{3.19}$$

$$H_2A_{aq} + mic \rightleftharpoons H_2A_{mic} \tag{3.20}$$

$$K_{s}^{H_2A} = \frac{[H_2A_{mic}]}{[H_2A_{aq}][mic]} \tag{3.21}$$

and combining these equilibria lead to the expression for KTZ cocrystal solubility. This can be generated for a 1:1 cocrystal of a dibasic drug with diprotic coformer[15]

$$S_{cc} = \sqrt{K_{sp}(1 + K_s^B[mic] + \frac{[H_{aq}^{+}]}{K_{a2}^B} + \frac{[H_{aq}^{+}]^2}{K_{a1}^B K_{a2}^B})(1 + K_s^{H_2A}[mic] + \frac{K_{a1}^{H_2A}}{[H_{aq}^{+}]} + \frac{K_{a1}^{H_2A} K_{a2}^{H_2A}}{[H_{aq}^{+}]^2})} \tag{3.22}$$

where the cocrystal solubility product (K_{sp}), hydrogen ion ($[H_{aq}^{+}]$) and surfactant micelle ($[mic]$) concentrations, ionization constants for drug (K_{a1}^{B},K_{a2}^{B}) and coformer ($K_{a1}^{H_2A}$, $K_{a2}^{H_2A}$), and the solubilization constants for drug (K_{s}^{B}) and coformer ($K_{s}^{H_2A}$) control cocrystal solubility.

Ketoconazole's nature as a weak base exibits an exponential decrease in solubility as pH increases, as is described by equation (3.7). A previous study measuring KTZ cocrystal solubilities showed cocrystallization with carboxylic acids leads to a U-shaped curve generated by plotting equation (3.22), as coformer ionization contributes to increased cocrystal solubility at higher pH and drug ionization at lower pH values[10]. Comparing drug and cocrystal solubility plots, the curves meet at an intersection point refered to as the pH_{max} (Figure 3.1). At pH values above this point, the cocrystal has a solubility advantage over the drug and supersaturation can be achieved. Below it, the drug is more soluble and the cocrystal is the more stable form.

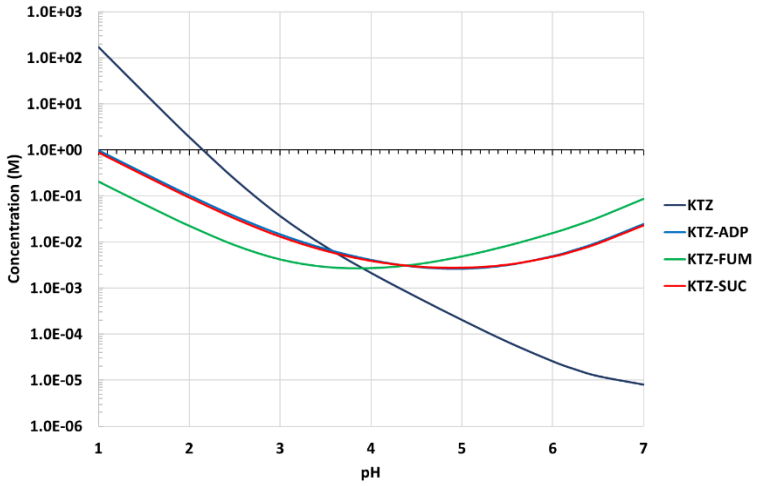

Figure 3.1: Stoichiometric solubilty curves of KTZ (—) according to equation (3.7) and cocrystals KTZ-ADP (—), KTZ-FUM (—), and KTZ-SUC (—) according to equation (3.22) as a function of bulk pH.

Table 3.1: Relevant KTZ and coformer ionization constants[15]

	KTZ	ADP	FUM	SUC
pK_{a1}	3.17	4.44	2.85	4.00
pK_{a2}	6.63	5.44	4.10	5.24

Table 3.2: KTZ cocrystal solubility products[10]

	KTZ-ADP	KTZ-FUM	KTZ-SUC
K_{sp} (M^2)	3.4 x 10^{-8}	1.5 x 10^{-9}	2.7 x 10^{-8}

Table 3.3: KTZ and coformer solubilization constants[15]

	pH	Ks (M^{-1})
KTZ	5	14400 ± 400
	6.5	1600 ± 70
ADP	5	0
FUM	5	29.1 ± 0.2
SUC	5	9.5 ±.02

Interfacial pH

Interfacial pH (pH_o) values for the KTZ cocrystals in unbuffered solutions were calculated according to the surface saturation model put forth by Cao et al. The model predicts coformer ionization to self buffer and create a plateau for KTZ cocrystal interfacial pH when bulk pH (pH_b) is in the intestinal range (pH 5-7) as shown in (Figure 3.2).

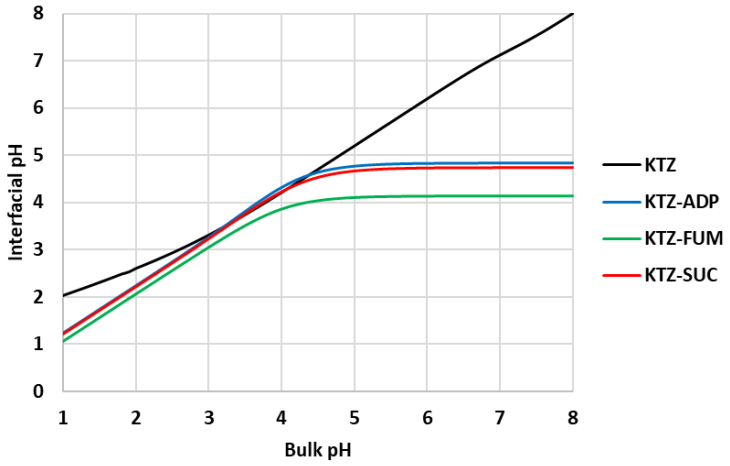

Figure 3.2: Interfacial pH estimates for KTZ (—), KTZ-ADP (—), KTZ-FUM (—), and KTZ-SUC (—) as a function of bulk pH in deionized water from Cao et al[11].

Supersaturation

In this study, supersaturation (σ) is a kinetic parameter defined as

$$\sigma = \frac{C_{drug}}{S_{drug}} \tag{3.23}$$

the ratio of the solution concentration of dissolved drug (C_{drug}) to the drug solubility (S_{drug}). It is a temporary value during a dissolution experiment that varies over time due to precipitation or pH changes.

Solubility Advantage

Solubility Advantage (SA) is a thermodynamic parameter defined as the ratio

$$SA = \frac{S_{cc}}{S_{drug}} \tag{3.24}$$

of cocrystal solubility (S_{cc}) to the drug solubility (S_{drug}). It is a theoretical limit to the amount of supersaturation that can be generated in a system if there is enough mass to generate saturation with respect to cocrystal.

Dose Number

Dose number (D_o) is defined as

$$D_o = \frac{dose/volume}{S_{drug}} \tag{3.25}$$

the dose in a given dissolution volume normalized by the drug solubility (S_{drug}). In the context of cocrystal dissolution, this parameter can serve as the theoretical limit of supersaturation that can be achieved in a dissolution system if the entire dose can completely dissolve.

Experimental Data from Literature

A study by Chen et al.[15] performed biorelevant particle dissolution experiments of Ketoconazole and its cocrystals with adipic, fumaric, and succinic acids in four dissolution media[15]. Surfactant containing Fed State Simulated Intestinal Fluid (FeSSIF) and Fasted State Simulated Intestinal Fluid (FaSSIF) in addition to both media without surfactants (Blank FeSSIF and Blank FaSSIF) were used to test the dissolution, supersaturation, and precipitation behavior

of the three KTZ cocrystals. The composition of the four dissolution media can be found in (Table 3.4).

Table 3.4: FeSSIF, FaSSIF, and blank media specifications.[16, 17]

	Blank FaSSIF	FaSSIF	Blank FeSSIF	FeSSIF
Sodium taurocholate	--	3 mM	--	15 mM
Lecithin	--	0.75 mM	--	3.75 mM
NaOH	8.7 mM	8.7 mM	101 mM	101 mM
$NaH_2PO_4*H_2O$	29 mM	29 mM	--	--
CH_3CO_2H	--	--	144 mM	144 mM
NaCl	106 mM	106 mM	203 mM	203 mM
pH	6.5	6.5	5.0	5.0

Varying levels of dissolution, supersaturation, and precipitation were exhibited amoung the three cocrystals across the different dissolution conditions (Figure 3.3). Parameters such as the apparent initial dissolution rate (AIDR), maximum supersaturation (σ_{max}), and the area under the curve from t = 0-180 minutes ($AUC_{0\text{-}180min}$) can be obtained from these concentration profiles and used for analysis.

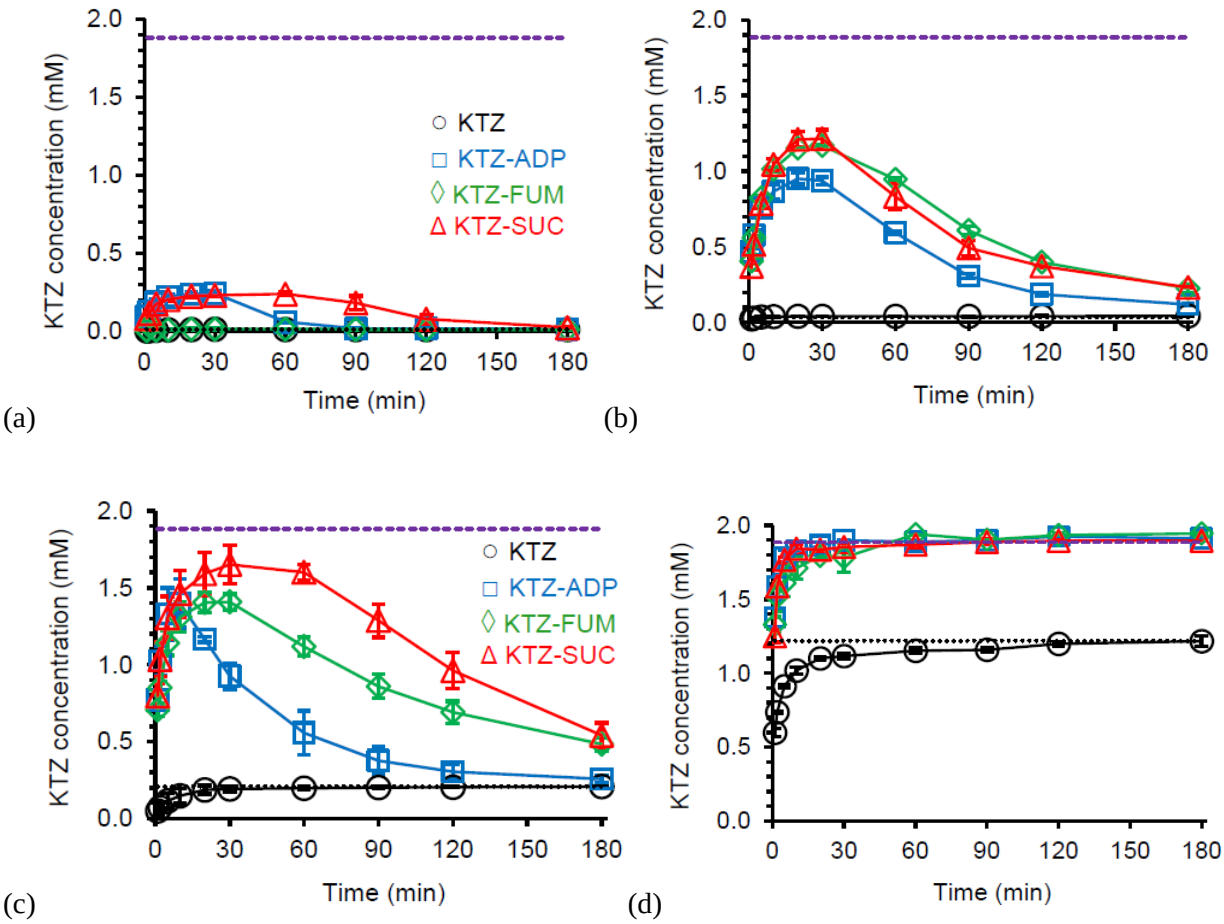

Figure 3.3: Concentration-time profiles of KTZ (—), KTZ-ADP (—), KTZ-FUM (—), and KTZ-SUC (—) in biorelevant dissolution media (a) blank FaSSIF, (b) FaSSIF, (c) blank FeSSIF, and (d) FeSSIF. Drug solubility (…) and cocrystal concentration when completely dissolved (---) shown for reference.

Results

Interfacial pH and Solubility Advantage

The focus of this study was to investigate connections between thermodynamic expressions for drug and cocrystal solubilities and experimentally measured kinetic dissolution profiles. Solubility estimations of the three KTZ cocrystals (equation 3.22) and parent drug (equation 3.7) were made for the bulk and interfacial pH conditions of biorelevant dissolution media from Chen et al[15]. The interfacial pH values were estimated using the surface saturation model from Cao et al[11]. and placed into cocrystal and drug solubility expressions. All values are compiled in (Table

Table 3.5: Interfacial pH (unbuffered) and bulk pH values with calculated cocrystal and drug solubilities in biorelevant conditions.

Blank FeSSIF	Interface				Bulk			
	Interfacial pH	Cocrystal Solubility (mM)	Drug Solubility (mM)	S_{cc}/S_{drug}	Bulk pH	Cocrystal Solubility (mM)	Drug Solubility (mM)	S_{cc}/S_{drug}
KTZ-ADP	4.77	3.03	0.45	6.72	5	2.99	0.26	11.3
KTZ-FUM	4.10	4.57	2.27	2.02	5	9.16	0.26	34.5
KTZ-SUC	4.66	4.22	0.58	7.22	5	4.48	0.26	16.8
Blank FaSSIF	Interface				Bulk			
	Interfacial pH	Cocrystal Solubility (mM)	Drug Solubility (mM)	S_{cc}/S_{drug}	Bulk pH	Cocrystal Solubility (mM)	Drug Solubility (mM)	S_{cc}/S_{drug}
KTZ-ADP	4.84	3.00	0.38	7.28	6.5	10.7	0.014	759
KTZ-FUM	4.14	4.63	2.07	2.23	6.5	63.0	0.014	4470
KTZ-SUC	4.73	4.23	0.50	8.50	6.5	19.6	0.014	1390
FeSSIF	Interface				Bulk			
	Interfacial pH	Cocrystal Solubility (mM)	Drug Solubility (mM)	S_{cc}/S_{drug}	Bulk pH	Cocrystal Solubility (mM)	Drug Solubility (mM)	S_{cc}/S_{drug}
KTZ-ADP	4.77	3.80	1.75	2.17	5	4.53	1.53	2.90
KTZ-FUM	4.10	5.75	3.57	1.61	5	22.2	1.53	14.2
KTZ-SUC	4.66	7.67	1.88	4.07	5	10.9	1.53	6.98
FaSSIF	Interface				Bulk			
	Interfacial pH	Cocrystal Solubility (mM)	Drug Solubility (mM)	S_{cc}/S_{drug}	Bulk pH	Cocrystal Solubility (mM)	Drug Solubility (mM)	S_{cc}/S_{drug}
KTZ-ADP	4.84	3.11	0.42	7.42	6.5	16.8	0.043	392
KTZ-FUM	4.14	4.66	2.14	2.17	6.5	110	0.043	2560
KTZ-SUC	4.73	4.36	0.52	8.28	6.5	34.2	0.043	798

3.5). Interfacial pH values of the KTZ cocrystals are lower than the bulk pH in the four biorelevant dissolution media due to the ionization of the coformer. Because of a lower pH at the interface, the ratio of the estimated cocrystal and drug solubility, or solubility advantage (SA), is lower at the interface than in the bulk dissolution media.

Contributions of Buffer to Interfacial Solubility Advantage

KTZ cocrystal pH_o values from Cao et al.[11] do not consider contributions from buffer species within the dissolution media. Biorelevant dissolution media contain buffer species that must be accounted for to solve for cocrystal pH_o in acetate buffer for Blank FeSSIF and FeSSIF, and for phosphate buffer for Blank FaSSIF and FaSSIF. Estimations reveal that an increase in the pH_o plateau is associated with increases in acetate and phosphate buffer concentrations (Figure

3.4). This increased plateau assomptotically approaches an upper limit where the buffer species cannot diffuse fast enough to react at the interface. The buffer species also plays a role in determining the plateau pH as acetate buffer has a higher plateau due to it being a smaller and therefore faster diffusing molecule than phosphate, which is more susceptable to diffusion rate limiting the reaction at the interface (Figure 3.4). This leads to phosphate having a lower ability to buffer the interfacial pH caused by the ionization of the coformer when the cocrystal dissolves at intestinal pH values.

Estimations of interfacial pH considering the appropriate bulk buffer and hydrogen ion concentrations for the biorelevant media were made. Table 3.6 contains these pH_o estimations and the interfacial solubilities calculated with them. All three cocrystals maintained a lower interfacial pH than bulk pH, however, the calculated interfacial solubility advantages for buffer

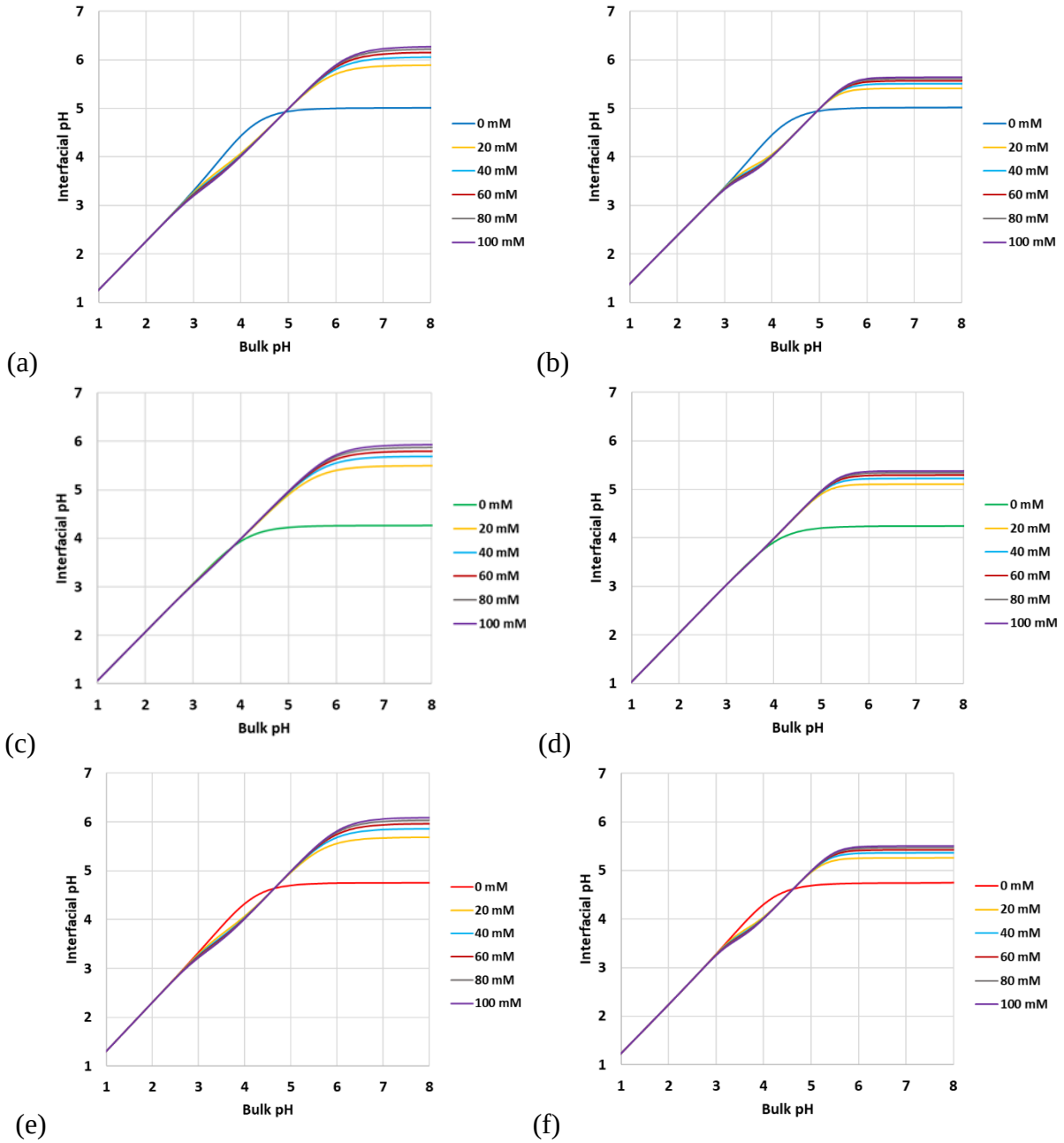

Figure 3.4: Interfacial pH estimations as a function of bulk pH for (a,b) KTZ-ADP (—), (c,d) KTZ-FUM (—), and (e,f) KTZ-SUC (—) varying total acetate (a,c,e) and phosphate (b,d,f) buffer concentrations 20 mM (—), 40 mM (—), 60 mM (—), 80 mM (—), and 100 mM (—).

were higher than the values estimated in the absence of buffer. This suggests that KTZ cocrystals may experience higher interfacial supersatuation when dissolving in a dissolution media that contains a buffering agent.

Table 3.6: Interfacial pH (buffered) and bulk pH values with calculated cocrystal and drug solubilities in biorelevant conditions.

Blank FeSSIF	Interface				Bulk			
	Interfacial pH	Cocrystal Solubility (mM)	Drug Solubility (mM)	S_{cc}/S_{drug}	Bulk pH	Cocrystal Solubility (mM)	Drug Solubility (mM)	S_{cc}/S_{drug}
KTZ-ADP	4.99	2.99	0.27	11.0	5	2.99	0.26	11.3
KTZ-FUM	4.96	8.80	0.29	30.2	5	9.16	0.26	34.5
KTZ-SUC	4.99	4.46	0.27	16.4	5	4.48	0.26	16.8
Blank FaSSIF	Interface				Bulk			
	Interfacial pH	Cocrystal Solubility (mM)	Drug Solubility (mM)	S_{cc}/S_{drug}	Bulk pH	Cocrystal Solubility (mM)	Drug Solubility (mM)	S_{cc}/S_{drug}
KTZ-ADP	5.36	3.30	0.12	27.9	6.5	10.7	0.014	759
KTZ-FUM	4.80	7.52	0.42	17.9	6.5	63.0	0.014	4470
KTZ-SUC	5.34	5.30	0.12	42.8	6.5	19.6	0.014	1390
FeSSIF	Interface				Bulk			
	Interfacial pH	Cocrystal Solubility (mM)	Drug Solubility (mM)	S_{cc}/S_{drug}	Bulk pH	Cocrystal Solubility (mM)	Drug Solubility (mM)	S_{cc}/S_{drug}
KTZ-ADP	4.99	4.48	1.57	2.86	5	4.53	1.53	2.90
KTZ-FUM	4.96	20.5	1.59	12.9	5	22.2	1.53	14.2
KTZ-SUC	4.99	10.8	1.57	6.86	5	10.9	1.53	6.98
FaSSIF	Interface				Bulk			
	Interfacial pH	Cocrystal Solubility (mM)	Drug Solubility (mM)	S_{cc}/S_{drug}	Bulk pH	Cocrystal Solubility (mM)	Drug Solubility (mM)	S_{cc}/S_{drug}
KTZ-ADP	5.36	3.68	0.15	25.0	6.5	18.6	0.043	435
KTZ-FUM	4.80	7.77	0.45	17.3	6.5	110	0.043	2560
KTZ-SUC	5.34	5.89	0.15	38.6	6.5	34.2	0.043	798

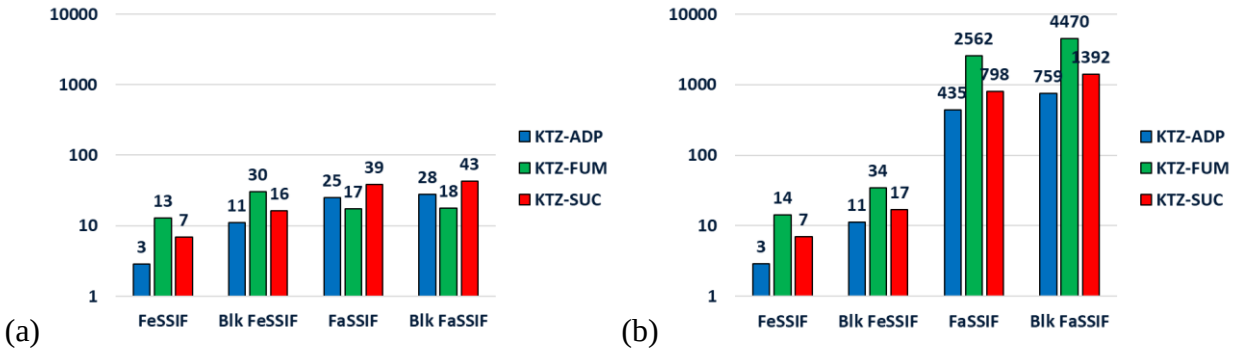

Figure 3.5: (a) Interfacial and (b) bulk solubility advantages calculated using buffered pH_o estimations and pH_b for KTZ-ADP (■), KTZ-FUM (■), and KTZ-SUC (■) in FeSSIF, blank FeSSIF, FaSSIF, and blank FaSSIF.

Bulk Solubility Advantage to Evaluate Precipitation Risk

A goal of this study was to assess the ability of the thermodynamic solubility equations derived for cocrystal and drug to correlate to kinetic parameters seen in cocrystal dissolution

experiments. In this capacity, AIDR, σ_{max}, and $AUC_{0\text{-}180min}$ were extracted from the concentration-time profiles in (Figure 3.3) for all three KTZ cocrystals and plotted in (Figure 3.6). Rank order for AIDR and $AUC_{0\text{-}180min}$ were similar for the four dissolution media with fastest dissolution rate to slowest: FeSSIF>Blank FeSSIF>FaSSIF>Blank FaSSIF. Maximum supersaturation values were lowest in FeSSIF and highest in FaSSIF.

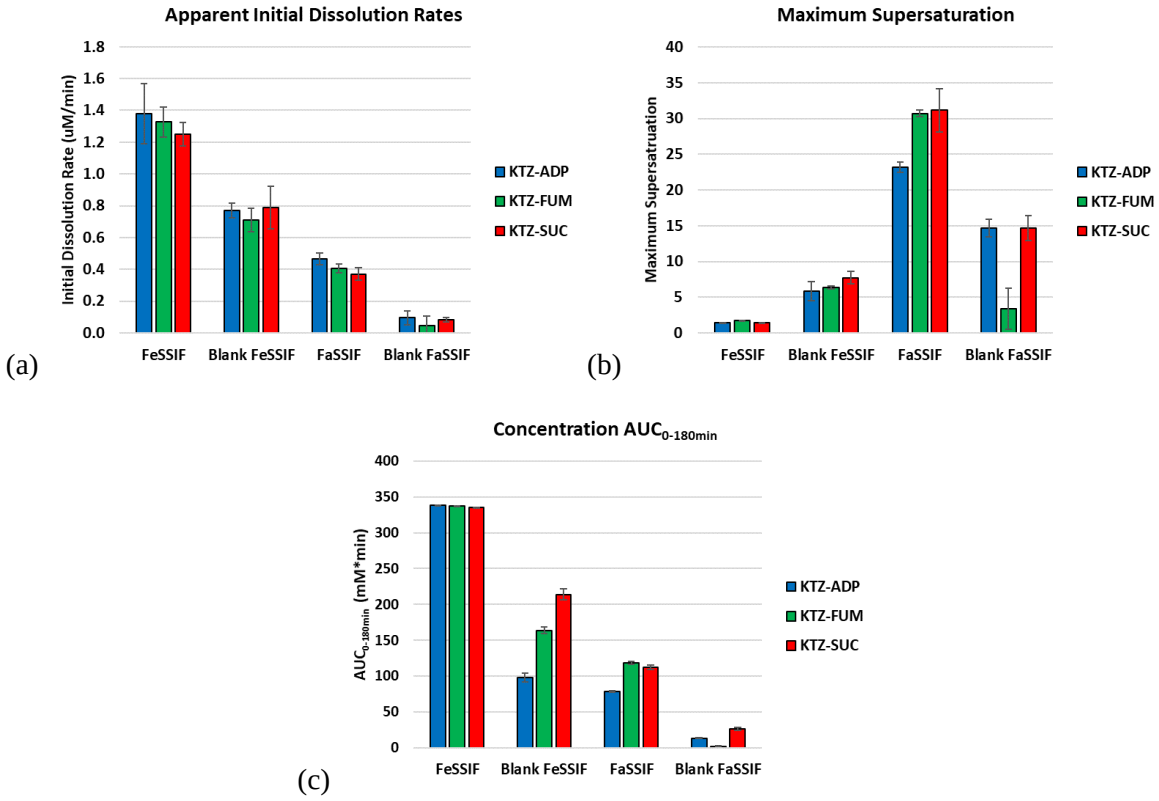

Figure 3.6: Values of experimental parameters (a) apparent initial dissolution rate (AIDR), (b) maximum supersaturation (σ_{max}), and (c) concentration area under the curve ($AUC_{0\text{-}180min}$) taken from KTZ-ADP (■), KTZ-FUM (■), and KTZ-SUC (■) cocrystal dissolution experiments in FeSSIF, blank FeSSIF, FaSSIF and blank FaSSIF.

Solubility advantage (SA) values for the biorelevant dissolution media serve as the highest possible supersaturation, assuming the system saturates with respect to cocrystal. Although not always obtainable in solution, this estimated value could serve as a quick assessment for the precipitation potential in the given media. Plotting the experimental parameters against SA values revealed trends among the biorelevant dissolution data. Exponentially decreasing AIDR and

$AUC_{0\text{-}180min}$ values were associated with increasing SA. As SA values exponentially increased, σ_{max} values increased 30-fold before decreasing.

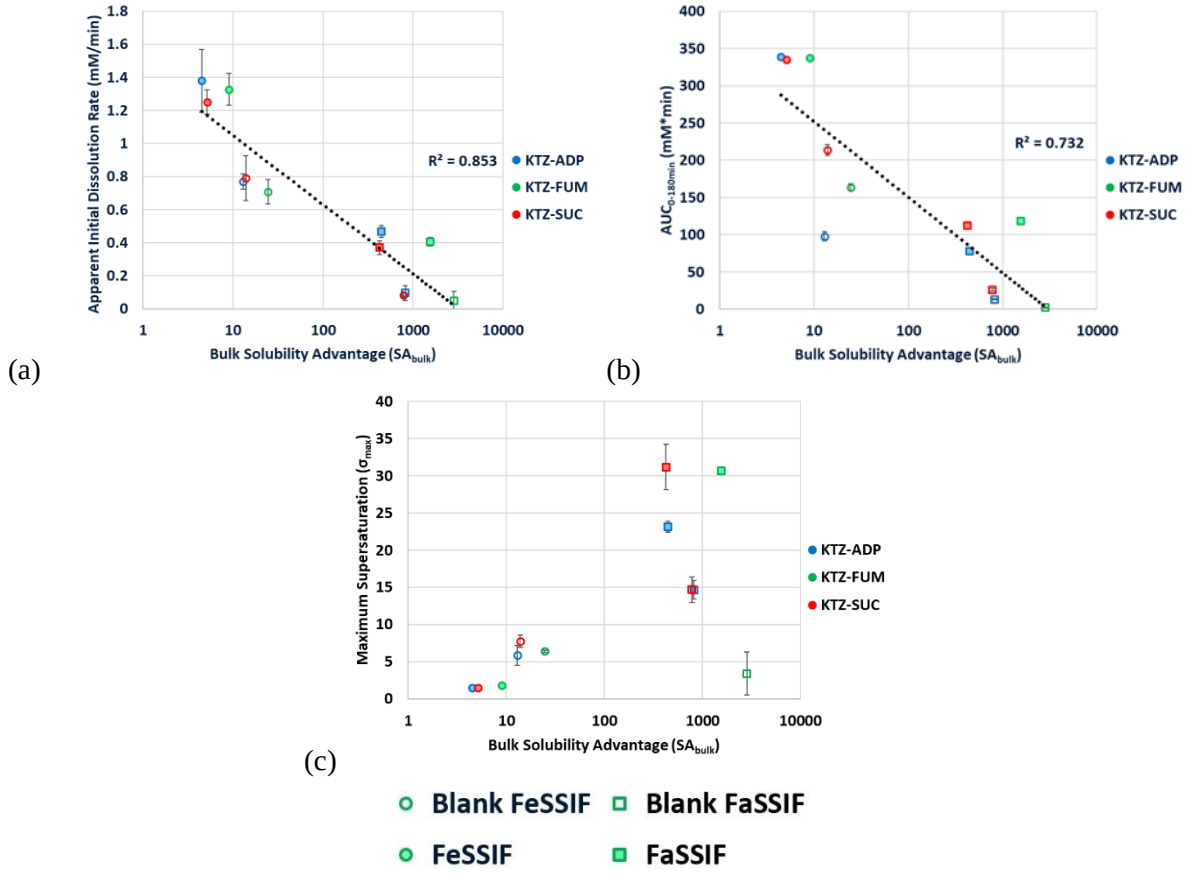

Figure 3.7: Plots comparing experimental parameters (a) apparent initial dissolution rate (AIDR), (b) concentration area under the curve ($AUC_{0\text{-}180min}$), and (c) maximum supersaturation (σ_{max}) to calculated bulk solubility advantage (SA_{bulk}) for KTZ-ADP (●), KTZ-FUM (●), and KTZ-SUC (●) in FeSSIF (●,●,●), blank FeSSIF (○,○,○), FaSSIF (■,■,■), and blank FaSSIF (□,□,□).

Dose Number to Evaluate Precipitation Risk

Solubility advantages assume excess solid is present in the system and saturation with respect to the cocrystal can be achieved. Oftentimes, experimental conditions do not contain sufficient solid phase to saturate the system, as is the case in the dissolution media from Chen. In this study, it is proposed that dose number (D_o) can be used in lieu of solubility advantage to calculate the theoretical limit of supersaturation that can be achieved in the system. Dose numbers

were calculated for the four dissolution media using equation (3.25) and can be found (Table 3.7). The three cocrystals were dosed in equimolar amounts leading to the same dose number for each cocrystal in a given dissolution media. Dose numbers calculated showed an increasing trend from FeSSIF being the lowest and blank FaSSIF the highest, and all dose numbers are lower than estimated SA_{bulk} values.

Table 3.7: Calculated dose numbers in cocrystal biorelevant dissolution experiments

Media	D_o
FeSSIF	1.25
Blank FeSSIF	9.31
FaSSIF	45.9
Blank FaSSIF	155

Assuming the dose number values theoretical limits of supersaturation a cocrystal could generate when the experimental conditions could not saturate with respect to cocrystal, the estimated dose numbers should have a stronger correlation with the experimental dissolution, supersaturation, and concentration $AUC_{0\text{-}180min}$. As seen in (Figure 3.8), the trends in the correlations with SA_{bulk} are the same with dose number, however, the correlations with D_o are much tighter.

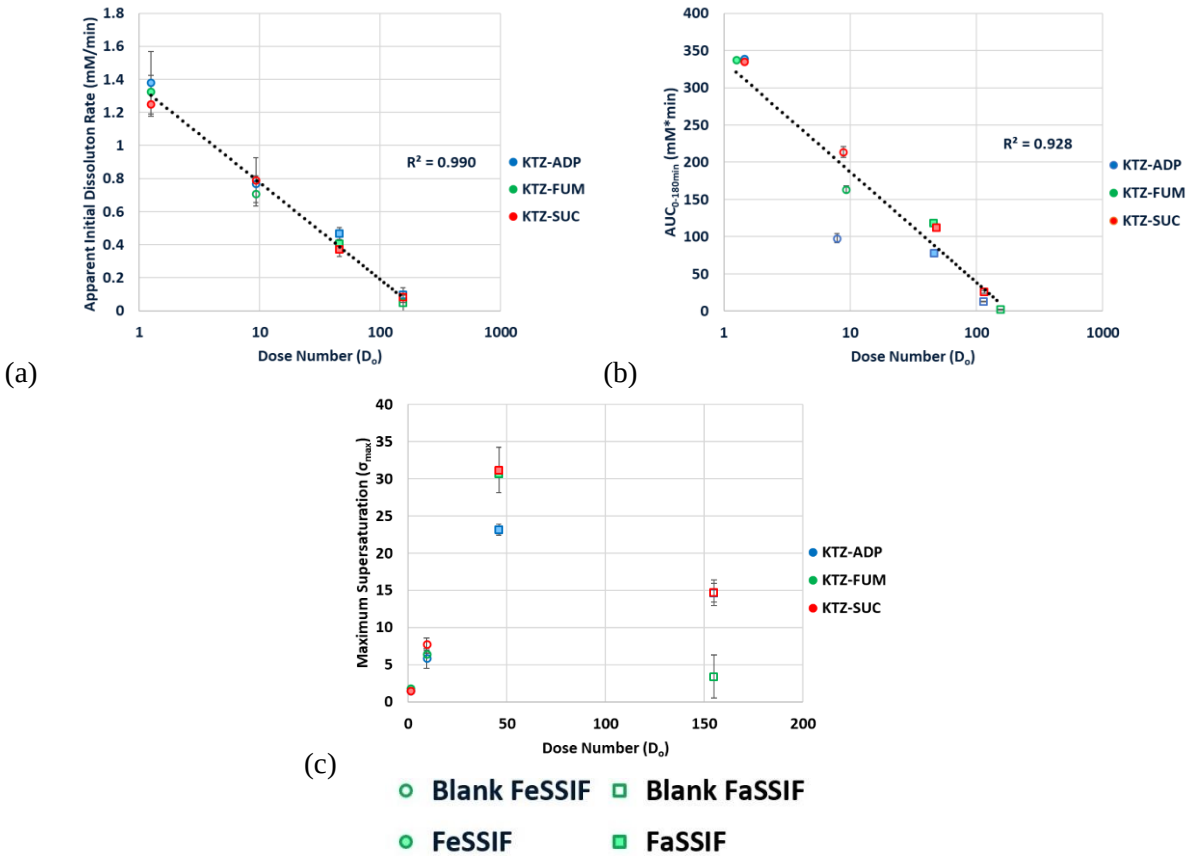

Figure 3.8: Plots comparing experimental parameters (a) apparent initial dissolution rate (AIDR), (b) concentration area under the curve ($AUC_{0\text{-}180min}$), and (c) maximum supersaturation (σ_{max}) to calculated dose number (D_o) for KTZ-ADP (●), KTZ-FUM (●), and KTZ-SUC (●) in FeSSIF (●,●,●), blank FeSSIF (○,○,○), FaSSIF (■,■,■), and blank FaSSIF (□,□,□).

Discussion

Cocrystals of weakly basic KTZ with its acidic coformers have an intrinsic behavior that is attractive to a pharmaceutical formulator. As Cao et al. had shown, dissolution of KTZ cocrystals at intestinal pH values leads to surface pH that is lower than the dissolution media because of coformer ionization (Figure 3.2). In other words, the coformer creates an environment at the interface that is consistent across the range of intestinal pH values. This could impart consistency in dissolution rates of the cocrystal across various pH values which could contribute to decreasing interpatient variability. More importantly, however, lowering the interfacial pH increases the drug solubility at the dissolving surface which could, in turn, create an environment

with lower supersaturation and less propensity for precipitation to occur (Table 3.5 and Figure 3.5). Acidic coformers can potentially impart an intrinsic ability to safeguard against interfacial precipitation when cocrystallized with basic drugs.

Part of this study aimed to investigate what might happen when cocrystals of weakly basic drugs dissolve in buffers of various concentrations and capacities. When dissolving at intestinal pH, estimates of cocrystal pH_o were shown to increase as buffer concentration was increased. The stable plateau region for each of the three cocrystals could increase by 1-2 pH units depending upon the buffer species and concentration (Figure 3.4). This could negatively affect dissolution as the cocrystals ability to decrease supersaturation is reduced leading to an increased risk of interfacial precipitation as buffer concentration increases (Tables 3.5 and 3.6).

The ability to estimate supersaturation at the interface and in bulk solution could identify risk areas where conditions may be most unfavorable for cocrystal dissolution and potential to sustain drug supersaturation. Estimates of cocrystal solubility advantage were able to correlate with previously obtained experimental results. Exponential decreases in apparent cocrystal initial dissolution rates and concentration $AUC_{0\text{-}180min}$ associating with increases in SA_{bulk} shows the merit of using thermodynamic solubility equations to estimate potential precipitation in a given system (Figure 3.7).

While SA_{bulk} gives a ceiling for the limit of achievable supersaturation and was able to correlate well with biorelevant dissolution data, this value cannot always be reached in the bulk dissolution media depending on the amount of solid present. D_o was observed to surpass the correlations SA_{bulk} had achieved (Figure 3.8) which suggests that it is a better value to assess the potential precipitation risks when the system is undersaturated with respect to cocrystal.

Conclusions

Thermodynamic solubility expressions for cocrystals and drug have promise to be powerful tools for pharmaceutical cocrystal development by using them to estimate potential cocrystal solution behavior over a wide range of experimental conditions. Calculating the interfacial and bulk supersaturations gives insight into the potential for precipitation to help avoid risky dissolution conditions. This study has shown the ability of cocrystals of weakly basic drugs with acidic coformers to reduce supersaturation at the interface of the dissolving solid. This knowledge could be used to help guide the rational selection of coformers to optimize cocrystal dissolution performance. However, it is also important to understand the role of buffer in determining pH_o as the theory put forth in this study suggests that the benefits of acidic coformers for weakly basic drugs could be inhibited significantly by the buffer species and concentration. Moreover, these cocrystal solubility expressions show the promise to estimate the supersaturation in the bulk dissolution media. Solubility advantages and dose numbers in this study were able to correlate with the overall dissolution performance of the three KTZ cocrystals suggesting that these values can be used as a guide to avoid regions of precipitation in the development of a cocrystal product.

Acknowledgements

The authors acknowledge the financial support from the University of Michigan College of Pharmacy.

References

1. Amidon, G.L., et al., *A Theoretical Basis for a Biopharmaceutic Drug Classification - the Correlation of in-Vitro Drug Product Dissolution and in-Vivo Bioavailability.* Pharmaceutical Research, 1995. **12**(3): p. 413-420.
2. Bak, A., et al., *The co-crystal approach to improve the exposure of a water-insoluble compound: AMG 517 sorbic acid co-crystal characterization and pharmacokinetics.* Journal of Pharmaceutical Sciences, 2008. **97**(9): p. 3942-3956.
3. Smith, A.J., et al., *Cocrystals of Quercetin with Improved Solubility and Oral Bioavailability.* Molecular Pharmaceutics, 2011. **8**(5): p. 1867-1876.
4. Cheney, M.L., et al., *Coformer Selection in Pharmaceutical Cocrystal Development: a Case Study of a Meloxicam Aspirin Cocrystal That Exhibits Enhanced Solubility and Pharmacokinetics.* Journal of Pharmaceutical Sciences, 2011. **100**(6): p. 2172-2181.
5. Childs, S.L., P. Kandi, and S.R. Lingireddy, *Formulation of a Danazol Cocrystal with Controlled Supersaturation Plays an Essential Role in Improving Bioavailability.* Molecular Pharmaceutics, 2013. **10**(8): p. 3112-3127.
6. Zheng, W.J., et al., *Selection of oral bioavailability enhancing formulations during drug discovery.* Drug Development and Industrial Pharmacy, 2012. **38**(2): p. 235-247.
7. Stanton, M.K., et al., *Improved Pharmacokinetics of AMG 517 Through Co-crystallization Part 2: Analysis of 12 Carboxylic Acid Co-crystals.* Journal of Pharmaceutical Sciences, 2011. **100**(7): p. 2734-2743.
8. Weyna, D.R., et al., *Improving Solubility and Pharmacokinetics of Meloxicam via Multiple-Component Crystal Formation.* Molecular Pharmaceutics, 2012. **9**(7): p. 2094-2102.
9. Martin, F.A., et al., *Ketoconazole Salt and Co-crystals with Enhanced Aqueous Solubility.* Crystal Growth & Design, 2013. **13**(10): p. 4295-4304.
10. Chen, Y.M. and N. Rodríguez-Hornedo, *Cocrystals Mitigate Negative Effects of High pH on Solubility and Dissolution of a Basic Drug.* Crystal Growth & Design, 2018. **18**(3): p. 1358-1366.
11. Cao, F.J., N. Rodriguez-Hornedo, and G.E. Amidon, *Mechanistic Analysis of Cocrystal Dissolution, Surface pH, and Dissolution Advantage as a Guide for Rational Selection.* Journal of Pharmaceutical Sciences, 2019. **108**(1): p. 243-251.
12. Mooney, K.G., et al., *Dissolution kinetics of carboxylic acids I: effect of pH under unbuffered conditions.* J Pharm Sci, 1981. **70**(1): p. 13-22.
13. Cao, F.J., et al., *Mechanistic Analysis of Cocrystal Dissolution as a Function of pH and Micellar Solubilization.* Molecular Pharmaceutics, 2016. **13**(3): p. 1030-1046.

14. Huang, N. and N. Rodriguez-Hornedo, *Engineering Cocrystal Solubility, Stability, and pH(max) by Micellar Solubilization.* Journal of Pharmaceutical Sciences, 2011. **100**(12): p. 5219-5234.

15. Chen, Y.M. and University of Michigan. Pharmaceutical Sciences., *Cocrystals Mitigate the Effect of pH on Solubility and Dissolution of Basic Drugs*. 2017, ProQuest Dissertations & Theses: Ann Arbor. p. 216 p.

16. Galia, E., et al., *Evaluation of Various Dissolution Media for Predicting In Vivo Performance of Class I and II Drugs.* Pharmaceutical Research, 1998. **15**(5): p. 698-705.

17. Kostewicz, E.S., et al., *Forecasting the Oral Absorption Behavior of Poorly Soluble Weak Bases Using Solubility and Dissolution Studies in Biorelevant Media.* Pharmaceutical Research, 2002. **19**(3): p. 345-349.

Appendix 3A

Dissolution of cocrystal with dibasic drug and diprotic coformer under buffered condition (monoprotic buffer such as acetate)

The reactions occurring while cocrystal dissolves in phosphate buffer are listed as follows:

$H_3O^+ + OH^- \rightleftarrows 2\,H_2O$		$K_w = [H_3O^+][OH^-]$
$(BH_2A)_{solid} \rightleftarrows B + H_2A$	k_f^{sp}, k_r^{sp}	$K_{sp} = [B][H_2A] = \frac{k_f^{sp}}{k_r^{sp}}$
$H_2O + BH_2^{2+} \rightleftarrows H_3O^+ + BH^+$	k_{a1f}^{B}, k_{a1r}^{B}	$K_{a1}^{B} = \frac{[H_3O^+][BH^+]}{[BH_2^{2+}]} = \frac{k_{a1f}^{B}}{k_{a1r}^{B}}$
$H_2O + BH^+ \rightleftarrows H_3O^+ + B$	k_{a2f}^{B}, k_{a2r}^{B}	$K_{a2}^{B} = \frac{[H_3O^+][B]}{[BH^+]} = \frac{k_{a2f}^{B}}{k_{a2r}^{B}}$
$H_2O + H_2A \rightleftarrows H_3O^+ + HA^-$	$k_{a1f}^{H_2A}, k_{a1r}^{H_2A}$	$K_{a1}^{H_2A} = \frac{[HA^-][H_3O^+]}{[H_2A]} = \frac{k_{a1f}^{H_2A}}{k_{a1r}^{H_2A}}$
$H_2O + HA^- \rightleftarrows H_3O^+ + A^{2-}$	$k_{a2f}^{H_2A}, k_{a2r}^{H_2A}$	$K_{a2}^{H_2A} = \frac{[H_3O^+][A^{2-}]}{[HA^-]} = \frac{k_{a2f}^{H_2A}}{k_{a2r}^{H_2A}}$
$OH^- + BH_2^{2+} \rightleftarrows H_2O + BH^+$	k_{1f}, k_{1r}	$K_1 = \frac{[BH^+]}{[BH_2^{2+}][OH^-]} = \frac{k_{1f}}{k_{1r}}$
$OH^- + BH^+ \rightleftarrows H_2O + B$	k_{2f}, k_{2r}	$K_2 = \frac{[B]}{[BH^+][OH^-]} = \frac{k_{2f}}{k_{2r}}$
$OH^- + H_2A \rightleftarrows H_2O + HA^-$	k_{3f}, k_{3r}	$K_3 = \frac{[HA^-]}{[H_2A][OH^-]} = \frac{k_{3f}}{k_{3r}}$
$OH^- + HA^- \rightleftarrows H_2O + A^{2-}$	k_{4f}, k_{4r}	$K_4 = \frac{[A^{2-}]}{[HA][OH^-]} = \frac{k_{4f}}{k_{4r}}$
$CH_3COOH + H_2O \rightleftarrows CH_3COO^- + H_3O^+$	k_{1f}^{b}, k_{1r}^{b}	$K_{a1} = \frac{[CH_3COO^-][H_3O^+]}{[CH_3COOH]} = \frac{k_{1f}^{b}}{k_{1r}^{b}}$

The hydration and dehydration reactions are in equilibrium in bulk but not at the solid-liquid interface. The Fick's second law of diffusion for transport with reaction, for component i is given by:

$$\frac{\partial C_i}{\partial t} + v\Delta C_i = D_i \Delta^2 C_i + \phi_i \qquad \text{(A3.1)}$$

where v is velocity field, D_i is the diffusion coefficient of i component, ϕ_i is the reaction term, and C_i is the concentration of i component. Simplifying it using the film model approach of Mooney et al.,[1] the differential equations defining the transport of different species at steady state, are defined as follows;

$$\frac{\partial[BH_2^{2+}]}{\partial t} = D_{BH_2^{2+}} \frac{\partial^2[BH_2^{2+}]}{\partial^2 x} + \phi_1 = 0 \qquad \text{(A3.2)}$$

$$\frac{\partial[BH^+]}{\partial t} = D_{BH^+} \frac{\partial^2[BH^+]}{\partial^2 x} + \phi_2 = 0 \qquad \text{(A3.3)}$$

$$\frac{\partial[B]}{\partial t} = D_B \frac{\partial^2[B]}{\partial^2 x} + \phi_3 = 0 \qquad \text{(A3.4)}$$

$$\frac{\partial[OH^-]}{\partial t} = D_{OH^-} \frac{\partial^2[OH^-]}{\partial^2 x} + \phi_4 = 0 \qquad \text{(A3.5)}$$

$$\frac{\partial[H_3O^+]}{\partial t} = D_{H_3O^+} \frac{\partial^2[H_3O^+]}{\partial^2 x} + \phi_5 = 0 \qquad \text{(A3.6)}$$

$$\frac{\partial[CH_3COO^-]}{\partial t} = D_{CH_3COO^-} \frac{\partial^2[CH_3COO^-]}{\partial^2 x} + \phi_6 = 0 \qquad \text{(A3.7)}$$

$$\frac{\partial[CH_3COOH]}{\partial t} = D_{CH_3COOH} \frac{\partial^2[CH_3COOH]}{\partial^2 x} + \phi_7 = 0 \qquad \text{(A3.8)}$$

$$\frac{\partial[H_2A]}{\partial t} = D_{H_2A} \frac{\partial^2[H_2A]}{\partial^2 x} + \phi_8 = 0 \qquad \text{(A3.9)}$$

$$\frac{\partial[HA^-]}{\partial t} = D_{HA^-} \frac{\partial^2[HA^-]}{\partial^2 x} + \phi_9 = 0 \qquad \text{(A3.10)}$$

$$\frac{\partial[A^{2-}]}{\partial t} = D_{A^{2-}} \frac{\partial^2[A^{2-}]}{\partial^2 x} + \phi_{10} = 0 \qquad (A3.11)$$

Defining ϕ_{1-11} for the differential equations:

$$\phi_1 = -k^{B}_{a1f}[BH_2^{2+}] + k^{B}_{a1r}[BH^+][H_3O^+] - k_{1f}[OH^-][BH_2^{2+}] + k_{1r}[BH^+]$$

$$\phi_2 = k^{B}_{a1f}[BH_2^{2+}] - k^{B}_{a1r}[BH^+][H_3O^+] - k^{B}_{a2f}[BH^+] + k^{B}_{a2r}[B][H_3O^+]$$
$$+ k_{1f}[OH^-][BH_2^{2+}] - k_{1r}[BH^+] - k_{2f}[BH^+][OH^-] + k_{2r}[B]$$

$$\phi_3 = k^{B}_{a2f}[BH^+] - k^{B}_{a2r}[B][H_3O^+] + k_{2f}[BH^+][OH^-] - k_{2r}[B] + k^{sp}_{f}[BH_2A]$$
$$- k^{sp}_{r}[B][H_2A]$$

$$\phi_4 = -k_{1f}[OH^-][BH_2^{2+}] + k_{1r}[BH^+] - k_{2f}[BH^+][OH^-] + k_{2r}[B] - k_{3f}[OH^-][H_2A]$$
$$+ k_{3r}[HA^-] - k_{4f}[OH^-][HA^-] + k_{4r}[A^{2-}]$$

$$\phi_5 = k^{B}_{a1f}[BH_2^{2+}] - k^{B}_{a1r}[BH^+][H_3O^+] + k^{B}_{a2f}[BH^+] - k^{B}_{a2r}[B][H_3O^+] + k^{H_2A}_{a1f}[H_2A]$$
$$- k^{H_2A}_{a1r}[HA^-][H_3O^+] + k^{H_2A}_{a2f}[HA^-] - k^{H_2A}_{a2r}[A^{2-}][H_3O^+]$$
$$+ k^{b}_{1f}[CH_3COOH] - k^{b}_{1r}[CH_3COO^-][H_3O^+]$$

$$\phi_6 = k^{b}_{1f}[CH_3COOH] - k^{b}_{1r}[CH_3COO^-][H_3O^+]$$

$$\phi_7 = -k^{b}_{1f}[CH_3COOH] + k^{b}_{1r}[CH_3COO^-][H_3O^+]$$

$$\phi_8 = k^{sp}_{f}[BH_2A] - k^{sp}_{r}[B][H_2A] - k^{H_2A}_{a1f}[H_2A] + k^{H_2A}_{a1r}[HA^-][H_3O^+] - k_{3f}[OH^-][H_2A]$$
$$+ k_{3r}[HA^-]$$

$$\phi_9 = k^{H_2A}_{a1f}[H_2A] - k^{H_2A}_{a1r}[HA^-][H_3O^+] - k^{H_2A}_{a2f}[HA^-] + k^{H_2A}_{a2r}[A^{2-}][H_3PO_4]$$
$$+ k_{3f}[OH^-][H_2A] - k_{3r}[HA^-] - k_{4f}[OH^-][HA^-] + k_{4r}[A^{2-}]$$

$$\phi_{10} = k^{H_2A}_{a2f}[HA^-] - k^{H_2A}_{a2r}[A^{2-}][H_3O^+] + k_{4f}[OH^-][HA^-] - k_{4r}[A^{2-}]$$

The boundary conditions for the differential equations are defined as:

$@x = 0$

$[BH_2^{2+}] = [BH_2^{2+}]_0$ Unknown

$[BH^+] = [BH^+]_0$ Unknown

$[B] = [B]_0$ Known

$[H_2A] = [H_2A]_0$ Known

$[HA^-] = [HA^-]_0$ Unknown

$[A^{2-}] = [A^{2-}]_0$ Unknown

$[OH^-] = [OH^-]_0$ Unknown

$[H_3O^+] = [H_3O^+]_0$ Unknown

$[CH_3COO^-] = [CH_3COO^-]_0$ Unknown

$[CH_3COOH] = [CH_3COOH]_0$ Unknown

@x = h

$[BH_2^{2+}] = [BH_2^{2+}]_h = 0$ Known

$[BH^+] = [BH^+]_h = 0$ Known

$[B] = [B]_h = 0$ Known

$[H_2A] = [H_2A]_h = 0$ Known

$[HA^-] = [HA^-]_h = 0$ Known

$[A^{2-}] = [A^{2-}]_h = 0$ Known

$[OH^-] = [OH^-]_h$ Given

$[H_3O^+] = [H_3O^+]_h$ Given

$[CH_3COO^-] = [CH_3COO^-]_h$ Given

$[CH_3COOH] = [CH_3COOH]_h$ Given

Mass and proton balance considerations give the following relationships between ϕ_i terms:

I $: \phi_1 + \phi_2 + \phi_3 = k_f^{sp}[BH_2A] - k_r^{sp}[B][H_2A]$

II $: \phi_8 + \phi_9 + \phi_{10} = k_f^{sp}[BH_2A] - k_r^{sp}[B][H_2A]$

III $: \phi_6 + \phi_7 = 0$

IV $: \phi_1 + \phi_5 + \phi_8 = \phi_4 + \phi_6 + \phi_{10} + \phi_3$

adding up equations A3.2, A3.3 and A3.4:

$$D_{BH_2^{2+}} \frac{\partial^2[BH_2^{2+}]}{\partial^2 x} + D_{BH^+} \frac{\partial^2[BH^+]}{\partial^2 x} + D_B \frac{\partial^2[B]}{\partial^2 x} = k_f^{sp}[BH_2A] - k_r^{sp}[B][H_2A] \quad (A3.12)$$

adding up equations A3.9, A3.10 and A3.11:

$$D_{H_2A} \frac{\partial^2[H_2A]}{\partial^2 x} + D_{HA^-} \frac{\partial^2[HA^-]}{\partial^2 x} + D_{A^{2-}} \frac{\partial^2[A^{2-}]}{\partial^2 x} = k_f^{sp}[BH_2A] - k_r^{sp}[B][H_2A] \quad (A3.13)$$

adding up equations A3.7, A3.8:

$$D_{CH_3COOH} \frac{\partial^2[CH_3COOH]}{\partial^2 x} + D_{CH_3COO^-} \frac{\partial^2[CH_3COO^-]}{\partial^2 x} = 0 \quad (A3.14)$$

adding up equations A3.2, A3.6, A3.9 and subtracting from summation of (A3.5, A3.7, A3.11, and A3.4) gives:

$$\begin{aligned} &D_{BH_2^{2+}} \frac{\partial^2[BH_2^{2+}]}{\partial^2 x} + D_{H_3O^+} \frac{\partial^2[H_3O^+]}{\partial^2 x} + D_{CH_3COOH} \frac{\partial^2[CH_3COOH]}{\partial^2 x} + D_{H_2A} \frac{\partial^2[H_2A]}{\partial^2 x} \\ &\quad - D_{OH^-} \frac{\partial^2[OH^-]}{\partial^2 x} - D_{CH_3COO^-} \frac{\partial^2[CH_3COO^-]}{\partial^2 x} - D_{A^{2-}} \frac{\partial^2[A^{2-}]}{\partial^2 x} - D_B \frac{\partial^2[B]}{\partial^2 x} \\ &\quad = 0 \end{aligned} \quad (A3.15)$$

simplifying equations A3.12 and A3.13 gives:

$$\begin{aligned} &D_{BH_2^{2+}} \frac{\partial^2[BH_2^{2+}]}{\partial^2 x} + D_{BH^+} \frac{\partial^2[BH^+]}{\partial^2 x} + D_B \frac{\partial^2[B]}{\partial^2 x} \\ &\quad = D_{H_2A} \frac{\partial^2[H_2A]}{\partial^2 x} + D_{HA^-} \frac{\partial^2[HA^-]}{\partial^2 x} + D_{A^{2-}} \frac{\partial^2[A^{2-}]}{\partial^2 x} \end{aligned} \quad (A3.16)$$

integrating equations A3.14, A3.15, and A3.16 respect to the x:

$$D_{CH_3COOH}\frac{\partial\,[CH_3COOH]}{\partial\,x}+D_{CH_3COO^-}\frac{\partial\,[CH_3COO^-]}{\partial\,x}=C_1 \quad (A3.17)$$

$$D_{BH_2^{2+}}\frac{\partial\,[BH_2^{2+}]}{\partial\,x}+D_{H_3O^+}\frac{\partial\,[H_3O^+]}{\partial\,x}+D_{CH_3COOH}\frac{\partial\,[CH_3COOH]}{\partial\,x}+D_{H_2A}\frac{\partial\,[H_2A]}{\partial\,x}-D_{OH^-}\frac{\partial\,[OH^-]}{\partial\,x}-$$

$$D_{CH_3COO^-}\frac{\partial\,[CH_3COO^-]}{\partial\,x}-D_{A^{2-}}\frac{\partial\,[A^{2-}]}{\partial\,x}-D_B\frac{\partial\,[B]}{\partial\,x}=$$

$$C_2 \quad (A3.18)$$

$$D_{BH_2^{2+}}\frac{\partial\,[BH_2^{2+}]}{\partial\,x}+D_{BH^+}\frac{\partial\,[BH^+]}{\partial\,x}+D_B\frac{\partial\,[B]}{\partial\,x}-D_{H_2A}\frac{\partial\,[H_2A]}{\partial\,x}-D_{HA^-}\frac{\partial\,[HA^-]}{\partial\,x}-D_{A^{2-}}\frac{\partial\,[A^{2-}]}{\partial\,x}=$$

$$C_3 \quad (A3.19)$$

The summation of the flux of the buffer species within the boundary layer is zero:

$$\sum(J_{CH_3COO^-}+J_{CH_3COOH})=0 \quad (A3.20)$$

Therefore,

$$C_1=0$$

The summation of the flux of the species reacting as an acid is equal to the summation of the flux of the species which react as base:

$$\sum(J_{BH_2^{2+}}+J_{H_3O^+}+J_{H_2A}+J_{CH_3COOH})$$

$$=\sum(J_{OH^-}+J_{CH_3COO^-}+J_{A^{2-}}+J_B) \quad (A3.21)$$

Therefore,

$$C_2=0$$

integrating the equations A3.17 through A3.19 with respect to x:

$$D_{CH_3COOH}[CH_3COOH]+D_{CH_3COO^-}[CH_3COO^-]=T_1 \quad (A3.22)$$

$$D_{BH_2^{2+}}[BH_2^{2+}]+D_{H_3O^+}[H_3O^+]+D_{CH_3COOH}[CH_3COOH]+D_{H_2A}[H_2A]-D_{OH^-}[OH^-]-$$

$$D_{CH_3COO^-}[CH_3COO^-]-D_{A^{2-}}[A^{2-}]-D_B[B]=$$

$$T_2 \quad (A3.23)$$

$$D_{BH_2^{2+}}[BH_2^{2+}] + D_{BH^+}[BH^+] + D_B[B] - D_{H_2A}[H_2A] - D_{HA^-}[HA^-] - D_{A^{2-}}[A^{2-}] = C_3x +$$

$$T_3 \qquad \text{(A3.24)}$$

Applying the boundary condition @ $x = 0$:

$$D_{CH_3COOH}[CH_3COOH]_0 + D_{CH_3COO^-}[CH_3COO^-]_0$$

$$= T_1 \qquad \text{(A3.25)}$$

$$D_{BH_2^{2+}}[BH_2^{2+}]_0 + D_{H_3O^+}[H_3O^+]_0 + D_{CH_3COOH}[CH_3COOH]_0 + D_{H_2A}[H_2A]_0 - D_{OH^-}[OH^-]_0 -$$

$$D_{CH_3COO^-}[CH_3COO^-]_0 - D_{A^{2-}}[A^{2-}]_0 - D_B[B]_0 =$$

$$T_2 \qquad \text{(A3.26)}$$

$$D_{BH_2^{2+}}[BH_2^{2+}]_0 + D_{BH^+}[BH^+]_0 + D_B[B]_0 - D_{H_2A}[H_2A]_0 - D_{HA^-}[HA^-]_0 - D_{A^{2-}}[A^{2-}]_0 =$$

$$T_3 \qquad \text{(A3.27)}$$

Applying the boundary condition @ $x = h$, with h being the boundary layer thickness:

$$D_{CH_3COOH}[CH_3COOH]_h + D_{CH_3COO^-}[CH_3COO^-]_h$$

$$= T_1 \qquad \text{(A3.28)}$$

$$D_{BH_2^{2+}}[BH_2^{2+}]_h + D_{H_3O^+}[H_3O^+]_h + D_{CH_3COOH}[CH_3COOH]_h + D_{H_2A}[H_2A]_h - D_{OH^-}[OH^-]_h -$$

$$D_{CH_3COO^-}[CH_3COO^-]_h - D_{A^{2-}}[A^{2-}]_h - D_B[B]_h =$$

$$T_2 \qquad \text{(A3.29)}$$

$$D_{BH_2^{2+}}[BH_2^{2+}]_h + D_{BH^+}[BH^+]_h + D_B[B]_h - D_{H_2A}[H_2A]_h - D_{HA^-}[HA^-]_h - D_{A^{2-}}[A^{2-}]_h =$$

$$C_3h +$$

$$T_3 \qquad \text{(A3.30)}$$

Under the sink condition, $C_3h + T_3 = 0$ therefore,

$$C_3 = -\frac{T_3}{h} = -\frac{1}{h} \times \left[D_{BH_2^{2+}}[BH_2^{2+}]_0 + D_{BH^+}[BH^+]_0 + D_B[B]_0 - D_{H_2A}[H_2A]_0 - D_{HA^-}[HA^-]_0 - D_{A^{2-}}[A^{2-}]_0\right]$$

subtracting equations A3.25 and A3.28 results in:

$$D_{CH_3COO^-}([CH_3COO^-]_0 - [CH_3COO^-]_h) + D_{CH_3COOH}([CH_3COOH]_0 - [CH_3COOH]_h) = 0 \quad (A3.31)$$

subtracting equations A3.26 and A3.29 results in:

$$D_{BH_2^{2+}}[BH_2^{2+}]_0 + D_{H_3O^+}([H_3O^+]_0 - [H_3O^+]_h) + D_{CH_3COOH}([CH_3COOH]_0 - [CH_3COOH]_h) + D_{H_2A}[H_2A]_0 - D_{OH^-}([OH^-]_0 - [OH^-]_h) - D_{CH_3COO^-}([CH_3COO^-]_0 - [CH_3COO^-]_h) - D_{A^{2-}}[A^{2-}]_0 - D_B[B]_0 = 0 \quad (A3.32)$$

Using the equilibrium relationships for ionization reactions such as:

$$K_{a1} = \frac{[CH_3COO^-][H_3O^+]}{[CH_3COOH]} \implies [CH_3COO^-] = \frac{K_{a1}[CH_3COOH]}{[H_3O^+]}$$

substituting the equilibrium relationships into equation A3.31:

$$D_{CH_3COO^-}\left(\frac{K_{a1}[CH_3COOH]_0}{[H_3O^+]_0} - [CH_3COO^-]_h\right) + D_{CH_3COOH}([CH_3COOH]_0 - [CH_3COOH]_h) = 0 \quad (A3.33)$$

solving for $[CH_3COOH]_0$ gives:

$$[CH_3COOH]_0 = \frac{D_{CH_3COO^-}[CH_3COO^-]_h + D_{CH_3COOH}[CH_3COOH]_h}{\frac{K_{a1}D_{CH_3COO^-}}{[H_3O^+]_0} + D_{CH_3COOH}} \quad (A3.34)$$

simplifying equation A3.34:

$$[CH_3COOH]_0$$

$$= \frac{A}{\frac{B}{[H_3O^+]_0} + E} \qquad (A3.35)$$

Where the constants are defined as:

$$A = D_{CH_3COO^-}[CH_3COO^-]_h + D_{CH_3COOH}[CH_3COOH]_h$$

$$B = K_{a1}D_{CH_3COO^-}$$

$$E = D_{CH_3COOH}$$

simplifying the equilibrium relationships gives:

$$K_{a1}^{B} = \frac{[H_3O^+][BH^+]}{[BH_2^{2+}]} \implies [BH_2^{2+}] = \frac{[H_3O^+][BH^+]}{K_{a1}^{B}} \implies [BH_2^{2+}] = \frac{[H_3O^+]^2[B]}{K_{a1}^{B}K_{a2}^{B}}$$

$$K_{a2}^{B} = \frac{[H_3O^+][B]}{[BH^+]} \implies [BH^+] = \frac{[H_3O^+][B]}{K_{a2}^{B}}$$

$$K_{a1}^{H_2A} = \frac{[HA^-][H_3O^+]}{[H_2A]} \implies [HA^-] = \frac{K_{a1}^{H_2A}[H_2A]}{[H_3O^+]}$$

$$K_{a2}^{H_2A} = \frac{[H_3O^+][A^{2-}]}{[HA^-]} \implies [A^{2-}] = \frac{K_{a2}^{H_2A}[HA^-]}{[H_3O^+]} \implies [A^{2-}] = \frac{K_{a2}^{H_2A}\,K_{a1}^{H_2A}[H_2A]}{[H_3O^+]^2}$$

Substituting the above equilibrium relationship into A3.32 results in:

$$D_{BH_2^{2+}}\frac{[H_3O^+]_0{}^2[B]_0}{K_{a1}^{B}K_{a2}^{B}} + D_{H_3O^+}([H_3O^+]_0 - [H_3O^+]_h) + D_{CH_3COOH}\left(\frac{[CH_3COO^-]_0[H_3O^+]_0}{K_{a1}}\right.$$

$$\left. - [CH_3COOH]_h\right) + D_{H_2A}[H_2A]_0 - D_{OH^-}\left(\frac{K_w}{[H_3O^+]_0} - [OH^-]_h\right)$$

$$- D_{CH_3COO^-}([CH_3COO^-]_0 - [CH_3COO^-]_h) - D_{A^{2-}}\frac{K_{a2}^{H_2A}\,K_{a1}^{H_2A}[H_2A]_0}{[H_3O^+]_0{}^2} - D_B[B]_0$$

$$= 0 \qquad (A3.35)$$

$$
-\frac{D_{OH^-}K_w}{[H_3O^+]_0} + D_{H_3O^+}[H_3O^+]_0 + \left(\frac{D_{CH_3COOH}[H_3O^+]_0}{K_{a1}} - D_{CH_3COO^-}\right)\left(\frac{A[H_3O^+]_0}{B + E[H_3O^+]_0}\right)
$$

$$
- D_{CH_3COOH}[CH_3COOH]_h + D_{CH_3COO^-}[CH_3COO^-]_h - D_{H_3O^+}[H_3O^+]_h + D_{OH^-}[OH^-]_h
$$

$$
+ \left(D_{H_2A}\left(\frac{D_B}{D_{H_2A}}\right)^{\frac{2}{3}} - \frac{D_{A^{2-}} K_{a2}^{H_2A} K_{a1}^{H_2A}\left(\frac{D_B}{D_{H_2A}}\right)^{\frac{2}{3}}}{[H_3O^+]_0{}^2} - D_B + \frac{D_{BH_2^{2+}}[H_3O^+]_0{}^2}{K_{a1}^B K_{a2}^B} \right)[B]_0
$$

$$
= 0 \qquad \text{(A3.36)}
$$

Where we have:

$$
[B]_0 = \frac{\sqrt{K_{sp}\left(1 + \frac{K_{a1}^{H_2A}}{[H_3O^+]} + \frac{K_{a1}^{H_2A}K_{a2}^{H_2A}}{[H_3O^+]^2}\right)\left(1 + \frac{[H_3O^+]}{K_{a2}^B} + \frac{[H_3O^+]^2}{K_{a1}^B K_{a2}^B}\right)}}{\left(1 + \frac{[H_3O^+]}{K_{a2}^B} + \frac{[H_3O^+]^2}{K_{a1}^B K_{a2}^B}\right)}
$$

$$
[H_2A]_0 = \frac{\left(\frac{D_B}{D_{H_2A}}\right)^{\frac{2}{3}}\sqrt{K_{sp}\left(1 + \frac{K_{a1}^{H_2A}}{[H_3O^+]} + \frac{K_{a1}^{H_2A}K_{a2}^{H_2A}}{[H_3O^+]^2}\right)\left(1 + \frac{[H_3O^+]}{K_{a2}^B} + \frac{[H_3O^+]^2}{K_{a1}^B K_{a2}^B}\right)}}{\left(1 + \frac{K_{a1}^{H_2A}}{[H_3O^+]} + \frac{K_{a1}^{H_2A}K_{a2}^{H_2A}}{[H_3O^+]^2}\right)}
$$

Substituting $[H_2A]_0$ and $[B]_0$ into A3.36 and finding the root of the nonlinear equation gives the estimation of interfacial pH.

Matlab code for estimating KTZ-FUM interfacial pH as a function of increasing acetate buffer

```
close all
clear all
%%%%%%%%%%%%%%%%%%%%%%%%%%%%%%%%%%%%%%%%%%%%%%%%%%%%%%%%%%%%
%%%%%%%%%%
%%%%%%%%%%%%%%%%%%%%%%%%%%%%% Setting
%%%%%%%%%%%%%%%%%%%%%%%%%%%%%%%%%%%
%%%%%%%%%%%%%%%%%%%%%%%%%%%%%%%%%%%%%%%%%%%%%%%%%%%%%%%%%%%%
%%%%%%%%%%
set(0,'DefaultTextInterpreter','latex')
set(0,'DefaultAxesFontsize',16)
set(0,'DefaultAxesXGrid','on','DefaultAxesYGrid','on')
set(0,'DefaultAxesGridLineStyle','--')
```

```
set(0,'DefaultAxesGridColor',[0,1,0])
set(0,'DefaultLineLineWidth',2)
set(0,'DefaultLineLineStyle','-.')
%%%%%%%%%%%%%%%%%%%%%%%%%%%%%%%%%%%%%%%%%%%%%%%%%%%%%%%%%%%%%%%%
%%%%%%%%%%%
%%%%%%%%%%%%%%%%%%%%%%%%%%%%%%%Input%%%%%%%%%%%%%%%%%%%%%%%%%%%%
%%%%%%%%%%%
%%%%%%%%%%%%%%%%%%%%%%%%%%%%%%%%%%%%%%%%%%%%%%%%%%%%%%%%%%%%%%%%
%%%%%%%%%%%
D_BH2 =3.56*10^-6;% Diffusion Coeff. of BH2++ (cm^2/s)
D_BH =3.56*10^-6;% Diffusion Coeff. of BH+ (cm^2/s)
D_B =3.56*10^-6;% Diffusion Coeff. of B (cm^2/s)

D_H2A =8.67*10^-6;% Diffusion Coeff. of H2A (cm^2/s)
D_HA =8.67*10^-6;% Diffusion Coeff. of HA- (cm^2/s)
D_A =8.67*10^-6;% Diffusion Coeff. of A-- (cm^2/s)

D_OH =52.8*10^-6;% Diffusion Coeff. of OH- (cm^2/s)
D_H =93.1*10^-6;% Diffusion Coeff. of H+ (cm^2/s)

D_CH3COO =8.84*10^-6;% Diffusion Coeff. of CH3COO- (cm^2/s)
D_CH3COOH =8.84*10^-6;% Diffusion Coeff. of CH3COOH (cm^2/s)

rpm = [200];%Rotation per minute
v = 0.00893 ;%Kinematic viscosity of solution in 37 C (cm^2/s)
pH_b =[eps:0.2:14];%Bulk pH range
Kw =1.008*10^-14*10^-3*10^-3; %Water dissociation constant
C_b = [0:20:100]*10^-6; %Total buffer concentration (mol/cm^3)

pka1_H2A =3.03; %H2A First pKa
pka2_H2A =4.38; %H2A Second pKa

pka1_B =2.94; %BH2 First pKa
pka2_B =6.51; %BH2 Second pKa

pka1 =4.6; %Buffer pKa

Ka1_H2A =10^(-pka1_H2A)*10^-3; %H2A First Ka
Ka2_H2A =10^(-pka2_H2A)*10^-3; %H2A Second Ka

Ka1_B =10^(-pka1_B)*10^-3; %BH2 First Ka
Ka2_B =10^(-pka2_B)*10^-3; %BH2 Second Ka

Ka1 =(10^(-pka1)*10^-3); %Buffer Kb

K_sp =0.15*10^-2*10^-12; %Drug Ksp (mM2 -> M2 -> (mol/cm3)^2)
```

```
H_s =zeros(length(C_b),length(pH_b));
pH_s =zeros(length(C_b),length(pH_b));
H2A_total =zeros(length(C_b),length(pH_b));
B_total =zeros(length(C_b),length(pH_b));
J_total =zeros(length(C_b),length(pH_b));
h_eff =zeros(length(C_b),length(pH_b));

%%%%%%%%%%%%%%%%%%%%%%%%%%%%%%%%%%%%%%%%%%%%%%%%%%%%%%%%%%%%%%%%
%%%%%%%%%%%
%%%%%%%%%%%%%%%%%%%%%%%%%%%%%%%Calculation%%%%%%%%%%%%%%%%%%%%%%
%%%%%%%%%%%
%%%%%%%%%%%%%%%%%%%%%%%%%%%%%%%%%%%%%%%%%%%%%%%%%%%%%%%%%%%%%%%%
%%%%%%%%%%%
for i=1:length(C_b)
for j=1:length(pH_b)

%Initial bulk concentrations:
H_b =10^(-pH_b(j)).*10^-3;
OH_b =Kw/H_b;
H2A_b =0;
HA_b =0;
A_b =0;
BH2_b =0;
BH_b =0;
B_b =0;
CH3COO_b =C_b(i)/(1+H_b/Ka1);
CH3COOH_b =C_b(i)-CH3COO_b;


%Finding the roots
H = (Ka1_B*Ka2_B);
G = (Ka1_H2A*Ka2_H2A);
A = D_CH3COOH*CH3COOH_b+D_CH3COO*CH3COO_b;
E = D_CH3COOH;
B = D_CH3COO*Ka1;
% B = D_H3PO4*(Kb1*Kb2*(A/(B+E*x+F*x^2))*x^2/Kw^2-H3PO4_b);
f = @(x)
((K_sp*(1+x/Ka2_B+x^2/H)*(1+Ka1_H2A/x+G/x^2))^0.5/(1+x/Ka2_B+x^2
/H))*(D_BH2*x^2/H-D_B)+
((D_B/D_H2A)^(2/3)*(K_sp*(1+x/Ka2_B+x^2/H)*(1+Ka1_H2A/x+G/x^2))^
0.5/(1+Ka1_H2A/x+G/x^2))*(D_H2A-
D_A*G/x^2)+(A*x/(B+E*x))*(D_CH3COOH-D_CH3COO*Ka1/x)+D_H*(x-
H_b)+D_OH*(OH_b-Kw/x)+D_CH3COO*CH3COO_b-D_CH3COOH*CH3COOH_b; %
function
x0 = [10^-17 10^-3]; % initial interval
r = fzero(f,x0);
```

```
r = r*10^3;
pH_s(i,j)= -log10(r);


%Solubility of H2A
H2A_total(i,j) =
(D_B/D_H2A)^(2/3)*(K_sp*(1+(r/1000)/Ka2_B+(r/1000)^2/H)*(1+Ka1_H
2A/(r/1000)+G/(r/1000)^2))^0.5;


%Solubility of B
B_total(i,j)
=(K_sp*(1+Ka1_H2A/(r/1000)+G/(r/1000)^2)*(1+(r/1000)/Ka2_B+(r/10
00)^2/H))^0.5;


%Effective boundary layer thickness
w = 2*pi*rpm;
h_eff=1.612*(D_B^(1/3))*(w^(-0.5))*(v^(1/6));

%Flux of drug
J_total(i,j) =D_B*B_total(i,j)/h_eff;


end
end

figure('Name','bulk pH vs. surface pH');
hold on
step = 1;
legend_array = cell(1,length(1:step:length(C_b)));
for i=1:length(C_b)
plot(pH_b, pH_s(i,:))
xlabel('Bulk pH')
ylabel('Surface pH')
 legend_array{1+(i-1)/step} ="C_{buffer} = " +
num2str(C_b(i)*10^6)+ ' mM ';

end
legend(legend_array)


figure('Name','bulk pH vs. drug solubility');
step = 1;
legend_array = cell(1,length(1:step:length(C_b)));
for i=1:length(C_b)
```

```
plot(pH_b, B_total(i,:)*10^6)
hold on
xlabel('Bulk pH')
xlim([1 8])
ylabel('Solubility of drug (mM)')
 legend_array{1+(i-1)/step} ="C_{buffer} = " +
num2str(C_b(i)*10^6)+ ' mM ';

end
legend(legend_array)


figure('Name','bulk pH vs. coformer solubility');
step = 1;
legend_array = cell(1,length(1:step:length(C_b)));
for i=1:length(C_b)
plot(pH_b, H2A_total(i,:)*10^6)
hold on
 legend_array{1+(i-1)/step} ="C_{acetate} = " +
num2str(C_b(i)*10^6)+ ' mM ';
xlabel('Bulk pH')
ylabel('Solubility of coformer (mM)')
end
legend(legend_array)


figure('Name','bulk pH vs. Flux');
step = 1;
legend_array = cell(1,length(1:step:length(C_b)));
for i=1:length(C_b)
semilogy(pH_b, J_total(i,:)*1000*60)
hold on
 legend_array{1+(i-1)/step} ="C_{buffer} = " +
num2str(C_b(i)*10^6)+ ' mM ';
xlabel('Bulk pH')
ylabel('Flux (mmol/ cm2 min)')
end
legend(legend_array)
```

CHAPTER IV

Simulation of Cocrystal Particle Dissolution Using a Dissolution-Precipitation Model

Introduction

Cocrystals are a promising tool in the world of pharmaceutical sciences. They have the potential to improve the oral bioavailability of poorly soluble drugs by generating supersaturated drug solutions in the gastrointestinal tract[1-6]. Development of a cocrystal product can be hindered by precipitation due to supersaturation, and this can lead to a library of cocrystals of the same drug having a wide range of pharmacokinetic profiles[6]. Due to the complex solution behavior and the nature of nucleation and growth kinetics, cocrystal behavior in solution is still not well understood. The ability to estimate cocrystal dissolution rate, the degree of supersaturation it may obtain, and the amount of associated precipitation could be a very powerful tool in understanding the mechanism by which cocrystals drive absorption advantages. This knowledge could help in reducing the amount of time and resources needed in developing a cocrystal and create options for active pharmaceutical ingredients previously thought to be unsuitable for development into an oral dosage form.

Mechanistic predictions of cocrystal dissolution in rotating disk dissolution experiments have been shown in the literature[7, 8]. However, more biorelevant estimations of cocrystal dissolution rates would be more appropriate to what would be achievable in the gastrointestinal tract. Classical dissolution theory states that the dissolution flux is a function of the interfacial

solubility[9, 10], and with ionizable species, estimations of the interfacial pH (pH_o) are needed to calculate the concentrations present at the solid-liquid interface. Cocrystals of the weakly basic drug ketoconazole (KTZ) with carboxylic acid coformers adipic (ADP), fumaric (FUM), and succinic (SUC) have been previously investigated in work which estimated pH_o and applied the calculated surface concentrations to rotating disk dissolution in unbuffered solutions[7, 8]. Biorelevant estimations of cocrystal dissolution would require an understanding of how buffer affects pH_o, and the surface concentrations would need to be applied not to a constant surface area like rotating disk but particle geometries as dosed *in vivo*.

KTZ cocrystals can generate varying amounts of supersaturation at intestinal pH values, and in turn, variable precipitation depending on the pH or surfactant concentrations of the dissolution media[11]. Particle dissolution experiments for these cocrystals in intestinally relevant dissolution media have shown no precipitation in some cases and precipitation in others[11, 12]. *In vitro* experiments exploring supersaturation and precipitation kinetics of weak bases caused by pH shift from gastric to intestinal compartments have been previously explored with mechanistic precipitation theories[13-15]. This makes KTZ cocrystals are an ideal model system for attempting to create a mathematical theory to approximate the dissolution and precipitation rates that control cocrystal solution behavior. A previous study investigated using a unified dissolution and precipitation theory to simulate amounts of drug in solution over time as a function of nucleation and crystal growth[16]. This approach adds merit to the feasibility of creating similar methods to simulate the concentration-time profiles of cocrystal systems.

The goal of this study was to develop a method to simulate the particle dissolution concentration profiles of KTZ cocrystals in the biorelevant dissolution media experiments performed by Chen et al[12]. Particle dissolution rates were simulated using pure diffusion theory

applied to spherical geometry as first explored by Higuchi and Hiestand[17]. To account for experiments that generate supersaturation, the approach taken by Jakubiak et al.[16] was modified for cocrystals by adding particle dissolution theory to terms for nucleation and growth of parent drug from supersaturated solutions. This approach aimed to simulate solution concentrations of KTZ cocrystals as a function of time in the presence and absence of bulk solution precipitation.

Materials and Methods

Particle Size Measurement

Measurement of cocrystal particle size used in the experiments of Chen et al[11]. was needed to simulate the dissolution rates. Sieving protocol used by the author was recreated and the reported sieve cut was isolated for measurement by brightfield microscopy. Dry cocrystals were placed into 96-well plates and mounted onto an inverted microscope (Leica DMi8). Images of the three KTZ cocrystals were processed using ImageJ software by placing an outline around each individual particle to obtain a two-dimensional area. This area was used as an equivalent circular area to solve for a particle radius. Assumption of a spherical particle to approximate actual particle size was justified due to equant nature of imaged cocrystal particles. Between 1100 and 1600 individual particles were analyzed for each KTZ cocrystal.

Cocrystal Particle Dissolution Simulations

Cocrystal dissolution rates in the absence of precipitation for FeSSIF dissolution media were estimated using paired differential equations (4.29) and (4.30) in Berkley Madonna (version 9.1.18). The simulations for dissolution were adapted from Higuchi-Hiestand[17] particle dissolution theory and assumed 1) dissolution is purely diffusion driven with no hydrodynamic enhancement, 2) monodisperse spherical particle radii, 3) interfacial pH estimated in buffered

conditions, and 4) no precipitation occurring at the interface of the dissolving cocrystal. Codes and parameters used for the dissolution simulations can be found in Appendix 4A.

Cocrystal Particle Dissolution Precipitation Simulations

Cocrystal dissolution data previously generated by Chen et al.[11] was fit using the Berkeley Madonna curve fitting tool. The growth rate constant (k_{grow}) was first found by fitting the terminal slope of the experimental data points. It was assumed that nucleation was not occurring in the bulk during the final data points of the dissolution run, and $-k_{grow}$ was determined by fitting the last three blank FeSSIF data points to equation (4.34). With a growth rate constant found, the entire experimental concentration-time profile from Chen et al. was fit using the curve fitting tool of Berkeley Madonna and the paired differential equations (4.35-4.37) by fitting the nucleation rate constant (k_{nuc}). The simplifying assumption of nucleation and growth occurring whenever supersaturation is generated was used for the fitting of these equations. Time steps of 0.1 min were used for all k_{nuc} and k_{grow} fittings. Codes and parameters used for the simulations and fittings can be found in Appendix 4A.

Theoretical

Drug and Cocrystal Solubility

The solubility of ketoconazole, a weakly dibasic drug (B), is influenced by the ionization and solubilization equilibria:

$$BH_{2\,aq}^{2+} \rightleftharpoons H_{aq}^{+} + BH_{aq}^{+} \tag{4.1}$$

$$K_{a1}^{B} = \frac{[H_{aq}^{+}][BH_{aq}^{+}]}{[BH_{2\,aq}^{2+}]} \tag{4.2}$$

$$BH_{aq}^{+} \rightleftharpoons H_{aq}^{+} + B_{aq} \tag{4.3}$$

$$K_{a2}^{B} = \frac{[H_{aq}^{+}][B_{aq}]}{[BH_{aq}^{+}]} \tag{4.4}$$

$$B_{aq} + mic \rightleftharpoons B_{mic} \tag{4.5}$$

$$K_{s}^{B} = \frac{[B_{mic}]}{[B_{aq}][mic]} \tag{4.6}$$

where the expressions for drug ionization (K_{a1}^{B}, K_{a2}^{B}) and solubilization (K_{s}^{B}) constants can be written in terms of their respective ionized ($BH_{aq}^{+}, BH_{2\,aq}^{2+}$) or solubilized ($B_m$) species as a function of hydrogen ion ($[H_{aq}^{+}]$) or micelle ($[mic]$) concentration. Combining and simplifying these expressions leads to the equation for drug solubility,

$$S_{drug} = S_o(1 + K_{s}^{B}[mic] + \frac{[H_{aq}^{+}]}{K_{a2}^{B}} + \frac{[H_{aq}^{+}]^2}{K_{a1}^{B}K_{a2}^{B}}) \tag{4.7}$$

where (S_o) is the intrinsic solubility of the unionized species.

Solubility of KTZ (B) cocrystals with diprotic carboxylic acids (H_2A) is a function of the ionization, solubilization, and dissociation equilibria:

$$BH_{2\,aq}^{2+} \rightleftharpoons H_{aq}^{+} + BH_{aq}^{+} \tag{4.8}$$

$$K_{a1}^{B} = \frac{[H_{aq}^{+}][BH_{aq}^{+}]}{[BH_{2\,aq}^{2+}]} \tag{4.9}$$

$$BH_{aq}^{+} \rightleftharpoons H_{aq}^{+} + B_{aq} \tag{4.10}$$

$$K_{a2}^{B} = \frac{[H_{aq}^{+}][B_{aq}]}{[BH_{aq}^{+}]} \tag{4.11}$$

$$B_{aq} + mic \rightleftharpoons B_{mic} \tag{4.12}$$

$$K_{s}^{B} = \frac{[B_{mic}]}{[B_{aq}][mic]} \tag{4.13}$$

$$H_2A \rightleftharpoons H_{aq}^{+} + HA_{aq}^{-} \tag{4.14}$$

$$K_{a1}^{H_2A} = \frac{[H_{aq}^{+}][HA_{aq}^{-}]}{[H_2A_{aq}]} \tag{4.15}$$

$$HA_{aq}^{-} \rightleftharpoons H_{aq}^{+} + A_{aq}^{2-} \tag{4.16}$$

$$K_{a2}^{H_2A} = \frac{[H_{aq}^{+}][A_{aq}^{2-}]}{[HA_{aq}^{-}]} \tag{4.17}$$

$$H_2A_{aq} + mic \rightleftharpoons H_2A_{mic} \tag{4.18}$$

$$K_s^{H_2A} = \frac{[H_2A_{mic}]}{[H_2A_{aq}][mic]} \tag{4.19}$$

$$(BH_2A)_s \rightleftharpoons B_{aq} + H_2A_{aq} \tag{4.20}$$

$$K_{sp} = [B_{aq}][H_2A_{aq}] \tag{4.21}$$

Combining the equilibrium expressions and rearranging results in the equation for stoichiometric solubility (S_{cc})

$$S_{cc} = \sqrt{K_{sp}(1 + K_s^B[mic] + \frac{[H_{aq}^{+}]}{K_{a2}^B} + \frac{[H_{aq}^{+}]^2}{K_{a1}^B K_{a2}^B})(1 + K_s^{H_2A}[mic] + \frac{K_{a1}^{H_2A}}{[H_{aq}^{+}]} + \frac{K_{a1}^{H_2A}K_{a2}^{H_2A}}{[H_{aq}^{+}]^2})} \tag{4.22}$$

which was previously derived[12].

Higuchi-Hiestand Particle Dissolution Adapted for Cocrystals

Higuchi and Hiestand proposed a particle dissolution theory in which dissolution is controlled by pure diffusion and applied Fick's first law to a spherical geometry[17]

$$\frac{dM}{dt} = 4\pi r^2 D_{aq} \frac{dC}{dr} \tag{4.23}$$

where the rate at which the particle mass changes ($\frac{dM}{dt}$) is controlled by the aqueous diffusion coefficient (D_{aq}) and the concentration gradient ($\frac{dC}{dr}$) along the radius (r) of spherical diffusion.

Integrating with respect to r from particle of radius (a) to infinity, applying the difference in concentration between the interface and bulk (ΔC) leads to

$$\frac{dM}{dt} = 4\pi a D_{aq} \Delta C \tag{4.24}$$

and multiplying this expression by the total number of particles (N) dissolving will give the total flux

$$\frac{dM}{dt} = N 4\pi a D_{aq} \Delta C \tag{4.25}$$

where, N can be expressed

$$N = \frac{3M}{4\pi a^3 \rho} \tag{4.26}$$

with the total mass (M) divided by the mass of a single particle given in terms of the density (ρ) and volume of a sphere with radius (a). Incorporating the expression for (N) and applying the bulk dissolution media volume (V) an expression for the rate at which the bulk concentration (C_b) changes as a function of time

$$\frac{dC_b}{dt} = \frac{3MD_{aq}}{a^2 \rho V}(C_s - C_b) \tag{4.27}$$

where the expression for ΔC has been written in terms of the concentration at the surface of the dissolving particle (C_s) and the bulk concentration (C_b). For cocrystal dissolution, the surface saturation model proposed by Cao et al.[7] states that the concentration of drug at interface is equal to that of the stoichiometric cocrystal solubility (S_{cc})[7] and incorperating this to equation (4.27) results in

$$\frac{dC_b}{dt} = \frac{3MD_{aq}}{a^2 \rho V}(S_{cc} - C_b) \tag{4.28}$$

a general expression for non-sink dissolution of cocrystals. Applying equation (4.22) to equation (4.28) and assuming sink conditions ($C_b = 0$), the final expression used for estimating cocrystal

particle dissolution was paired with a differential equation representing the mass of solid cocrystal available for dissolution. Assuming mass balance any solid cocrystal dissolved would be expressed in the concentration compartment. The paired differential equations

$$\frac{dC_b}{dt} = \frac{3MD_{aq}}{a^2\rho V}\sqrt{K_{sp}(1 + K_s^B[mic] + \frac{[H_{aq}^+]}{K_{a2}^B} + \frac{[H_{aq}^+]^2}{K_{a1}^B K_{a2}^B})(1 + K_s^{H_2A}[mic] + \frac{K_{a1}^{H_2A}}{[H_{aq}^+]} + \frac{K_{a1}^{H_2A}K_{a2}^{H_2A}}{[H_{aq}^+]^2})} \quad (4.29)$$

$$\frac{dM}{dt} = -\frac{3MD_{aq}}{a^2\rho}\sqrt{K_{sp}(1 + K_s^B[mic] + \frac{[H_{aq}^+]}{K_{a2}^B} + \frac{[H_{aq}^+]^2}{K_{a1}^B K_{a2}^B})(1 + K_s^{H_2A}[mic] + \frac{K_{a1}^{H_2A}}{[H_{aq}^+]} + \frac{K_{a1}^{H_2A}K_{a2}^{H_2A}}{[H_{aq}^+]^2})} \quad (4.30)$$

were used for simulations with parameter values independently estimated or sourced from the literature that can be found in Appendix 4A. Drug solubilization into surfactant micelles alters the aqueous diffusion coefficient and was accounted for by calculating an effective diffusion coefficient

$$D_{eff} = f_{aq}D_{aq} + f_{mic}D_{mic} \quad (4.31)$$

according the fractions of free (f_{aq}) and solubilized (f_{mic}) drug that would diffuse according to drug (D_{aq}) or micelle (D_{mic}) diffusion coefficients[18].

Particle Dissolution and Precipitation

When a cocrystal dissolves, bulk solution concentrations as a function of time are increased by dissolution and decreased by precipitation. In this same manner, the rate of change in bulk concentration can be expressed as

$$\frac{dC_b}{dt} = Dissolution - Precipitation \quad (4.32)$$

with a positive term for dissolution and a negative term for precipitation. The previous section discussed the development of a particle dissolution term for cocrystal dissolution. Terms for bulk

precipitation were modified from Jakubiak et al[19]. by considering precipitation as a function of nucleation and growth driven by supersaturation,

$$Nucleation\ Rate = k_{nuc}(C_b - S_{drug})^{\alpha} \tag{4.33}$$

$$Growth\ Rate = \frac{k_{grow}A_s}{V}\left(C_b - S_{drug}\right)^{1.5} \tag{4.34}$$

where (k_{nuc}) and (k_{grow}) are the nucleation and growth rate constants and supersaturation is defined as the difference between the bulk concentration (C_b) and drug solubility (S_{drug}). Nucleation involves molecules colliding to form a nucleus and (α) is a molecularity index that represents the average number of molecules required for that process. Solid drug precipitate (A_s) is formed from nucleation and is needed for growth to proceed in the bulk media volume (V). Growth rate is assumed to follow a quasiparabolic rate law[20].

The expressions for dissolution, nucleation, and growth were placed into an equation to represent change in concentration as a function of time, amount of solid cocrystal available for dissolution and the amount of solid drug that had precipitated. Paired differential equations were then created for the rate of change of solid drug ($\frac{dA_s}{dt}$) and solid cocrystal ($\frac{dM}{dt}$) assuming mass balance.

$$\frac{dC_b}{dt} = \frac{3MD_{aq}}{a^2\rho V}(S_{cc} - C_b) - k_{nuc}\left(C_b - S_{drug}\right)^{\alpha} - \frac{k_{grow}A_s}{V}\left(C_b - S_{drug}\right)^{1.5} \tag{4.35}$$

$$\frac{dA_s}{dt} = Vk_{nuc}\left(C_b - S_{drug}\right)^{\alpha} + k_{grow}A_s\left(C_b - S_{drug}\right)^{1.5} \tag{4.36}$$

$$\frac{dM}{dt} = -\frac{3MD_{aq}}{a^2\rho}(S_{cc} - C_b) \tag{4.37}$$

For simplicity, this approach assumes that nucleation and growth occur at any concentration higher than the drug solubility. This is a limiting assumption of the model as it does not include

contributions of lag time and metastable zone width that would affect the concentration-time profile.

Definition of Terms			
K_{a1}^{B}	First drug ionization constant	M	Total mass
K_{a2}^{B}	Second drug ionization constant	N	Total number of particles
K_{s}^{B}	Drug solubilization constant	C	Concentration
$K_{a1}^{H_2A}$	First coformer ionization constant	C_b	Bulk Concentration
$K_{a2}^{H_2A}$	Second coformer ionization constant	C_s	Surface concentration
$K_{s}^{H_2A}$	Coformer solubilization constant	ρ	Solid density
K_{sp}	Cocrystal solubility product	D_{aq}	Aqueous diffusion coefficient
S_o	Intrinsic drug solubility	D_{mic}	Micellar diffusion coefficient
S_{drug}	Drug solubility	D_{eff}	Effective diffusion coefficient
S_{cc}	Cocrystal stoichiometric solubility	f_{aq}	Fraction of drug in aqeous phase
mic	Micellar concentration	f_{mic}	Fraction of drug in micellar phase
t	Time	k_{nuc}	Nucleation rate constant
r	Diffusion radius	α	Molecularity index
a	Particle radius	k_{grow}	Growth rate constant
V	Dissolution volume	A_s	Amount of precipitated solid drug

Experimental Data from Literature

To explore the merit of mathematical approximations of cocrystal solution behavior, the previously performed dissolution experiments from Chen et al.[12] were examined. The surfactant containing biorelevant dissolution media, Fed State Simulated Intestinal Fluid (FeSSIF), and the sans surfactant equivalent buffer (Blank FeSSIF) are the focus of this study. Only the dissolution rate was simulated for the FeSSIF experiments (Figure 4.1a), as no bulk precipitation was observed, and blank FeSSIF experiments (Figure 4.1b) were used to explore the merit of equations (4.35-4.37) to describe the dissolution and precipitation profiles.

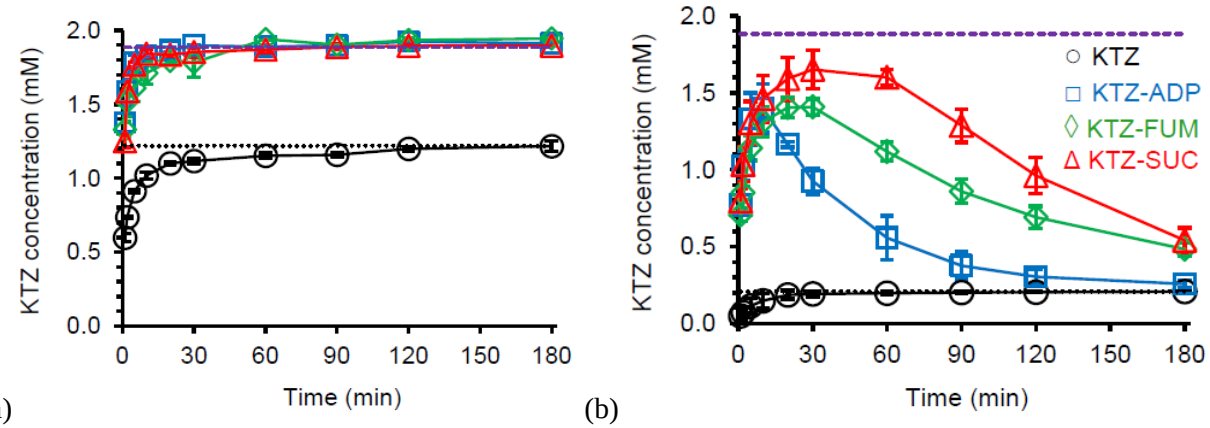

Figure 4.1: Concentration-time profiles of KTZ (—), KTZ-ADP (—), KTZ-FUM (—), and KTZ-SUC (—) in biorelevant dissolution media (a) FeSSIF, and (b) blank FeSSIF from Chen et al.[12]

Results

Simulating Cocrystal Particle Dissolution in the Absence of Precipitation

The KTZ cocrystal experimental data in the biorelevant media FeSSIF was the foundation for developing cocrystal particle dissolution theory in the absence of precipitation. To estimate the dissolution rate, there are two main aspects that need to be understood. The first aspect is the solubility of the cocrystal at the dissolving interface which depends heavily on the interfacial pH (pH_o), the second aspect being the surface area available for dissolution. Assuming the particles are spherical in nature, the particle radius controls the calculation of surface area that drives dissolution.

Cocrystal Equilibrium pH as a Interfacial pH Estimate

The previous chapter explored the addition of buffer equilibria to the estimation of KTZ cocrystal interfacial pH. Buffer was shown to decrease the ability of the coformers to lower the interfacial pH, showing estimations of buffered interfacial pH to be 1-2 pH units higher than the unbuffered at bulk intestinal pH values.

Table 4.1: Estimated values of KTZ cocrystal pH_o and experimental solubility equilibrium pH

FeSSIF	Unbuffered pH_o	Buffered pH_o	Equilibrium pH (pH_{eq})
KTZ-ADP	4.70	4.99	4.67±0.03
KTZ-FUM	4.05	4.96	4.37±0.04
KTZ-SUC	4.70	4.99	4.63±0.01
Blank FeSSIF	Unbuffered pH_o	Buffered pH_o	Equilibrium pH (pH_{eq})
KTZ-ADP	4.70	4.99	4.59±0.03
KTZ-FUM	4.05	4.96	4.26±0.04
KTZ-SUC	4.70	4.99	4.62±0.01

This process could be time consuming and it could be advantageous to quickly estimate the interfacial pH from a surrogate measurement that could be available in the literature. The first experiment to assess the solution behavior of a solid form is to measure the solubility, which by definition is when the solution becomes saturated with respect to the dissolving solid. At the dissolving surface, the concentration is assumed to be equal to that of saturation, and hypotheically, the saturation concentrations found in a solubility measurement could closely resemble the conditions at the interface. In other words, the interfacial pH may be estimated by measuring the pH of a saturated solution[21]. For cocrystals, measuring the solubility requires that the solution be saturated with respect to both drug and cocrystal[22-24]. Measuring the equilibrium pH (pH_{eq}) of a cocrystal solubility experiment may give a reasonable estimate of interfacial pH.

In the case of the KTZ cocrystals, solubility experiments in different aqueous buffer conditions were previously done to calculate the solubility product[11]. Equilibrium pH values were also recorded from these experiments. These equilibrium bulk pH values were then plotted against the previous unbuffered estimates of cocrystal interfacial pH from Cao et al.[8]. The equilibrium

pH values for the three KTZ cocrystals are within 0.5 pH units of the unbuffered interfacial pH estimates.

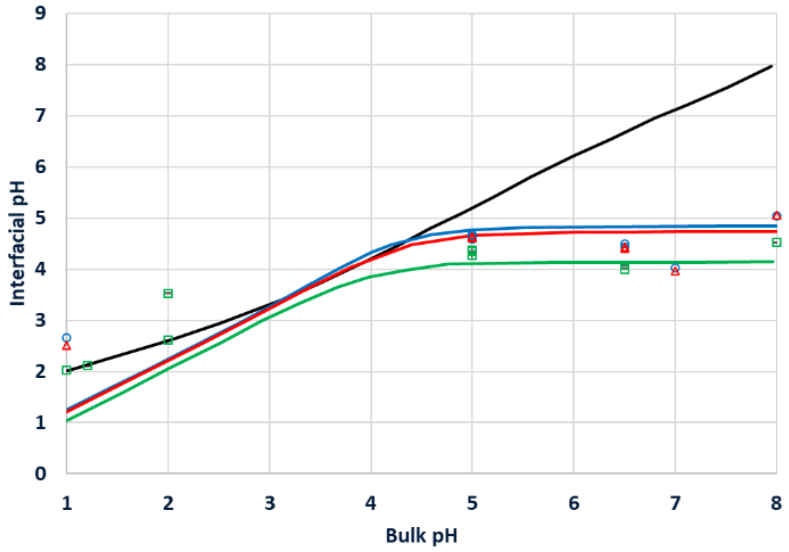

Figure 4.2: Estimated interfacial pH for KTZ (—), KTZ-ADP (—), KTZ-FUM (—), and KTZ-SUC (—) as a function of bulk pH from Cao et al[8]. Measured equilibrium pH values (y-axis) with initial pH (x-axis) for KTZ-ADP (○), KTZ-FUM (□), and KTZ-SUC (Δ) in phosphate, acetate, and hydrochloric acid buffers of varying concentrations.

Measured pH_{eq} values from (Figure 4.2) are from solutions that contain various concentrations of multiple types of buffer species that range from 29-150 mM. For the purposes of estimating the dissolution of KTZ cocrystals, it is more relevant to compare the values pH_{eq} to the buffered interfacial pH estimates. (Table 4.1) shows the measured values of equilibrium pH for the biorelevant dissolution media from Chen et al.[12] (Figure 4.3) shows the estimation of interfacial pH as a function of bulk pH considering the effect of acetate and phosphate buffer. Plotting the pH_{eq}, it is clear that the estimations of interfacial pH agree relatively well. There is a common theme amoung all cocrystals. The measured pH_{eq} always underestimates the estimated buffered pH_o. For FeSSIF and blank FeSSIF buffers at pH 5, the pH_{eq} and pH_o are within, at most, 0.5 pH units.

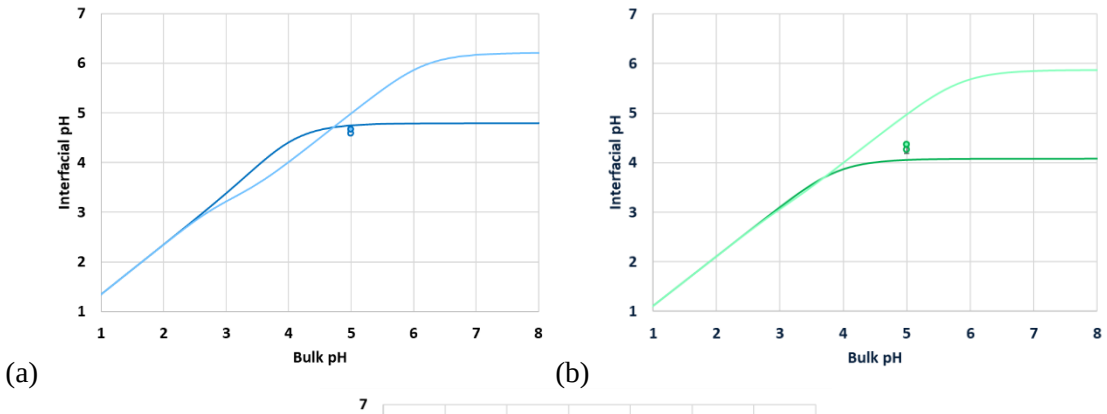

Figure 4.3: Estimated interfacial pH for (a) KTZ-ADP (—), (b) KTZ-FUM (—), and (c) KTZ-SUC (—) as a function of bulk pH adjusting for acetate buffer concentrations for FeSSIF/blank FeSSIF. Measured values of pH_{eq} (y-axis) for (a) KTZ-ADP, (b) KTZ-FUM, and (c) KTZ-SUC in FeSSIF (●, ●, ●) and blank FeSSIF (○, ○, ○) with an initial pH_{bulk} = 5 (x-axis). Error bars plotted for pH_{eq}.

Differences between pH_{eq} and pH_o are expected when taking into account the conditions of the cocrystal solubility experiments. The estimations of pH_o assume that there are concentration around stoichiometric solubility, where drug and coformer are equal. In an aqueous media where a cocrystal is more soluble than the parent drug, cocrystal solubility must be depressed to meet drug solubility. According to the cocrystal solublity product, the solubility of the cocrystal will decrease as coformer concentration increases as shown in (Figure 4.4).

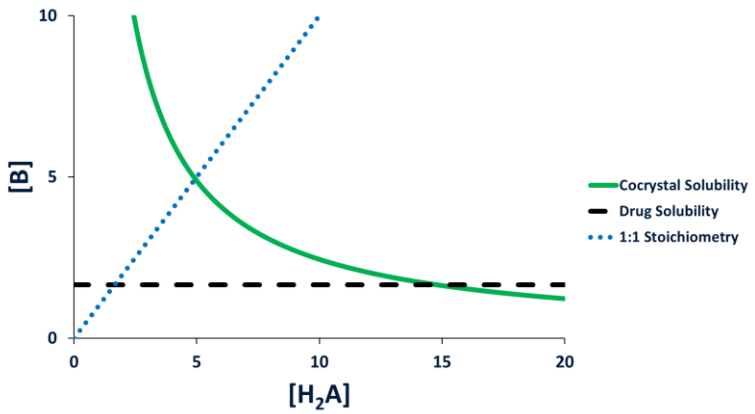

Figure 4.4: Schematic of KTZ-FUM (—) solubility as a function of drug and coformer concentrations. Drug solubility (- - -) and stoichiometric concentration (…) plotted for reference.

This means that cocrystal must increase the coformer concentration substantially to decrease cocrystal solubility so that drug and cocrystal can be at equilibrium with solution. Solubility experiments, where the pH_{eq} is measured, have measured coformer concentrations higher than drug for this reason and a lower pH would be associated with an increased acidic coformer and decreased basic drug concentration. A quick estimate of pH_{eq} can be made by applying acid-base calculations to the measured pH_{eq} and adjusting for the change in concentration between equilibrium and assumed interfacial concentrations.

Particle Size of Cocrystal Dissolution Experiments

Calculated interfacial solubilities estimated using the appropriate pH_o values need a surface area to simulate dissolution rates observed in the KTZ cocrystal dissolution experiments. The dissolution theory assumes a monodisperse distribution of spherical particles, therefore an equivalent average spherical particle radius was found for the cocrystal particles used experimentally. Brightfield microscopy was utilized to image particles obtained from the sieving protocol used by Chen et al.[12] and spherical equivalent particle radii measured for the three cocrystals are compiled in Table 4.2. Particles measured were relatively equant, justifying use of a spherical equilvalent radius, and an average radius of approximately 5 μm was measured for all

three cocrystals. Due to a small number of large particles containing a large percentage of the total mass (Figure 4.5), it was deemed that a mass median radius (R50) would be more appropriate for describing the average particle radius in simulations. The R50 values measured were found to be approximately 10 μm for all three cocrystals and which was used for mdissolution simulations.

Table 4.2: Measured cocrystal particle radii

	Average Sphereical Particle Radius (μm)	Mass Median Radius (R50) (μm)
KTZ-ADP	5.38±3.02	10.21
KTZ-FUM	4.59±2.85	9.51
KTZ-SUC	4.48±2.79	9.71

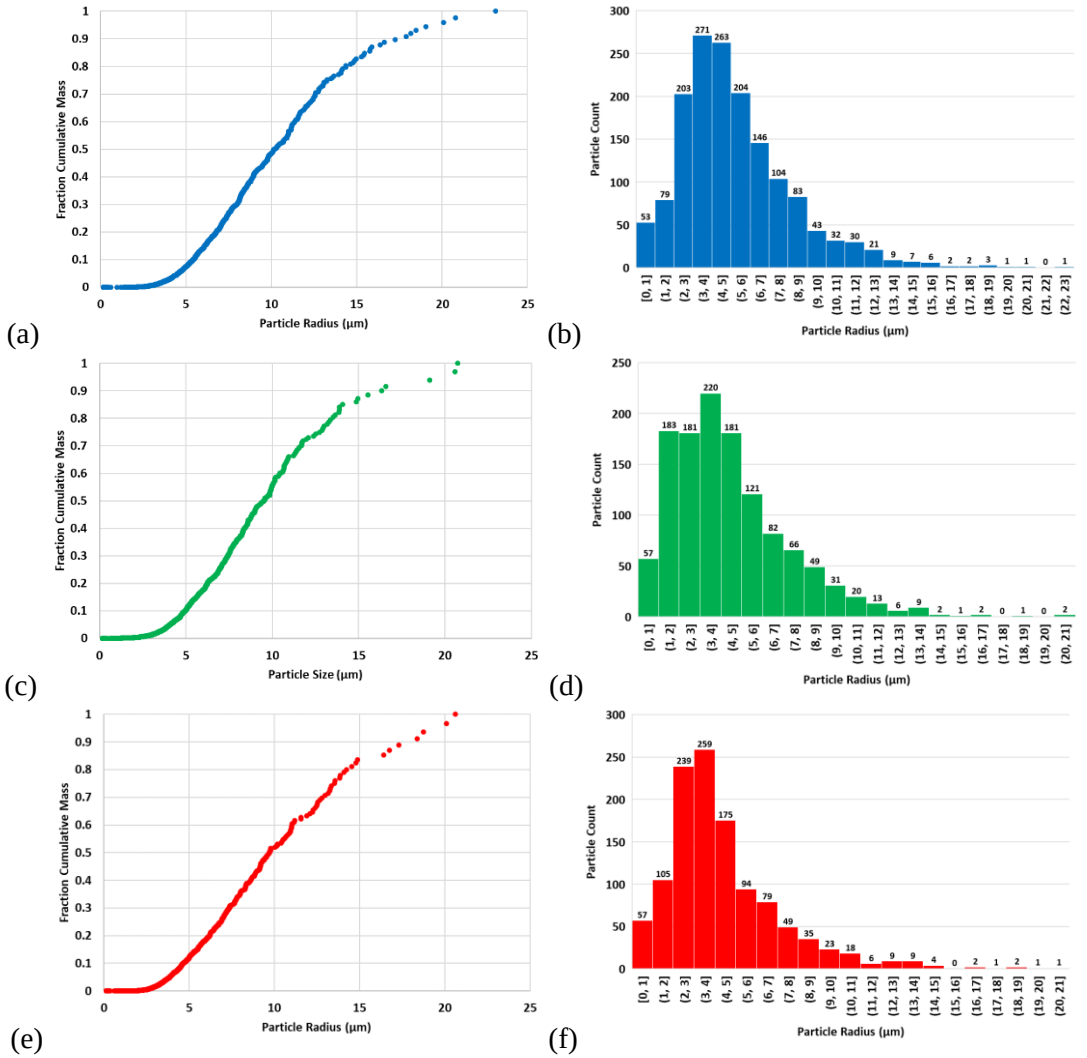

Figure 4.5: Fraction cumulative mass as a function of particle radius for (a) KTZ-ADP (●), (c) KTZ-FUM (●), and (e) KTZ-SUC (●). Binned particle size distributions for (b) KTZ-ADP (■), (d) KTZ-FUM (■), and (f) KTZ-SUC (■)

KTZ Cocrystal Simulations in FeSSIF

Necessary parameters were either estimated or gathered from literature to complete equations (4.29-4.30) in order to execute simulations of the KTZ cocrystal dissolution in blank FeSSIF. Rapid dissolution due to small particle size caused solid cocrystal to completely dissolve within 30 minutes and Figure 4.6 shows the dissolution data and simulations during this time frame. There is good agreement between the dissolution theory and the experimental data with simulation residuals being less than 0.15 mM away from observed data on average according to calculated root mean square error (RMSE) values compiled in Table 4.3. For all three cocrystals, simulations were often within the standard deviation of experimental data points.

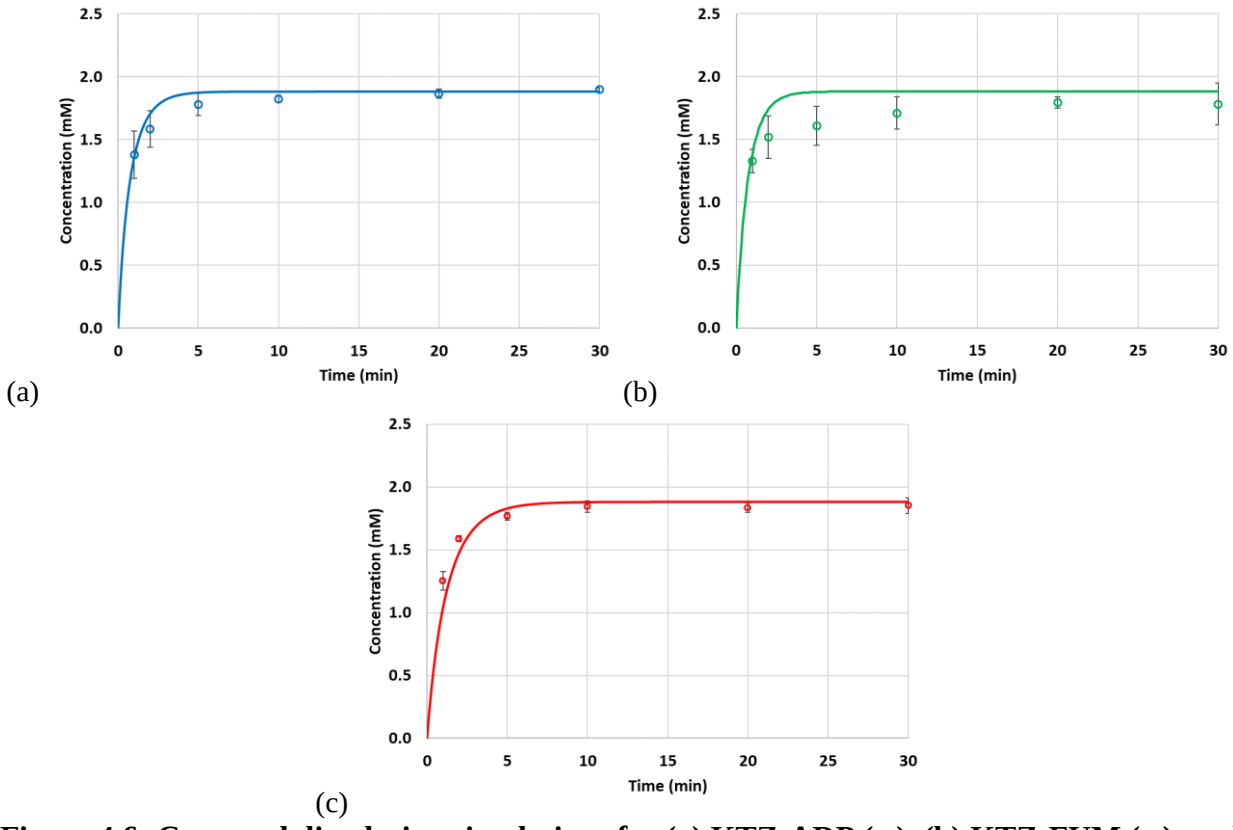

Figure 4.6: Cocrystal dissolution simulations for (a) KTZ-ADP (—), (b) KTZ-FUM (—), and (c) KTZ-SUC (—) over the first 30 minutes of dissolution experiments in pH 5 FeSSIF. Data points are experimental concentrations of (a) KTZ-ADP (●), (b) KTZ-FUM (●), and (c) KTZ-SUC (●) found in (Figure 4.1a).

Table 4.3: FeSSIF particle dissolution (0 ≤ t ≤180min) simulation root mean square error values (RMSE)

	RMSE (mM)
KTZ-ADP	0.056
KTZ-FUM	0.135
KTZ-SUC	0.112

Sensitivity analysis investigating the influence of particle size on the initial dissolution rate of KTZ-FUM was simulated and plotted in (Figure 4.7). A two-fold increase in particle radius creates a four-fold decrease in the initial dissolution rate, supporting the ability of the dissolution theory with measured particle sizes to estimate the concentration time profiles of these KTZ cocrystals.

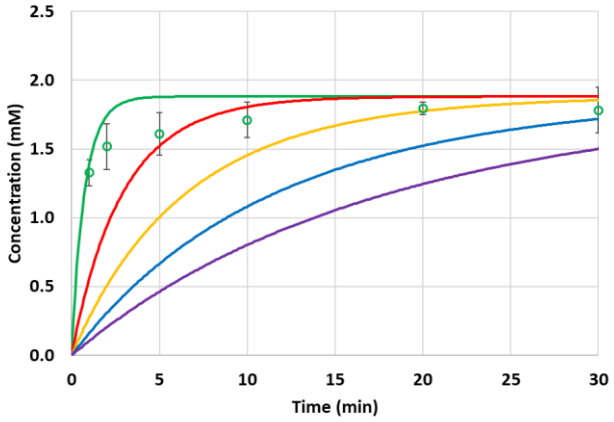

Figure 4.7: KTZ-FUM dissolution simulations in pH 5 FeSSIF with particle radii 10 µm (—), 20 µm (—), 30 µm (—), 40 µm (—), and 50 µm (—). Measured KTZ concentrations (○) from (Figure 4.1a) shown for reference.

Simulating KTZ Cocrystal Dissolution in Blank FeSSIF

The same approach for simulating FeSSIF concentration profiles was also done for blank FeSSIF. Simulations were in good agreement with the measured coformer concentrations from KTZ-FUM experiments as shown in (Figure 4.8b). However, drug concentrations were not able to be simulated as a function of time due to drug precipitation. It should be noted that the first two time points for all three cocrystals appear to be in good agreement with the respective dissolution simulations before bulk precipitation occurs as evidenced by the decreasing experimental bulk

concentrations (Figure 4.8). Terms for precipitation would need to be added in order to simulate blank FeSSIF concentration profiles of the entire dissolution experiment.

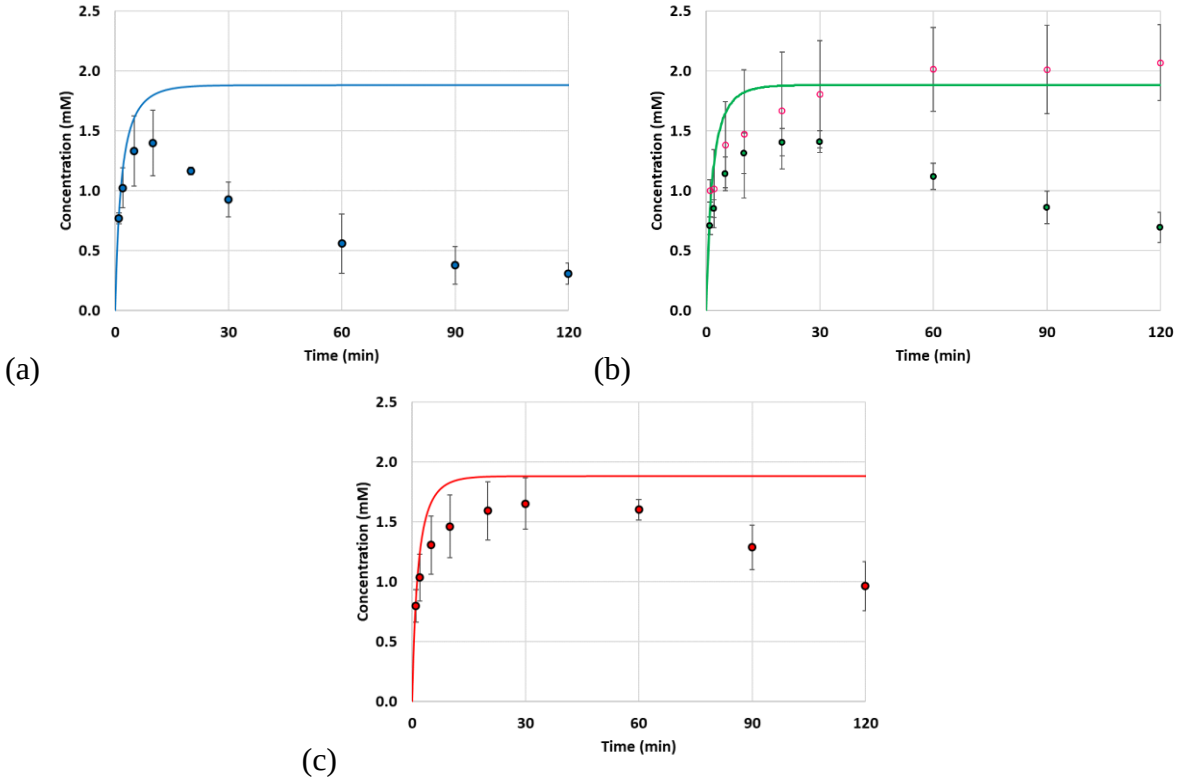

Figure 4.8: Simulations of cocrystal particle dissolution from (a) KTZ-ADP (—), (b) KTZ-FUM (—), and (c) KTZ-SUC (—) in blank FeSSIF. Measured concentrations of drug from (a) KTZ-ADP (●), (b) KTZ-FUM (●), and KTZ-SUC (●) cocrystal dissolution in blank FeSSIF (Figure 4.1b) shown for reference. Experimental coformer concentration from cocrystal dissolution in blank FeSSIF was only detectable for (b) FUM (○).

Fitting Precipitation Growth Rate Constant

Building upon the theory to simulate KTZ cocrystal dissolution rates in the absence of precipitation, mathematical terms for the approximation of precipitation rates were added to account for nucleation and growth of solid drug in the bulk dissolution media. The resulting equations (4.35-4.37) have only two parameters, nucleation rate constant (k_{nuc}) and the growth rate constant (k_{grow}) that could not be calculated or sourced from literature to generate concentration-time profiles for blank FeSSIF dissolution experiments. Simplifying assumptions for the model assume that nucleation and growth occur whenever there is supersaturation. Realistically,

however, nucleation typically does not occur when concentrations are within the metastable zone width. Assuming that nucleation is negligible for t = 90-180 min, a growth rate constant can be calculated by fitting the concentration data points to equation (4.34). Fits of KTZ cocrystal concentration-time profiles ($90 \leq t \leq 180$ min) are shown in (Figure 4.9) and the calculated values of k_{grow} and their associated root mean square error are compiled in (Table 4.4).

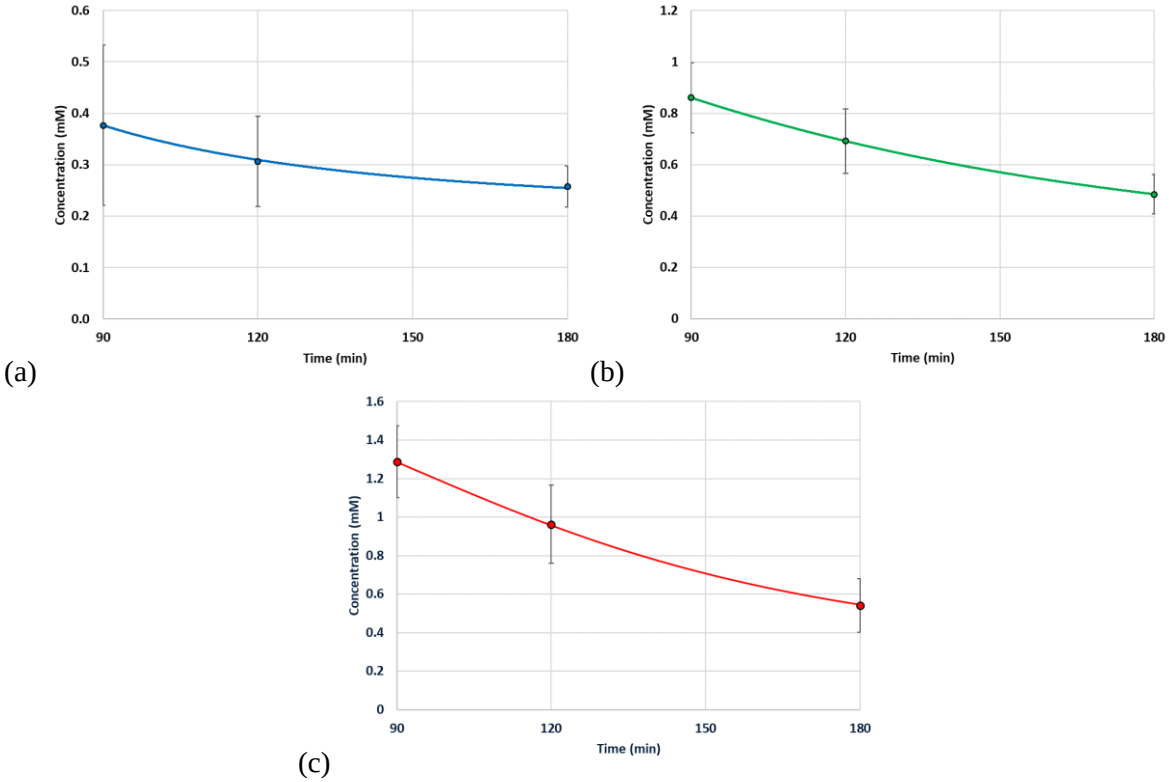

Figure 4.9: Concentration-time profiles of (a) KTZ-ADP (—), (b) KTZ-FUM (—), and (c) KTZ-SUC (—) fit to measured concentrations of drug from (a) KTZ-ADP (●), (b) KTZ-FUM (●), and (c) KTZ-SUC (●) dissolution in blank FeSSIF ($90 \leq t \leq 180$ min).

Table 4.4: Growth rate constants and root mean square error (RMSE) values from fitted blank FeSSIF concentration-time profiles ($90 \leq t \leq 180$ min).

	k_{grow} ($\mu M^{-1} min^{-1}$)	RMSE (μM)
KTZ-ADP	8.49×10^{-7}	2.66
KTZ-FUM	3.46×10^{-7}	0.08
KTZ-SUC	4.90×10^{-7}	3.21

Fitting Precipitation Nucleation Rate Constant

With values of k_{grow} obtained, the concentration-time profile from t = 0-180 minutes can be simulated and fit to the experimentally measured values by changing only k_{nuc}. Best fits of dissolution-precipitation model are shown in (Figure 4.10) and show good agreement with the experimental profiles. Root mean square error values calculated for the KTZ cocrystals can be found in Table 4.5 and are of similar magnitudes as the experimental concentration standard deviations. There are limitations to the model shown by the overprediction of the maximum concentrations and underprediction of the exponentially decreasing portion of the curves that indicate modifications are necessary to improve predictions of the concentration-time profiles.

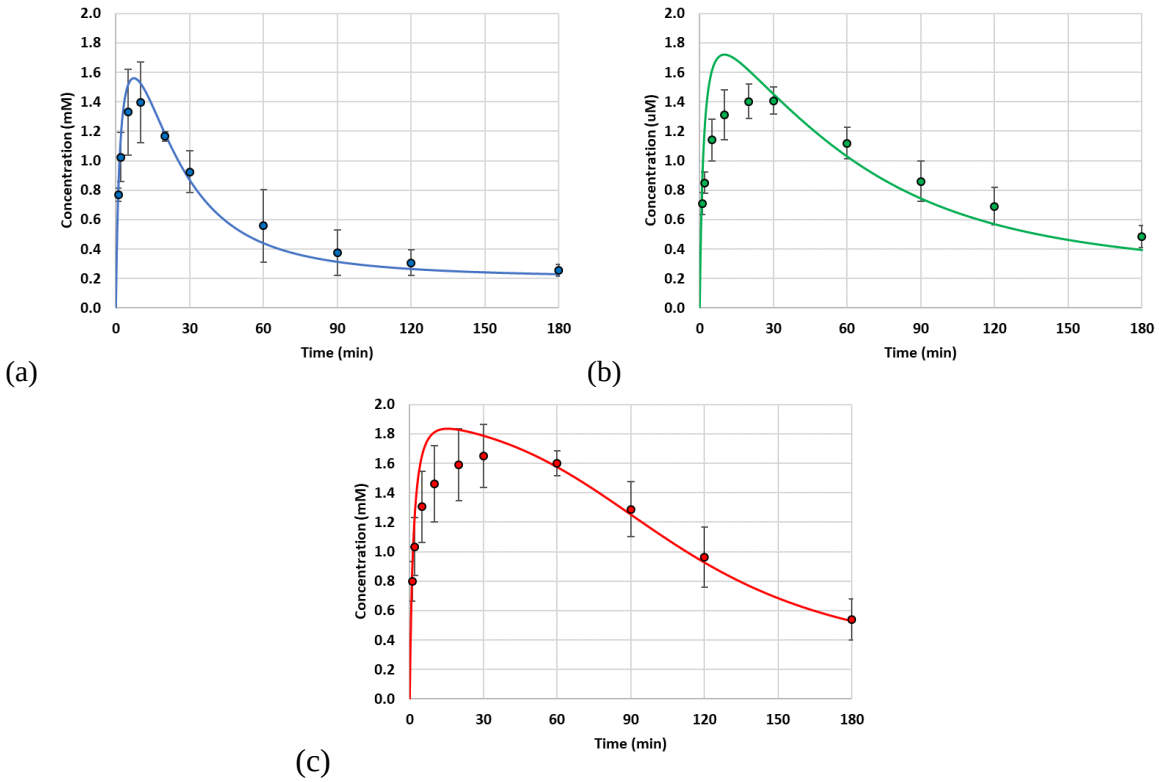

Figure 4.10: Simulations of (a) KTZ-ADP (—), (b) KTZ-FUM (—), and (c) KTZ-SUC (—) fit to measured concentration-time profiles for KTZ-ADP (●), (b) KTZ-FUM (●), and (c) KTZ-SUC (●) dissolution in blank FeSSIF using k_{grow}, k_{nuc}, and α values from Tables 4.4 and 4.5.

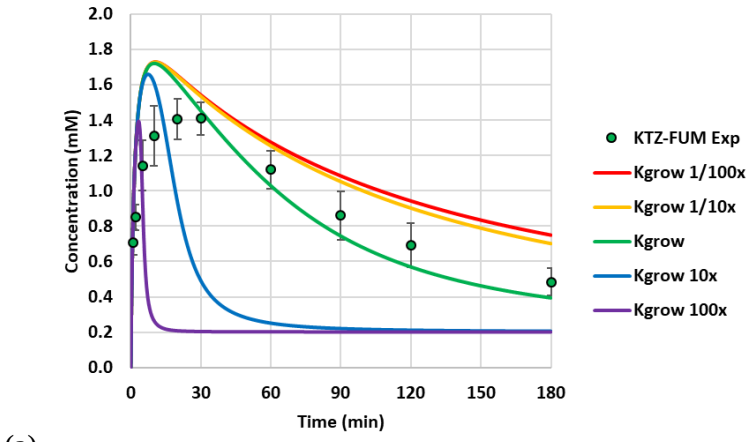

(a)

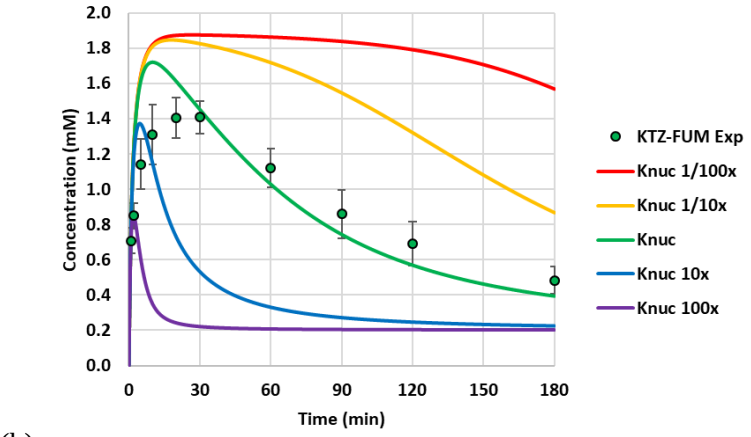

(b)

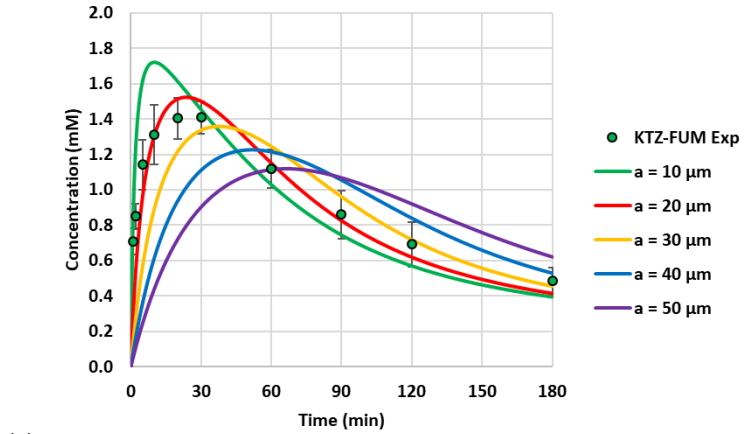

(c)

Figure 4.11: Sensitivity analyses of KTZ-FUM dissolution simulation (—) in blank FeSSIF changing (a) growth rate constant, (b) nucleation rate constant, or (c) particle size. (a,b) Values of k_{nuc} and k_{grow} multiplied by 1/100- (—), 1/10- (—), 10- (—), 100-fold (—) the obtained value. (c) Particle sizes used were 10 µm (—), 20 µm (—), 30 µm (—), 40 µm (—), and 50 µm (—). Measured concentrations of KTZ-FUM (●) in blank FeSSIF shown for reference.

Table 4.5: Nucleation rate constants and root mean square error (RMSE) values obtained from cocrystal dissolution experiments in blank FeSSIF.

	k_{nuc} ($\mu M^{-(1-\alpha)} min^{-1}$)	α	RMSE (μM)
KTZ-ADP	9.39×10^{-4}	1.44	97.6
KTZ-FUM	8.57×10^{-5}	1.63	252.5
KTZ-SUC	6.85×10^{-6}	1.71	191.6

Sensitivity analyses of the dissolution-precipitation simulations were undertaken to explore how changes in k_{grow}, k_{nuc}, and particle size affected the concentration-time profiles. Increasing k_{grow} (Figure 4.11a) does not greatly change the maximum concentration (C_{max}) or the time of the maximum (t_{max}) as these values range over 0.3 mM and between t = 5 and 15 minutes, respectively, however the concentrations in the precipitation interval ($t_{max} < t < \infty$) more rapidly decrease. If k_{nuc} is increased (Figure 4.11b), C_{max} and t_{max} both decrease and show a much larger range of values than seen in the k_{grow} sensitivity analysis. Changing dissolution rates by increasing particle size (Figure 4.11c) creates a slower dissolution rate associated with smaller values of C_{max} and later values of t_{max}.

Discussion

The ability to estimate the interfacial pH of KTZ cocrystal has been shown previously for rotating disk dissolution in solution void of buffering species[8]. Ignoring the effects of buffer limits the variables needed to be considered in the development of a mechanistic dissolution theory, however, does not represent biorelevant conditions. To estimate the dissolution rates of KTZ cocrystals under intestinally relevant, *in vitro* conditions tested by Chen et al.[12], more complexity must be added to the dissolution theory to account for buffer and its effect on cocrystal interfacial solubility. Previous work has shown that KTZ cocrystals are able to stabilize their interfacial pH lower than that of intestinal bulk pH ranges (Figure 4.2). Buffer limits this ability of the cocrystal and raises the interfacial pH plateau as buffer increases (Figure 4.3). Rough estimates of the

interfacial pH of a cocrystal dissolving in a dissolution buffer could potentially be estimated by a surrogate measurement of the pH_{eq} of a cocrystal solubility experiment as evidenced by the proximity of these values to estimated pH_o values (Figures 4.2 & 4.3). The estimated pH_o for blank FeSSIF and the measured pH_{eq} are within 0.5 pH units. There is a caveat to the pH_{eq} estimate of pH_o as the concentrations that are measured at equilibrium are not equal to those assumed at the interface. In the case of KTZ cocrystals, the pH_{eq} value will always underestimate pH_o due to concentrations of acidic coformer being higher and basic drug lower than stoichiometric concentrations assumed at the interface (Figure 4.4). Knowledge of this difference can allow for a more accurate estimation of pH_o from pH_{eq} and provide a practical estimate for calculating dissolution rates from data potentially previously generated in the cocrystal development process.

Calculations of the dissolution rates in FeSSIF were made using buffered estimates of pH_o. The particle sizes of the cocrystals used in the experiments were not provided and the sieving protocol from Chen et al[11]. was recreated to measure the particles isolated from the appropriate sieve cuts. The particles were equant aiding the assumption of a spherical equivalent particle size that was obtained via brightfield microscopy. An approximate monodisperse particle radius based on a mass median average radius (R50) was calculated for each KTZ cocrystal (Table 4.2) due to the particle size distributions observed. These particle radii and their respective pH_o values were combined to calculate the diffusive flux that could be achieved by a cocrystal in FeSSIF. Applying this flux to Higuchi-Hiestand particle dissolution theory was able to generate a dissolution simulation that is in great agreement with the measured concentration-time profiles measured for the three KTZ cocrystals in FeSSIF (Figure 4.6).

Using the same approach, the particle dissolution theory was also applied to the conditions for blank FeSSIF. Again, the simulations of concentration-time profiles agreed with experimental

results from blank FeSSIF as the concentrations of FUM were within a standard deviation of the simulated profile (Figure 4.8b). The first two drug time points matched simulations of all KTZ cocrystals but after five minutes of dissolution, bulk precipitation caused measured concentrations lower than simulations (Figure 4.8). Addition of terms for bulk nucleation and growth of the parent drug would be needed in order to simulate complete drug concentration profiles in blank FeSSIF dissolution experiments.

A combined dissolution and precipitation mathematical theory proposed by Jakubiak et al explains precipitation of poorly soluble drugs from solution according to their nucleation and growth. Terms were modified to be used in conjunction with the Higuchi-Hiestand particle dissolution theory to simulate experimental solution concentrations measured in blank FeSSIF. The values for the nucleation and growth rate constants were the only fitted values as the molecularity index was already found for the KTZ cocrystals in unpublished work within the Rodríguez lab. The unknown k_{grow} value for blank FeSSIF was obtained first by fitting the exponentially decreasing concentration-time profile of the KTZ cocrystal dissolution experiments (Figure 4.9). This assumed the contributions of nucleation to the decreasing drug concentrations were negligible and growth was the dominant term at these saturations.

A fitted value for k_{grow} allowed the complete experimental concentration-time profiles to be fit to equations (4.35-4.37) by optimizing the value of k_{nuc}. The results found in (Figure 4.10) show that this process has merit to obtain a simulation that has good agreement with previously generated KTZ dissolution data as a majority of simulation residuals are within experimental standard deviations. Discrepancies in the simulation and the experimental concentration profiles such as the overpredictions of C_{max} and slight underprediction of the later concentration time points show the limitations of the assumptions of the model. This suggests that nucleation event of the

drug is stronger than the model predicts early in the generation of supersaturation and, once stable nuclei are present, growth drives the decrease in solution concentrations seen. Further iterations of the equations and assumptions could be modified to account for these more real-world mechanisms of crystal nucleation and growth.

Conclusions

This work has shown the potential of pH_o estimations to calculate the profiles of cocrystal particle dissolution in biorelevant dissolution media. Knowledge gained from a solubility experiment is enough to allow for a simulation of cocrystal dissolution rate. The solubility experiment provides a K_{sp} and pH_o estimate in the form of its pH_{eq} that could be applied to the dissolution theory proposed in this work for a preliminary estimate of dissolution rate before *in vitro* or *in vivo* testing. The dissolution theory proposed in this study has simplifying assumptions that do not wholly translate to real world situations and further refinements of this model with hydrodynamic conscious particle dissolution theories like Wang-Flanagan[25] or accounting for particle size distributions could be added.

This work has also shown the ability of a modified dissolution-precipitation model to simulate the concentration time profiles of cocrystals in a dissolution experiment. Combining the dissolution theory with terms for both nucleation and growth create a relatively simple model for simulating the solution kinetics of cocrystals. This approach is a foundation that can be built upon with modifications and better assumptions for biorelevant conditions that could more accurately fit cocrystal dissolution profiles. Also, further work to estimate k_{nuc} and k_{grow} values from theory could allow for simulations of amounts of drug available for absorption before any benchtop experiment. This could limit the amount of wasteful experiments done in the development process and save both time and resources in the development of a viable cocrystal system.

Acknowledgements

The authors acknowledge the financial support from the University of Michigan College of Pharmacy.

References

1. Childs, S.L., P. Kandi, and S.R. Lingireddy, *Formulation of a Danazol Cocrystal with Controlled Supersaturation Plays an Essential Role in Improving Bioavailability.* Molecular Pharmaceutics, 2013. **10**(8): p. 3112-3127.
2. Bak, A., et al., *The co-crystal approach to improve the exposure of a water-insoluble compound: AMG 517 sorbic acid co-crystal characterization and pharmacokinetics.* Journal of Pharmaceutical Sciences, 2008. **97**(9): p. 3942-3956.
3. Smith, A.J., et al., *Cocrystals of Quercetin with Improved Solubility and Oral Bioavailability.* Molecular Pharmaceutics, 2011. **8**(5): p. 1867-1876.
4. Cheney, M.L., et al., *Effects of Crystal Form on Solubility and Pharmacokinetics: A Crystal Engineering Case Study of Lamotrigine.* Crystal Growth & Design, 2010. **10**(1): p. 394-405.
5. Cheney, M.L., et al., *Coformer Selection in Pharmaceutical Cocrystal Development: a Case Study of a Meloxicam Aspirin Cocrystal That Exhibits Enhanced Solubility and Pharmacokinetics.* Journal of Pharmaceutical Sciences, 2011. **100**(6): p. 2172-2181.
6. Stanton, M.K., et al., *Improved Pharmacokinetics of AMG 517 Through Co-crystallization Part 2: Analysis of 12 Carboxylic Acid Co-crystals.* Journal of Pharmaceutical Sciences, 2011. **100**(7): p. 2734-2743.
7. Cao, F.J., et al., *Mechanistic Analysis of Cocrystal Dissolution as a Function of pH and Micellar Solubilization.* Molecular Pharmaceutics, 2016. **13**(3): p. 1030-1046.
8. Cao, F.J., N. Rodriguez-Hornedo, and G.E. Amidon, *Mechanistic Analysis of Cocrystal Dissolution, Surface pH, and Dissolution Advantage as a Guide for Rational Selection.* Journal of Pharmaceutical Sciences, 2019. **108**(1): p. 243-251.
9. Fick, A., *Ueber diffusion.* Annalen der Physik, 1855. **170**(1): p. 59-86.
10. Brunner, E., *Reaktionsgeschwindigkeit in heterogenen Systemen*. 1903: Georg-Augusts-Universitat, Gottingen.
11. Chen, Y.M. and N. Rodríguez-Hornedo, *Cocrystals Mitigate Negative Effects of High pH on Solubility and Dissolution of a Basic Drug.* Crystal Growth & Design, 2018. **18**(3): p. 1358-1366.
12. Chen, Y.M. and University of Michigan. Pharmaceutical Sciences., *Cocrystals Mitigate the Effect of pH on Solubility and Dissolution of Basic Drugs*. 2017, ProQuest Dissertations & Theses: Ann Arbor. p. 216 p.
13. Ruff, A., T. Fiolka, and E.S. Kostewicz, *Prediction of Ketoconazole absorption using an updated in vitro transfer model coupled to physiologically based pharmacokinetic modelling.* European Journal of Pharmaceutical Sciences, 2017. **100**: p. 42-55.

14. Kostewicz, E.S., et al., *Predicting the precipitation of poorly soluble weak bases upon entry in the small intestine.* Journal of Pharmacy and Pharmacology, 2004. **56**(1): p. 43-51.

15. Kambayashi, A., T. Yasuji, and J.B. Dressman, *Prediction of the precipitation profiles of weak base drugs in the small intestine using a simplified transfer ("dumping") model coupled with in silico modeling and simulation approach.* European Journal of Pharmaceutics and Biopharmaceutics, 2016. **103**: p. 95-103.

16. Jakubiak, P., et al., *Development of a Unified Dissolution and Precipitation Model and Its Use for the Prediction of Oral Drug Absorption.* Molecular Pharmaceutics, 2016. **13**(2): p. 586-598.

17. Higuchi, W.I. and E.N. Hiestand, *Dissolution rates of finely divided drug powders. I. Effect of a distribution of particle sizes in a diffusion-controlled process.* J Pharm Sci, 1963. **52**: p. 67-71.

18. Amidon, G.E., W.I. Higuchi, and N.F. Ho, *Theoretical and experimental studies of transport of micelle-solubilized solutes.* J Pharm Sci, 1982. **71**(1): p. 77-84.

19. Jakubiak, P., et al., *Development of a Unified Dissolution and Precipitation Model and Its Use for the Prediction of Oral Drug Absorption.* Molecular Pharmaceutics, 2016. **13**(2): p. 586-598.

20. Nielsen, A.E., *RATE LAWS AND RATE CONSTANTS IN CRYSTAL-GROWTH.* Croatica Chemica Acta, 1987. **60**(3): p. 531-539.

21. Serajuddin, A.T.M. and C.I. Jarowski, *Effect of diffusion layer pH and solubility on the dissolution rate of pharmaceutical acids and their sodium salts II: Salicylic acid, theophylline, and benzoic acid.* Journal of Pharmaceutical Sciences, 1985. **74**(2): p. 148-154.

22. Good, D.J. and N. Rodriguez-Hornedo, *Cocrystal Eutectic Constants and Prediction of Solubility Behavior.* Crystal Growth & Design, 2010. **10**(3): p. 1028-1032.

23. Good, D.J. and N. Rodriguez-Hornedo, *Solubility Advantage of Pharmaceutical Cocrystals.* Crystal Growth & Design, 2009. **9**(5): p. 2252-2264.

24. Roy, L., M.P. Lipert, and N. Rodriguez-Hornedo, *Co-crystal Solubility and Thermodynamic Stability*, in *Pharmaceutical Salts and Co-Crystals*, J. Wouters and L. Quere, Editors. 2011, Royal Soc Chemistry: Cambridge. p. 247-279.

25. Wang, J.Z. and D.R. Flanagan, *General solution for diffusion controlled dissolution of spherical particles. 1. Theory.* Journal of Pharmaceutical Sciences, 1999. **88**(7): p. 731-738.

Appendix 4A

Berkeley Madonna codes for FeSSIF dissolution simulations.

KTZ-ADP

```
METHOD RK4
STARTTIME=0
STOPTIME=180
DT=0.1
;dissolved compound
d/dt(C1) = (1 / V) * (3 * M * DaqB*60) / (p * a^2) * ( Scc - C1)
d/dt(M) = -(3 * M * DaqB*60) / (p*1000 * a^2) * ( Scc - C1 )
;initial conditions
Init(C1) = 0 ; dissolved uM
Init(M) =  5.64515e1; solidundissolved umol
;cocrystal solubility
Scc = (Ksp * (1 + (KsA*mic) + (Ka1A / H0) + (Ka1A * Ka2A / H0^2)) * (1 + (KsB*mic) + (H0
/ Ka2B) + (H0^2 / Ka1B / Ka2B)))^(1 / 2)
;parameters [ADP FeSSIF]
Ksp = 3.4e4 ; uM^2
Ka1A = 3.63078e-5
Ka2A = 3.63078e-6
Ka1B = 1.15e-3
Ka2B = 3.09e-7
KsA = 0
KsB = 0.0144 ; uM-1
H0 = 1.023e-5
Hb = 1e-5
DaqB = 1.69e-6; cm^2/s
```

V = 30 ; cm^3

a = 0.001 ; cm

p = 2634.40; umol/cm^3

mic = 15000 ;uM

KTZ-FUM

METHOD RK4

STARTTIME=0

STOPTIME=180

DT=0.1

;dissolved compound

d/dt(C1) = (1 / V) * (3 * M * DaqB*60) / (p * a^2) * (Scc - C1)

d/dt(M) = -(3 * M * DaqB*60) / (p*1000 * a^2) * (Scc - C1)

;initial conditions

Init(C1) = 0; dissolved uM

Init(M) = 5.64515e1; solidundissolved umol

;cocrystal solubility

Scc = (Ksp * (1 + (KsA*mic) + (Ka1A / H0) + (Ka1A * Ka2A / H0^2)) * (1 + (KsB*mic) + (H0 / Ka2B) + (H0^2 / Ka1B / Ka2B)))^(1 / 2)

;parameters [FUM FeSSIF]

Ksp = 1.5e3; uM^2

Ka1A = 9.33e-4

Ka2A = 4.17e-5

Ka1B = 1.15e-3

Ka2B = 3.09e-7

KsA = 2.9e-5; uM-1

KsB = 0.0144; uM-1

H0 = 1.09648e-05

Hb = 1e-5

DaqB = 1.69e-6; cm^2/s

V = 30; cm^3

a = 0.001 ; cm

p = 2634.40; umol/cm^3

mic = 15000; uM

KTZ-SUC

METHOD RK4

STARTTIME=0

STOPTIME=180

DT=0.1

;dissolved compound

d/dt(C1) = (1 / V) * (3 * M * DaqB*60) / (p * a^2) * (Scc - C1)

d/dt(M) = -(3 * M * DaqB*60) / (p*1000 * a^2) * (Scc - C1)

;initial conditions

Init(C1) = 0; dissolved uM

Init(M) = 5.64515e1; solidundissolved umol

;cocrystal solubility

Scc = (Ksp * (1 + (KsA*mic) + (Ka1A / H0) + (Ka1A * Ka2A / H0^2)) * (1 + (KsB*mic) + (H0 / Ka2B) + (H0^2 / Ka1B / Ka2B)))^(1 / 2)

;parameters [SUC FeSSIF]

Ksp = 2.7e4; uM^2

Ka1A = 6.17e-5

Ka2A = 2.34e-6

Ka1B = 1.15e-3

Ka2B = 3.09e-7

KsA = 9.5e-6; uM-1

KsB = 0.0144; uM-1

H0 = 1.023e-5

Hb = 1e-5

DaqB = 1.69e-6; cm^2/s

V = 30; cm^3

a = 0.001; cm

p = 2634.40; umol/cm^3

mic = 15000; uM

Berkeley Madonna codes for blank FeSSIF dissolution simulations.

KTZ-ADP

```
METHOD RK4
STARTTIME=0
STOPTIME=180
DT=0.1
;dissolved compound
d/dt(C1) = (1 / V) * (3 * M * DaqB*60) / (p * a^2) * ( Scc - C1)
d/dt(M) = -(3 * M * DaqB*60) / (p*1000 * a^2) * ( Scc - C1 )
;initial conditions
Init(C1) = 0 ;dissolved uM
Init(M) = 5.64515e1; solidundissolved umol
;cocrystal solubility
Scc = (Ksp * (1 + (KsA*mic) + (Ka1A / H0) + (Ka1A * Ka2A / H0^2)) * (1 + (KsB*mic) + (H0
/ Ka2B) + (H0^2 / Ka1B / Ka2B)))^(1 / 2)
;parameters [ADP FeSSIF]
Ksp = 3.4e4; uM^2
Ka1A = 3.63078e-5
Ka2A = 3.63078e-6
Ka1B = 1.15e-3
Ka2B = 3.09e-7
KsA = 0
KsB = 0.0144; uM-1
H0 = 1.023e-5
Hb = 1e-5
DaqB = 3.81e-6; cm^2/s
V = 30; cm^3
a = 0.001; cm
p = 2634.40; umol/cm^3
mic = 0; uM
```

KTZ-FUM

METHOD RK4

STARTTIME=0

STOPTIME=180

DT=0.1

;dissolved compound

d/dt(C1) = (1 / V) * (3 * M * DaqB*60) / (p * a^2) * (Scc - C1)

d/dt(M) = -(3 * M * DaqB*60) / (p*1000 * a^2) * (Scc - C1)

;initial conditions

Init(C1) = 0; dissolved uM

Init(M) = 5.64515e1; solidundissolved umol

;cocrystal solubility

Scc = (Ksp * (1 + (KsA*mic) + (Ka1A / H0) + (Ka1A * Ka2A / H0^2)) * (1 + (KsB*mic) + (H0 / Ka2B) + (H0^2 / Ka1B / Ka2B)))^(1 / 2)

;parameters [FUM FeSSIF]

Ksp = 1.5e3; uM^2

Ka1A = 9.33e-4

Ka2A = 4.17e-5

Ka1B = 1.15e-3

Ka2B = 3.09e-7

KsA = 2.9e-5; uM-1

KsB = 0.0144; uM-1

H0 = 1.09648e-05

Hb = 1e-5

DaqB = 3.81e-6; cm^2/s

V = 30; cm^3

a = 0.001; cm

p = 2634.40; umol/cm^3

mic = 0; uM

KTZ-SUC

METHOD RK4

STARTTIME=0

STOPTIME=180

DT=0.1

;dissolved compound

d/dt(C1) = (1 / V) * (3 * M * DaqB*60) / (p * a^2) * (Scc - C1)

d/dt(M) = -(3 * M * DaqB*60) / (p*1000 * a^2) * (Scc - C1)

;initial conditions

Init(C1) = 0; dissolved uM

Init(M) = 5.64515e1; solidundissolved umol

;cocrystal solubility

Scc = (Ksp * (1 + (KsA*mic) + (Ka1A / H0) + (Ka1A * Ka2A / H0^2)) * (1 + (KsB*mic) + (H0 / Ka2B) + (H0^2 / Ka1B / Ka2B)))^(1 / 2)

;parameters [SUC FeSSIF]

Ksp = 2.7e4; uM^2

Ka1A = 6.17e-5

Ka2A = 2.34e-6

Ka1B = 1.15e-3

Ka2B = 3.09e-7

KsA = 9.5e-6; uM-1

KsB = 0.0144; uM-1

H0 = 1.023e-5

Hb = 1e-5

DaqB = 3.81e-6; cm^2/s

V = 30; cm^3

a = 0.001; cm

p = 2634.40; umol/cm^3

mic = 0; uM

Berkeley Madonna codes for blank FeSSIF crystal growth fitting

KTZ-ADP

```
METHOD RK4
STARTTIME=90
STOPTIME=180
DT=0.1
;dissolved compound
d/dt(C1) = - (kgrow * As * (1/(V/1000)) * ((C1-Css))^b)
d/dt(As) = (kgrow * As * ((C1-Css))^b)
;initial conditions
Init(C1) = 376.65372; dissolved uM
Init(As) = 50.1115426 ; solidundissolved uM
;drug solubility
Css = So * (1 + (KsB*mic) + (Hb / Ka2B) + (Hb^2 / (Ka1B * Ka2B)))
;parameters [ADP Blank FeSSIF]
Ka1B = 6.76e-3
Ka2B = 2.34e-7
KsB=0.0144; uM-1
Hb = 1e-5
mic = 0
V = 30; cm^3
So = 4.7e0; uM
kgrow = 8.49e-6; uM-1*min-1
b = 1.5
```

KTZ-FUM

METHOD RK4

STARTTIME=90

STOPTIME=180

DT=0.01

;dissolved compound

d/dt(C1) = - (kgrow * As * (1/(V/1000)) * ((C1-Css))^b)

d/dt(As) = (kgrow * As * ((C1-Css))^b)

;initial conditions

Init(C1) = 860.31; dissolved uM

Init(As) = 33.989; solidundissolved uM

;drug solubility

Css = So * (1 + (KsB*mic) + (Hb / Ka2B) + (Hb^2 / (Ka1B * Ka2B)))

;parameters [FUM Blank FeSSIF]

Ka1B = 6.76E-04

Ka2B = 2.34E-07

KsB=0.0144; uM-1

Hb = 1e-5

V = 30; cm^3

So = 4.7e0; uM

mic = 0; uM

kgrow =3.46e-7; uM^-1*min^-1

b = 1.5

KTZ-SUC

METHOD RK4

STARTTIME=90

STOPTIME=180

DT=0.1

;dissolved compound

d/dt(C1) = - (kgrow * As * (1/(V/1000)) * ((C1-Css))^b)

d/dt(As) = (kgrow * As * ((C1-Css))^b)

;initial conditions

Init(C1) = 1287.357559; dissolved uM

Init(As) = 19.7547; solidundissolved uM

;drug solubility

Css = So * (1 + (KsB*mic) + (Hb / Ka2B) + (Hb^2 / (Ka1B * Ka2B)))

;parameters [SUC Blank FeSSIF]

Ka1B = 6.76E-04

Ka2B = 2.34E-07

KsB = 0.0144; uM-1

Hb = 1e-5

V = 30; cm^3

So = 4.7e0; uM

mic = 0

kgrow = 4.90e-7; uM-1min-1

b=1.5

Berkeley Madonna Codes for blank FeSSIF dissolution-precipitation simulations.

KTZ-ADP

```
METHOD RK4
STARTTIME=0
STOPTIME=180
DT=0.1
;dissolved compound
d/dt(C1) = IF TIME < 0.2 THEN ((3 * M * DaqB*60) / (V*p* a^2) * ( Scc - C1 )) ELSE (3 * M * DaqB*60) / (V*p* a^2) * ( Scc - C1 ) - (kgrow * As * (1/(V/1000)) * ((C1-Css))^b) - (knuc * (C1-Css)^q)
d/dt(As) = IF TIME < 0.2 THEN 0 ELSE (kgrow * As * ((C1-Css))^b) + ((V/1000) * knuc * (C1-Css)^q)
d/dt(M) = -(3 * M * DaqB*60) / (p * 1000 * a^2) * ( Scc - C1 )
;initial conditions
Init(C1) = 0; dissolved uM
Init(As) = 0; solidundissolved uM
Init(M) = 56.4459; solidundissolved umol
;cocrystal solubility
Scc = (Ksp * (1 + (KsA*mic) + (Ka1A / H0) + (Ka1A * Ka2A / H0^2)) * (1 + (KsB*mic) + (H0 / Ka2B) + (H0^2 / Ka1B / Ka2B)))^(1 / 2)
;drug solubility
Css = So * (1 + (KsB*mic) + (Hb / Ka2B) + (Hb^2 / (Ka1B * Ka2B)))
;parameters [ADP Blk FeSSIF]
Ksp = 3.4e4; uM^2
Ka1A = 3.63078e-5
Ka2A = 3.63078e-6
Ka1B = 1.15e-3
Ka2B = 3.09e-7
KsA = 0
KsB = 0.0144; uM-1
```

H0 = 1.6982e-5

Hb = 1e-5

DaqA = 9.95e-6; cm^2/s

DaqB = 3.81e-6; cm^2/s

V = 30; cm^3

a = 0.001; cm

p = 2634.40; umol/cm^3

So = 6e0; uM

mic = 0; uM

kgrow = 8.4901e-7

knuc = 9.39e-4

q = 1.44015

b = 1.5

KTZ-FUM

METHOD RK4

STARTTIME = 0

STOPTIME = 180

DT = 0.1

;dissolved compound

d/dt(C1) = IF TIME < 0.2 THEN ((3 * M * DaqB*60) / (V*p* a^2) * (Scc - C1)) ELSE (3 * M * DaqB*60) / (V*p* a^2) * (Scc - C1) - (kgrow * As * (1/(V/1000)) * ((C1-Css))^b) - (knuc * (C1-Css)^q)

d/dt(As) = IF TIME < 0.2 THEN 0 ELSE (kgrow * As * ((C1-Css))^b) + ((V/1000) * knuc * (C1-Css)^q)

d/dt(M) = -(3 * M * DaqB*60) / (p * 1000 * a^2) * (Scc - C1)

;initial conditions

Init(C1) = 0; dissolved uM

Init(As) = 0; solidundissolved uM

Init(M) =56.4459; solidundissolved umol

;cocrystal solubility

Scc = (Ksp * (1 + (KsA*mic) + (Ka1A / H0) + (Ka1A * Ka2A / H0^2)) * (1 + (KsB*mic) + (H0 / Ka2B) + (H0^2 / Ka1B / Ka2B)))^(1 / 2)

;drug solubility

Css = So * (1 + (KsB*mic) + (Hb / Ka2B) + (Hb^2 / (Ka1B * Ka2B)))

;parameters [FUM Blank FeSSIF]

Ksp = 1.5e3; uM^2

Ka1A = 9.33e-4

Ka2A = 4.17e-5

Ka1B = 1.15e-3

Ka2B = 3.09e-7

KsA = 2.9e-5; uM-1

KsB = 0.0144; uM-1

H0 = 7.90679e-5

Hb = 1e-5

DaqA = 9.95e-6; cm^2/s

DaqB = 3.81e-6; cm^2/s

V = 30; cm^3

a = 0.001; cm

p = 2634.40; umol/cm^3

So = 6.0e0; uM

mic = 0; uM

kgrow = 3.457e-7; uM^-1*min^-1

knuc = 8.5734e-5; uM^(1-q)*min^-1

q = 1.62804

b = 1.5

KTZ-SUC

METHOD RK4

STARTTIME = 0

STOPTIME = 180

DT = 0.1

;dissolved compound

d/dt(C1) = IF TIME < 0.2 THEN ((3 * M * DaqB*60) / (V*p* a^2) * (Scc - C1)) ELSE (3 * M * DaqB*60) / (V*p* a^2) * (Scc - C1) - (kgrow * As * (1/(V/1000)) * ((C1-Css))^b) - (knuc * (C1-Css)^q)

d/dt(As) = IF TIME < 0.2 THEN 0 ELSE (kgrow * As * ((C1-Css))^b) + ((V/1000) * knuc * (C1-Css)^q)

d/dt(M) = -(3 * M * DaqB*60) / (p * 1000 * a^2) * (Scc - C1)

;initial conditions

Init(C1) = 0; dissolved uM

Init(As) = 0 ; solidundissolved uM

Init(M) = 56.4459; solidundissolved umol

;cocrystal solubility

Scc = (Ksp * (1 + (KsA*mic) + (Ka1A / H0) + (Ka1A * Ka2A / H0^2)) * (1 + (KsB*mic) + (H0 / Ka2B) + (H0^2 / Ka1B / Ka2B)))^(1 / 2)

;drug solubility

Css = So * (1 + (KsB*mic) + (Hb / Ka2B) + (Hb^2 / (Ka1B * Ka2B)))

;parameters [SUC Blank FeSSIF]

Ksp = 2.7e4; uM^2

Ka1A = 6.17e-5

Ka2A = 2.34e-6

Ka1B = 1.15e-3

Ka2B = 3.09e-7

KsA = 9.5e-6; uM-1

KsB = 0.0144; uM-1

H0 = 2.1877e-5

Hb = 1e-5

DaqA = 9.95e-6; cm^2/s

DaqB = 3.81e-6; cm^2/s

V = 30; cm^3

a = 0.001; cm

p = 2634.40; umol/cm^3

So = 6e0; uM

mic = 0

kgrow = 4.9021e-7

knuc = 6.8473e-6

b = 1.5

q = 1.7136

CHAPTER V

Cocrystal Particle Dissolution Simulations in the Presence of an Absorption Compartment

Introduction

Cocrystals are a great tool for generating supersaturation and boosting the oral performance of a poorly soluble drug[1-5]. For this reason, cocrystals are a viable formulation strategy for a Biopharmaceutics Classification System (BCS) class II drug molecules that have good ability to permeate lipid membranes but do not have intestinal concentrations high enough to drive absorption due to poor solubility. The generation of supersaturation is associated with precipitation which adds more variables to an already complicated set of solution equilibria. This has led to cocrystal *in vitro* dissolution experiments not aligning with *in vivo* plasma concentrations[6, 7]. Due to the lack of understanding of cocrystal precipitation rates, experimental studies test entire libraries of cocrystals *in vitro* and *in vivo* to assess if an absorption advantage exists[7]. The ability to simulate cocrystal kinetic solution concentrations controlled by dissolution, supersaturation, and precipitation, could limit the number of experiments needed on cocrystal libraries to select the best performing candidate. Eliminating poorly performing cocrystals before starting benchtop or animal experiments could save time and resources in the development of a cocrystal product.

Mathematical expressions capable of simulating cocrystal dissolution for rotating disk (Chapter 2) and particle dissolution (Chapter 4) have been explored for ketoconazole (KTZ)

cocrystals with adipic (ADP), fumaric (FUM), and succinic (SUC) acids. Expressions for the processes of precipitation in biorelevant dissolution media (Chapter 4), and partitioning mass transport into an absorption compartment (Chapter 2) have also been independently studied. This work aims to unite the expressions for particle dissolution, precipitation, and biphasic partitioning previously independently developed to explore the interplay of these processes in controlling amounts of drug that could be absorbed from cocrystals.

Methods

Cocrystal Particle Biphasic Dissolution and Precipitation Simulations

Simulations of cocrystal particle dissolution in a biphasic system were performed using Berkeley Madonna Software (version 9.1.18). Runge-Kutta 4th order method with time steps of 0.1 minutes was used to simulate cocrystal dissolution, precipitation, and partitioning under a biphasic scenario over 180 minutes according to the dependent differential equations (5.11-5.14). Initial conditions, variable values, and codes used for simulations can be found in Appendix 5A.

Theoretical

Cocrystal Dissolution, Precipitation, and Partitioning Simulations

To simulate cocrystal dissolution behavior in an absorption environment, expressions for the fundamental processes that control solution concentrations must be derived. A simple two-compartment model where the rates of change in bulk concentrations of the donor compartment ($C_{b,d}$) are assumed to be a function of three terms

$$\frac{dC_{b,d}}{dt} = Dissolution - Precipitation - Absorption \quad (5.1)$$

where 1) dissolution adds to and 2) precipitation and 3) absorption detract from $C_{b,d}$. In the biphasic system, mass balance is assumed to be maintained. Every molecule that leaves the donor

compartment, must be accounted for in the receiver compartment and the bulk concentration of the receiver phase ($C_{b,r}$) is defined as

$$\frac{dC_{b,r}}{dt} = Absorption \tag{5.2}$$

where the only mass added to the compartment comes from absorption from the donor phase. Terms for these three processes have been defined in previous chapters of this dissertation and can be combined to simulate a proposed scenario of KTZ cocrystal particle dissolution in a biphasic system. Particle dissolution of a cocrystal was previously derived in Chapter 4 and is defined as a mass balanced set of paired differential equations

$$\frac{dC_{b,d}}{dt} = \frac{3MD_{aq}}{a^2\rho V_d}(S_{cc} - C_{b,d}) \tag{5.3}$$

$$\frac{dM}{dt} = -\frac{3MD_{aq}}{a^2\rho}(S_{cc} - C_{b,d}) \tag{5.4}$$

where dissolution rate is a function of the particle surface area expressed in terms of mass available for dissolution (M), particle radius (a), solid density (ρ), and the solubility of the dissolving cocrystal (S_{cc}) in the donor phase volume (V_d). In the case of KTZ cocrystals, assuming sink conditions, the solubility expression can be substituted into equation (5.3-5.4) to create

$$\frac{dC_{b,d}}{dt} = \frac{3MD_{aq}}{a^2\rho V_d}\sqrt{K_{sp}(1 + \frac{[H^+]_0}{K_{a2}^B} + \frac{[H^+]_0^2}{K_{a1}^B K_{a2}^B})(1 + \frac{K_{a1}^{H_2A}}{[H^+]_0} + \frac{K_{a1}^{H_2A}K_{a2}^{H_2A}}{[H^+]_0^2})} \tag{5.5}$$

$$\frac{dM}{dt} = -\frac{3MD_{aq}}{a^2\rho}\sqrt{K_{sp}(1 + \frac{[H^+]_0}{K_{a2}^B} + \frac{[H^+]_0^2}{K_{a1}^B K_{a2}^B})(1 + \frac{K_{a1}^{H_2A}}{[H^+]_0} + \frac{K_{a1}^{H_2A}K_{a2}^{H_2A}}{[H^+]_0^2})} \tag{5.6}$$

which describes dissolution rate in terms of the solubility product (K_{sp}), the dissociation constants for the dibasic drug (K_{a1}^B, K_{a2}^B) and diprotic coformer ($K_{a1}^{H_2A}, K_{a2}^{H_2A}$), and the interfacial proton concentration ($[H^+]_0$). In Chapter 4, the term for precipitation was split into nucleation and growth and defined as,

$$Precipitation = Nucleation + Growth \tag{5.7}$$

$$Nucleation\ Rate = \frac{dC_{b,d}}{dt} = -k_{nuc}(C_{b,d} - S_{drug})^{\alpha} \tag{5.8}$$

$$Growth\ Rate = \frac{dC_{b,d}}{dt} = -\frac{k_{grow}A_s}{V_d}\left(C_{b,d} - S_{drug}\right)^{1.5} \tag{5.9}$$

where nucleation rate is a function of supersaturation $\left(C_{b,d} - S_{drug}\right)$, molecularity index ($\alpha$), and nucleation rate constant (k_{nuc}). Likewise, growth rate is a function of supersaturation, growth rate constant (k_{grow}) and the surface area of precipitated drug (A_s).

Absorption of the drug into the receiver phase is the last process to define in order to simulate cocrystal dissolution in a biphasic scenario. Chapter 2 defined the absorption term as

$$Absorption = \frac{dC_{b,r}}{dt} = \frac{A}{V_r}k_p\Delta C = -\frac{dC_{b,d}}{dt} = -\frac{A}{V_d}k_p\Delta C \tag{5.10}$$

in which the rate at which the bulk receiver phase concentration ($C_{b,r}$) increases is a function of the area of the donor/receiver interface (A), the volume of the receiver phase (V_r), the drug mass transfer coefficient for partitioning (k_p) and the concentration gradient between donor and receiver phase (ΔC). Donor phase concentration decreases due to partitioning and thus carries a negative sign. In addition, the solubility of the drug in 1-octanol is large enough that the receiver phase is under sink conditions and the concentration gradient expressed as $C_{b,d}$ for simplification. Combining equations (5.3), (5.8), (5.9), and (5.10) create the expression for donor phase. Mass entering the donor phase comes from dissolution of the solid cocrystal phase (M) and mass leaving the donor phase enters the receiver phase ($C_{b,r}$) or precipitates into the solid drug phase (A_s) to maintain mass balance. This creates the following four dependent differential equations

$$\frac{dC_{b,d}}{dt} = \frac{3MD_{aq}}{a^2\rho V_d}(S_{cc} - C_{b,d}) - k_{nuc}(C_{b,d} - S_{drug})^{\alpha} - \frac{k_{grow}A_s}{V_d}(C_{b,d} - S_{drug})^{1.5} - \frac{A}{V_d}k_pC_{b,d} \tag{5.11}$$

$$\frac{dC_{b,r}}{dt} = \frac{A}{V_r}k_pC_{b,d} \tag{5.12}$$

$$\frac{dA_s}{dt} = V_r k_{nuc}\left(C_b - S_{drug}\right)^{\alpha} + k_{grow} A_s \left(C_{b,d} - S_{drug}\right)^{1.5} \quad (5.13)$$

$$\frac{dM}{dt} = -\frac{3MD_{aq}}{a^2\rho}\left(S_{cc} - C_b\right) \quad (5.14)$$

for the simulation of biphasic cocrystal particle dissolution. Values for the variables defined below can be found in the Appendix 5A.

Definition of Terms			
$C_{b,d}$	Donor phase bulk concentration	K_{a1}^{B}	First drug ionization constant
$C_{b,r}$	Receiver phase bulk concentration	K_{a2}^{B}	Second drug ionization constant
t	Time	K_{s}^{B}	Drug solubilization constant
M	Mass available for dissolution	$K_{a1}^{H_2A}$	First coformer ionization constant
D_{aq}	Aqueous diffusion coefficient	$K_{a2}^{H_2A}$	Second coformer ionization constant
a	Particle radius	k_{nuc}	Nucleation rate constant
ρ	Solid density	α	Molecularity index
V_d	Donor phase volume	k_{grow}	Growth rate constant
S_{cc}	Cocrystal stoichiometric solubility	A_s	Amount of precipitated solid drug
S_{drug}	Drug solubility	A	Surface Area of Aq/Org Interface
K_{sp}	Cocrystal solubility product	V_r	Receiver phase volume
$[H^+]_0$	Interfacial proton concentration	k_p	Drug mass transfer coefficient

Results

Cocrystal Biphasic Dissolution and Precipitation Simulations

Cocrystal particle dissolution concentration-time profiles in pH 5 blank FeSSIF were simulated in Chapter 4 by fitting equations (4.35-4.37) to experimental data collected by Chen et al.[8] The results of these single phase simulations in pH 5 blank FeSSIF (Figure 5.1 a,c,e) and their obtained nucleation and growth rate constants were applied to an *in silico* biphasic dissolution scenario. Biphasic simulations for aqueous (Figure 5.1 a,c,e) and organic phases (Figure 5.2 b,d,f) show biphasic donor concentration-time profiles to be lower than single phase simulations in the absence of a 1-octanol receiver compartment.

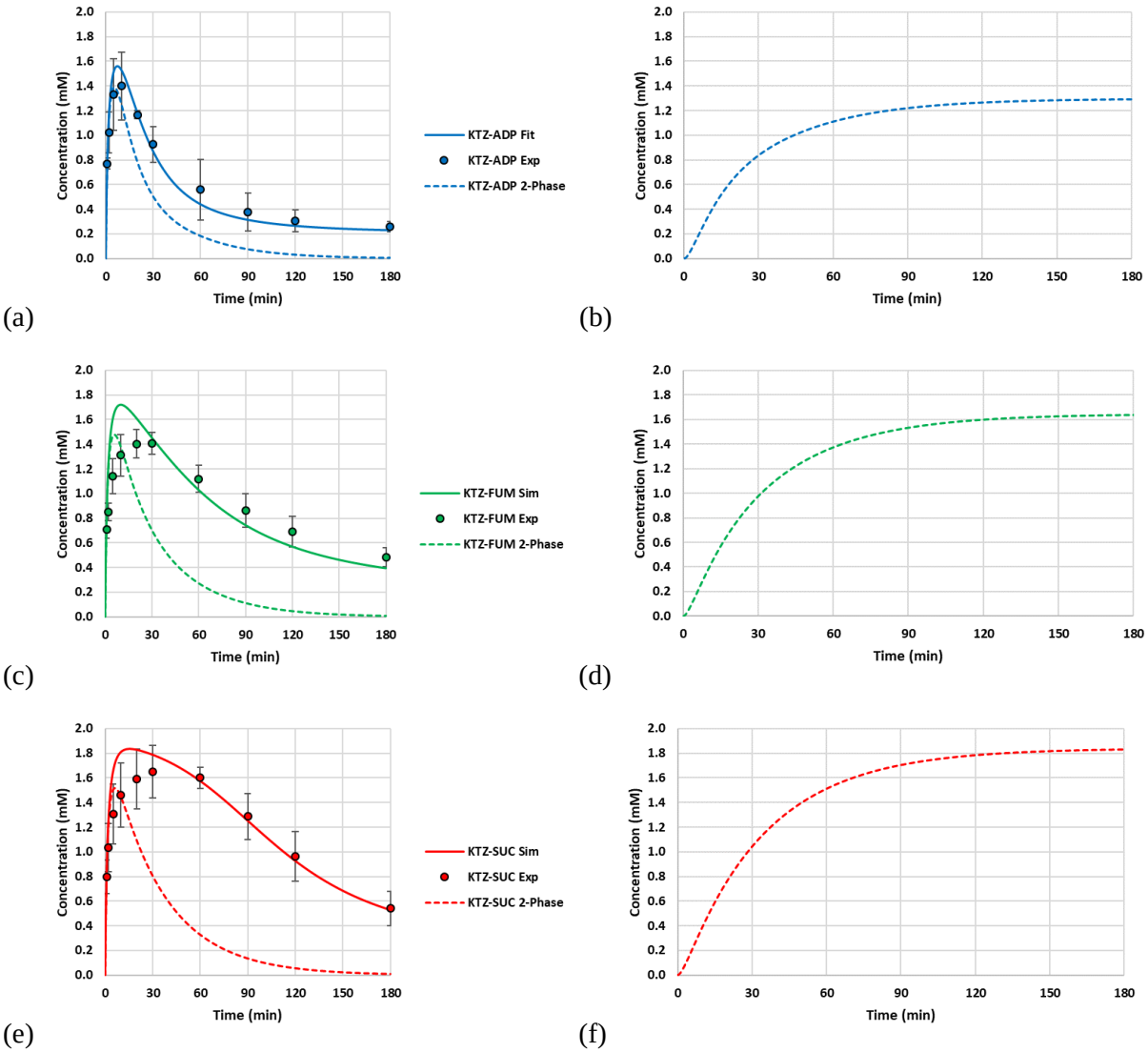

Figure 5.1: Particle dissolution concentration-time profiles for (a) KTZ-ADP (●), (c) KTZ-FUM, (●), and (e) KTZ-SUC (●) measured in pH 5 blank FeSSIF. Single phase simulations with fitted nucleation and growth rate constants for (a) KTZ-ADP (—), (b) KTZ-FUM, (—), and (c) KTZ-SUC (—) in pH 5 blank FeSSIF. Biphasic simulations of KTZ-ADP (- - -), KTZ-FUM, (- - -), and KTZ-SUC (- - -) particle dissolution in pH 5 blank FeSSIF donor compartment (a,c,e) partitioning into octanol receiver phase (b,d,f).

The KTZ cocrystals had varying levels of precipitation and partitioning over the course of the three simulations (Figure 5.2). SUC generated the highest concentrations in the receiver compartment and ADP the least over a 180-minute simulation. All cocrystal simulations generated higher concentrations in both donor and receiver phases compared to an equal molar dose and particle size of drug.

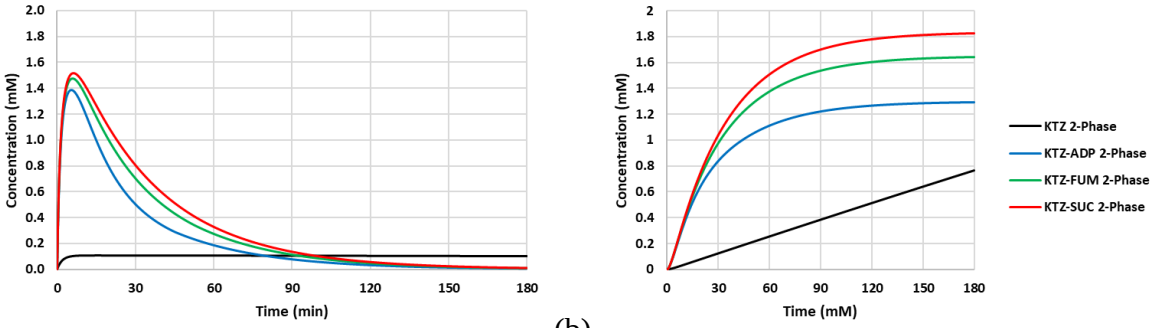

(a) (b)

Figure 5.2: Simulated concentration-time profiles of biphasic particle dissolution for KTZ (—), KTZ-ADP (—), KTZ-FUM, (—) and KTZ-SUC (—) in (a) aqueous pH 5 blank FeSSIF donor phase and (b) octanol receiver phase.

The cocrystals on average were able to partition 84 percent of the total dose into the organic phase over the 180-minute simulations whereas the parent drug was only able to partition almost 41 percent of the total dose (Figure 5.3).

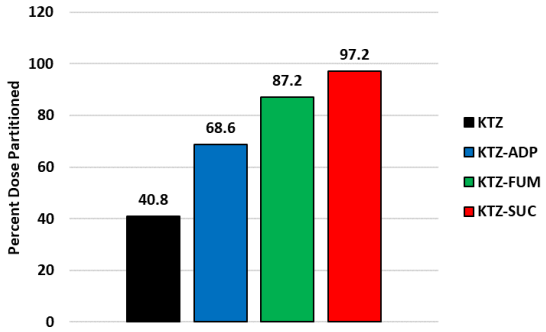

Figure 5.3: Calculated percent of initial dose partitioned into the receiver phase at the end of 180 min biphasic particle dissolution simulations of KTZ (■), KTZ-ADP (■), KTZ-FUM (■), and KTZ-SUC (■).

Modifying Dissolution Rate

Sensitivity analysis of the KTZ-FUM simulation to changes in dissolution rate displayed an increase in particle size correlated to a reduction in the dissolution rate and a decreased in the maximum concentration (C_{max}) and time to maximum concentration (t_{max}) in the aqueous phase (Figure 5.4a). Because of lower solution concentrations, there was a longer duration of supersaturation with the larger particle radii which caused higher amounts of partitioning to occur

(Figure 5.4b). Faster particle dissolution caused greater supersaturation and therefore more of the dissolving cocrystal dose to precipitate to solid drug and remain unavailable for partitioning.

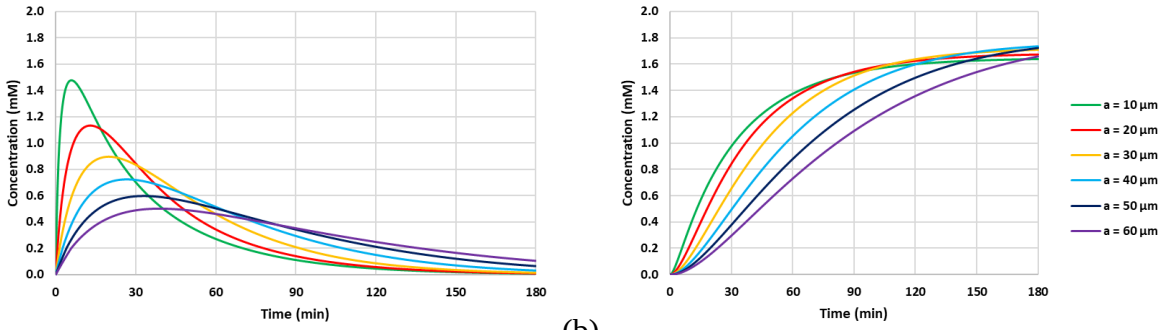

(a) (b)

Figure 5.4: Concentration-time profile simulations of KTZ-FUM biphasic particle dissolution in pH 5 blank FeSSIF (a) aqueous donor phase and (b) octanol receiver phase with particle radii 10 µm (—), 20 µm (—), 30 µm (—), 40 µm (—), 50 µm (—), and 60 µm (—).

Slowing the dissolution rate was associated with a decrease in the amount of initial dose that precipitated into solid drug phase over the course of the simulation (Figure 5.5a). Lower amounts of precipitation did not necessarily mean greater levels of partitioning. There was an optimal particle size of 40 µm that balanced dissolution, precipitation, and partitioning rates to

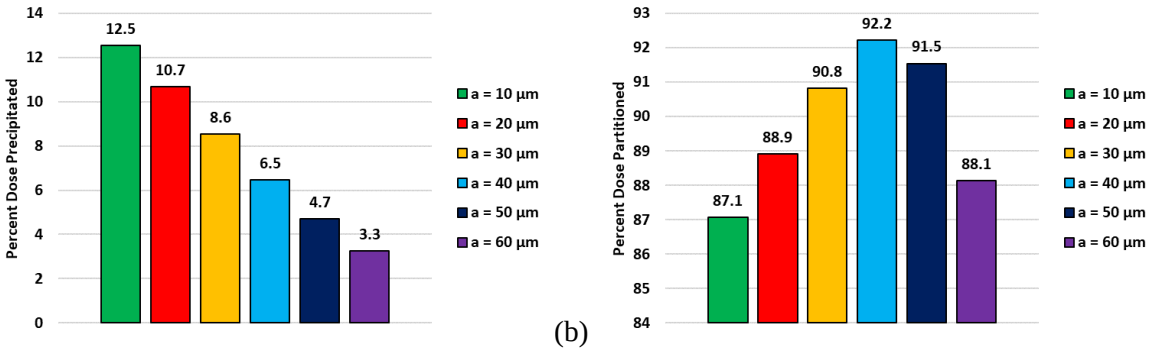

(a) (b)

Figure 5.5: Calculated percent of initial dose (a) precipitated as solid drug in donor phase and (b) partitioned into octanol receiver phase at t = 180 minutes in biphasic particle dissolution simulations of KTZ-FUM in pH 5 blank FeSSIF for particle radii 10 µm (■), 20 µm (■), 30 µm (■), 40 µm (■), 50 µm (■), and 60 µm (■).

obtain the highest fraction of initial dose in the receiver phase at the end of the 180-minute simulations (Figure 5.5b). Looking at the general trend of the organic concentration-time profiles,

the larger particle sizes with lower amounts of precipitation would obtain greater fractions of partitioned dose if simulations were run for a longer duration.

Modifying Nucleation Rate

A sensitivity analysis to assess the ability of the nucleation rate constant (k_{nuc}) to affect the concentration-time profiles of the biphasic simulation was explored (Figure 5.6). Decreasing k_{nuc} by 10-fold resulted in a 10 percent increase in the amount of cocrystal dose transported to the receiver phase. However, a 10-fold increase in k_{nuc} resulted in a 35 percent decrease in dose partitioned (Figure 5.7) due to the dose becoming sequestered as precipitated drug in the aqueous donor phase.

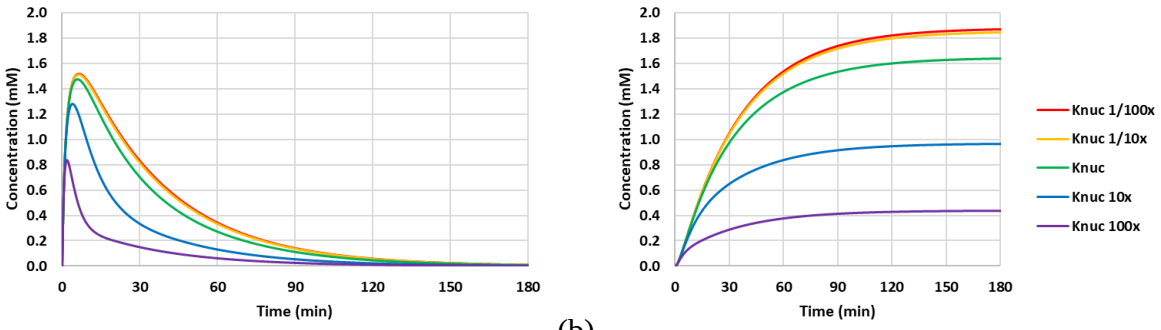

(a) (b)

Figure 5.6: Concentration-time profile simulations of KTZ-FUM biphasic particle dissolution in pH 5 blank FeSSIF aqueous donor phase (a) and octanol receiver phase (b) changing nucleation rate constant by 100- (—), 10- (—), 1/10- (—), and 1/100- (—) fold.

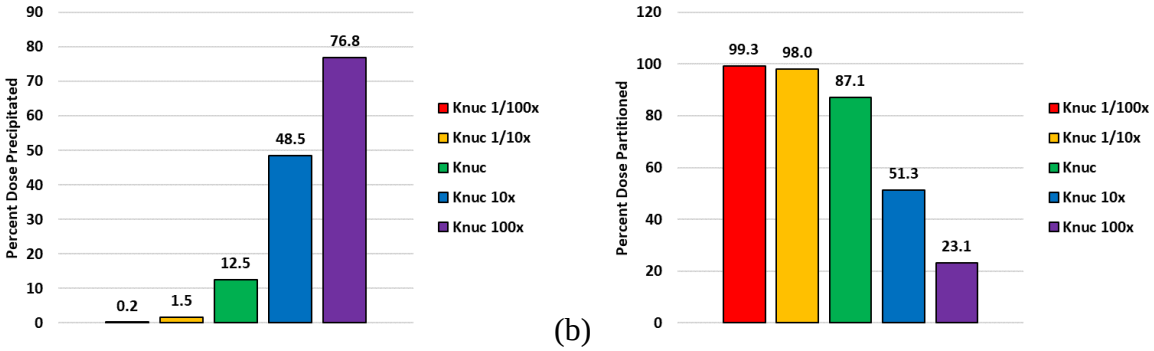

Figure 5.7: Calculated percent of initial dose (a) precipitated as solid drug in donor phase and (b) partitioned into octanol receiver phase at t = 180 minutes in biphasic particle dissolution simulations of KTZ-FUM in pH 5 blank FeSSIF for nucleation rate constant values 1/100- (■), 1/10- (■), 10- (■), and 100- (■) times the original fitted value (■).

Modifying Growth Rate

The sensitivity analysis to assess the effect of growth rate constant (k_{grow}) on concentration-time profiles of biphasic simulations had similar results to the k_{nuc} analysis (Figure 5.8). Levels of partitioning were less sensitive to changes in k_{grow} as 10 and 100-fold decreases resulted in less than two percent increases of partitioned dose. Whereas, a 10-fold increase in k_{grow} resulted in a 21 percent decrease in initial dose partitioned after 180-minutes (Figure 5.9).

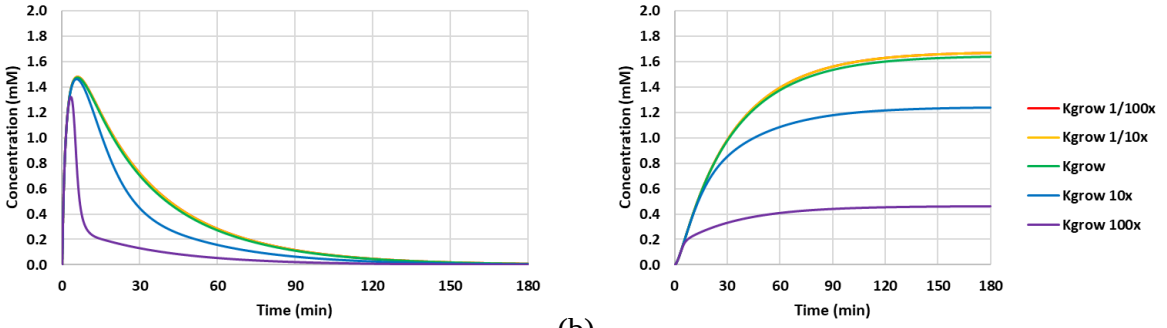

(a) (b)

Figure 5.8: Concentration-time profile simulations of KTZ-FUM biphasic particle dissolution in pH 5 blank FeSSIF (a) aqueous donor phase and (b) octanol receiver phase changing growth rate constant by 100- (—), 10- (—), 1/10- (—), and 1/100- (—) fold.

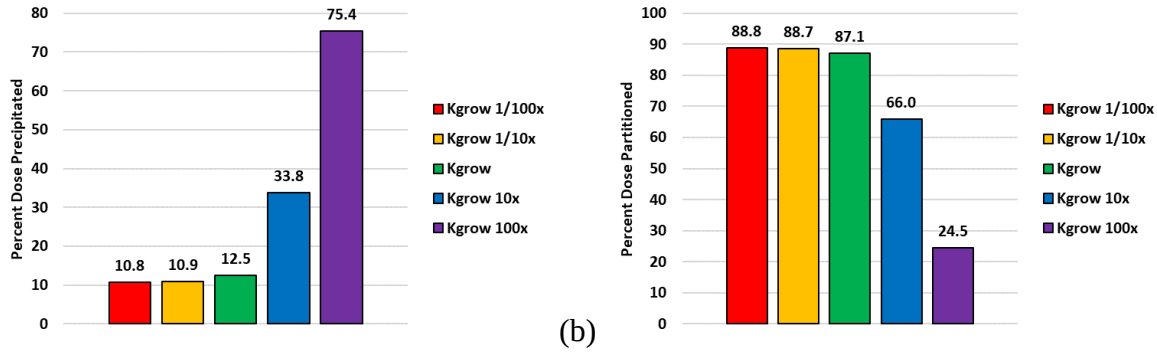

(a) (b)

Figure 5.9: Calculated percent of initial dose (a) precipitated as solid drug in donor phase and (b) partitioned into octanol receiver phase at t = 180 minutes in biphasic simulations of KTZ-FUM particle dissolution in pH 5 blank FeSSIF for growth rate constant values 1/100- (■), 1/10- (■), 10- (■), and 100- (■) times the original fitted value (■).

Modifying Partitioning Rate

Changing the partition mass transfer coefficient (k_p) was also investigated. Concentration-time profiles in both donor and receiver phases were more sensitive to changes in k_p than k_{nuc} or k_{grow} (Figure 5.8). Simulations showed that 5- and 10-fold decreases in k_p decreased the amount of initial dose partitioned by approximately 45 and 65 percent, respectively. What is interesting to note that 5 to 10-fold increases in k_p resulted in nearly the entire (~98%) simulated dose partitioning into the receiver phase due to the partition rate being fast enough to lower concentrations enough to reduce the amount of drug precipitation (Figure 5.9 & 5.10).

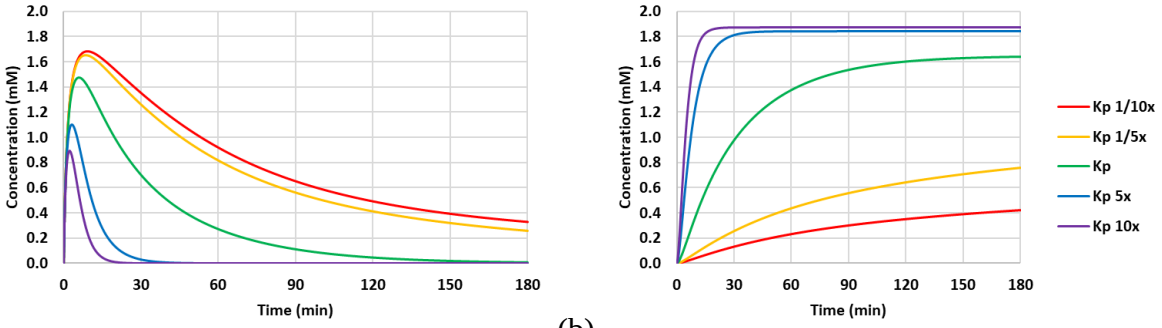

(a) (b)

Figure 5.10: Concentration-time profile simulations of KTZ-FUM (—) biphasic particle dissolution in pH 5 blank FeSSIF (a) aqueous donor phase and octanol receiver phase (b) changing partition mass transfer rate constant by 10- (—), 5- (—), 1/5- (—), and 1/10- (—) fold.

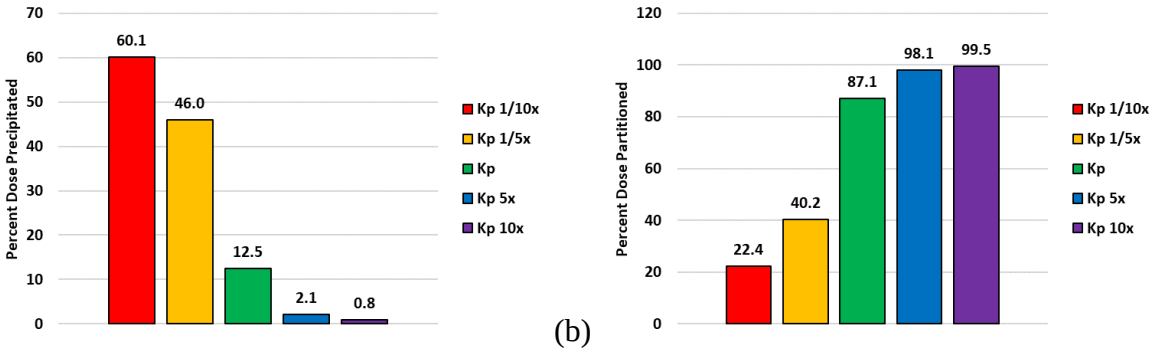

(a) (b)

Figure 5.11: Calculated percent of initial dose (a) precipitated as solid drug in donor phase and (b) partitioned into octanol receiver phase at t = 180 minutes in biphasic particle dissolution simulations of KTZ-FUM in pH 5 blank FeSSIF for partition mass transfer coefficient values 1/10- (■), 1/5- (■), 5- (■), and 10- (■) times the original fitted value (■).

Discussion

Diffusion driven passive absorption of a small molecule is a concentration driven process[9]. Therefore, it is important to have knowledge of the concentration available for absorption to have a sense how well a drug might perform as an oral dosage form. Combining the previously developed dissolution-supersaturation-precipitation simulations of KTZ cocrystal dissolution in blank FeSSIF and biphasic mass transport expressions gave the opportunity to simulate the amount of drug from cocrystal dissolution that is available for partitioning into an absorption compartment. The derived differential equations using parameters fitted from previous cocrystal dissolution experiments showed the ability of these KTZ cocrystals to generate

supersaturation in a donor compartment and drive higher amounts of partitioning compared to parent drug in a two-phase dissolution simulation (Figure 5.1). These simulations of cocrystal dissolution also revealed differences in partitioning between the three cocrystals of KTZ (Figure 5.2). KTZ-SUC had the highest and KTZ-ADP the lowest in terms of amount of initial dose partitioned into the receiver phase (Figure 5.3), showing promise that this approach could be a potential tool for rank ordering cocrystals for formulations. Further development of these analyses could help in the selection of cocrystals for development, especially if the values of nucleation, growth, and partitioning mass transport coefficients can be predicted *a priori*. This would likely reduce the number of experiments needed to develop a cocrystal product and save valuable time and resources.

Sensitivity analyses show that dissolution, precipitation, and partition rates all play a role in determining the concentration of drug from cocrystal dissolution available in solution to be absorbed. Simulations of different dissolution rates created by changing particle sizes of drug showed promise in limiting the amount of drug that precipitates in the aqueous donor phase (Figure 5.4). The slower the simulated cocrystal dissolution rate, the lower the amount of solid precipitated drug at t = 180 minutes (Figure 5.5a). However, the lower amount of precipitate did not necessarily lead to more partitioned drug at simulation end. Slower dissolution rates created lower concentration gradients and thus slowed the rate of partitioning. An optimal dissolution rate with particle radius of 40 μm balanced the rates of dissolution, precipitation, and partitioning to allow for the highest calculated percentage of initial dose in the receiver phase at the end of the biphasic dissolution simulations (Figure 5.5b). This result hints at the possibility of an optimal supersaturation where the rates of dissolution and precipitation are balanced to allow for the maximum possible amount of drug absorption from a cocrystal system.

A common formulation tactic is to increase exposure from supersaturating drug delivery systems by inhibiting nucleation and growth rates[4]. Sensitivity analyses mimicked this approach by changing the values of nucleation (Figure 5.6) and growth (Figure 5.8) rate constants. Decreasing the nucleation and growth rates did little to help improve the amounts of partitioning in the biphasic cocrystal simulations for the given set of initial conditions (Figure 5.7b and 5.9b). Increases in these values created large amounts of precipitated drug which decreased the calculated percent of initial dose that was able to partition.

The effect of partition mass transport coefficient on donor phase concentrations was also investigated. Increases in k_p decreased the simulated donor phase concentrations (Figure 5.10) and limited the amount of solid drug that precipitated (Figure 5.11a). This allowed higher percentages of the initial dose to be absorbed (Figure 5.11b). Smaller values of k_p resulted in higher simulated donor phase concentrations, more precipitation, and less of the initial dose able to partition into the receiver phase. Under these conditions, any abatement of nucleation or growth rate constants could have greater effect in boosting the amounts of drug able to partition.

Conclusions

The ability to simulate the concentration-time profiles of cocrystals could be a powerful tool for use in the development of viable cocrystal products. Absorption is a concentration driven process and knowledge of drug concentrations in solution can be used to estimate the amount that could potentially be absorbed. This work derived a set of differential equations able to create simulated concentration-time profiles for cocrystals and with them estimate amounts of the dissolution dose that could be absorbed in a biphasic system. These mathematical expressions were used to gain knowledge on how rates of cocrystal dissolution, supersaturation, and precipitation could interplay with each other to control drug absorption.

Sensitivity analyses showed that lowering dissolution rates or increasing partitioning rates limited simulated supersaturation and reduced amounts of precipitation that contributed to more simulated dose absorbed. Increasing the dissolution rate or decreasing the partitioning rate creates more supersaturation and a greater driving force for precipitation. Under these conditions, inhibition of nucleation or crystal growth would have more impact on facilitating increases in absorption. The knowledge gained from these simulations suggest the possibility of an optimal supersaturation where the processes of dissolution, precipitation, and partitioning are balanced to allow for the largest amount of drug to be absorbed. Targeting of this optimal supersaturation using cocrystal solubility, particle size, precipitation inhibitors, or dose would take less guessing out of experiments and bring a more mechanistic approach to helping improve the research and development of cocrystal. Further development of these simulations to include more biorelevant parameters for volume, surface areas, and intestinal permeation rates could create mathematical expressions capable of generating viable estimations of amounts of drug absorbed from a cocrystal system. Cocrystal dissolution simulations could be used to guide benchtop experiments, streamline the development process, reduce wasteful research, and save valuable time and resources.

Acknowledgements

The authors acknowledge the financial support from the University of Michigan College of Pharmacy.

References

1. Bak, A., et al., *The co-crystal approach to improve the exposure of a water-insoluble compound: AMG 517 sorbic acid co-crystal characterization and pharmacokinetics.* Journal of Pharmaceutical Sciences, 2008. **97**(9): p. 3942-3956.
2. Hickey, M.B., et al., *Performance comparison of a co-crystal of carbamazepine with marketed product.* European Journal of Pharmaceutics and Biopharmaceutics, 2007. **67**(1): p. 112-119.
3. Jung, M.S., et al., *Bioavailability of indomethacin-saccharin cocrystals.* Journal of Pharmacy and Pharmacology, 2010. **62**(11): p. 1560-1568.
4. Childs, S.L., P. Kandi, and S.R. Lingireddy, *Formulation of a Danazol Cocrystal with Controlled Supersaturation Plays an Essential Role in Improving Bioavailability.* Molecular Pharmaceutics, 2013. **10**(8): p. 3112-3127.
5. Smith, A.J., et al., *Cocrystals of Quercetin with Improved Solubility and Oral Bioavailability.* Molecular Pharmaceutics, 2011. **8**(5): p. 1867-1876.
6. Cheney, M.L., et al., *Effects of Crystal Form on Solubility and Pharmacokinetics: A Crystal Engineering Case Study of Lamotrigine.* Crystal Growth & Design, 2010. **10**(1): p. 394-405.
7. Stanton, M.K., et al., *Improved Pharmacokinetics of AMG 517 Through Co-crystallization Part 2: Analysis of 12 Carboxylic Acid Co-crystals.* Journal of Pharmaceutical Sciences, 2011. **100**(7): p. 2734-2743.
8. Chen, Y.M. and N. Rodríguez-Hornedo, *Cocrystals Mitigate Negative Effects of High pH on Solubility and Dissolution of a Basic Drug.* Crystal Growth & Design, 2018. **18**(3): p. 1358-1366.
9. Fick, A., *Ueber diffusion.* Annalen der Physik, 1855. **170**(1): p. 59-86.

Appendix 5A

Biphasic Cocrystal Particle Dissolution and Partitioning

KTZ-ADP

METHOD RK4

STARTTIME = 0

STOPTIME = 180

DT = 0.1

;dissolved compound

d/dt(C1) = IF TIME < 0.2 THEN ((3 * M * DaqB*60) / (V*p* a^2) * (Scc - C1)) ELSE IF TIME >56.6 THEN ((3 * M * DaqB*60) / (V*p* a^2) * (Scc - C1)) - (S / V2)* k1 * C1 ELSE (3 * M * DaqB*60) / (V*p* a^2) * (Scc - C1) - (kgrow * As * (1/(V/1000)) * ((C1-Css))^b) - (knuc * (C1-Css)^q) - (S / V2)* k1 * C1

d/dt(C2) = (S / V2) * k1 * C1

d/dt(As) = IF TIME < 0.2 THEN 0 ELSE IF TIME > 56.6 THEN 0 ELSE (kgrow * As * ((C1-Css))^b) + ((V/1000) * knuc * (C1-Css)^q)

d/dt(M) = - (3 * M * DaqB*60) / (p * 1000 * a^2) * (Scc - C1)

;initial conditions

Init(C1) = 0; dissolved uM

Init(C2) = 0; dissolved uM

Init(As) = 0 ; solidundissolved uM

Init(M) =56.4459; solidundissolved umol

;cocrystal solubility

Scc = (Ksp * (1 + (KsA*mic) + (Ka1A / H0) + (Ka1A * Ka2A / H0^2)) * (1 + (KsB*mic) + (H0 / Ka2B) + (H0^2 / Ka1B / Ka2B)))^(1 / 2)

;drug solubility

Css = So * (1 + (KsB*mic) + (Hb / Ka2B) + (Hb^2 / (Ka1B * Ka2B)))

;parameters [ADP Blank FeSSIF]

Ksp = 3.4e4; uM^2

Ka1A = 3.63078e-5

Ka2A = 3.63078e-6

Ka1B = 1.15e-3

Ka2B = 3.09e-7

KsA = 0

KsB = 0.0144; uM-1

H0 = 1.6982e-5

Hb = 1e-5

DaqA = 9.95e-6; cm^2/s

DaqB = 3.81e-6; cm^2/s

V = 30; cm^3

V2 = 30; cm^3

a = 0.001; cm

p = 2634.40; umol/cm^3

So = 6e0; uM

mic = 0; uM

kgrow = 8.4901e-7

knuc = 9.39e-4

q = 1.44015

b = 1.5

k1 = 0.02058; min^-1*cm^-1

S = 43.00840343; cm^2

KTZ-FUM

METHOD RK4

STARTTIME = 0

STOPTIME = 180

DT = 0.1

;dissolved compound

d/dt(C1) = IF TIME < 0.2 THEN ((3 * M * DaqB*60) / (V*p* a^2) * (Scc - C1)) ELSE IF TIME > 70.1 THEN ((3 * M * DaqB*60) / (V*p* a^2) * (Scc - C1)) -(S / V2)* k1 * C1 ELSE (3 * M * DaqB*60) / (V*p* a^2) * (Scc - C1) - (kgrow * As * (1/(V/1000)) * ((C1-Css))^b) - (knuc * (C1-Css)^q) - (S / V2)* k1 * C1

d/dt(C2) = (S / V2) * k1 * C1

d/dt(As) = IF TIME < 0.2 THEN 0 ELSE IF TIME > 70.1 THEN 0 ELSE (kgrow * As * ((C1-Css))^b) + ((V/1000) * knuc * (C1-Css)^q)

d/dt(M) = - (3 * M * DaqB*60) / (p * 1000 * a^2) * (Scc - C1)

;initial conditions

Init(C1) = 0; dissolved uM

Init(C2) = 0; dissolved uM

Init(As) = 0; solidundissolved uM

Init(M) =56.4459; solidundissolved umol

;cocrystal solubility

Scc = (Ksp * (1 + (KsA*mic) + (Ka1A / H0) + (Ka1A * Ka2A / H0^2)) * (1 + (KsB*mic) + (H0 / Ka2B) + (H0^2 / Ka1B / Ka2B)))^(1 / 2)

;drug solubility

Css = So * (1 + (KsB*mic) + (Hb / Ka2B) + (Hb^2 / (Ka1B * Ka2B)))

;parameters [FUM Blank FeSSIF]

Ksp = 1.5e3; uM^2

Ka1A = 9.33e-4

Ka2A = 4.17e-5

Ka1B = 1.15e-3

Ka2B = 3.09e-7

KsA = 2.9e-5; uM-1

KsB = 0.0144; uM-1

H0 = 7.90679e-5

Hb = 1e-5

DaqA = 9.95e-6; cm^2/s

DaqB = 3.81e-6; cm^2/s

V = 30; cm^3

V2 = 30; cm^3

a = 0.001; cm

p = 2634.40; umol/cm^3

So = 6.0e0; uM

mic = 0; uM

kgrow = 3.457e-7; uM^-1*min^-1

knuc = 8.5734e-5; uM^(1-q)*min^-1

q = 1.62804

b = 1.5

k1 = 0.02058; min^-1*cm^-1

S = 43.00840343; cm^2

KTZ-SUC

METHOD RK4

STARTTIME = 0

STOPTIME = 180

DT = 0.1

;dissolved compound

d/dt(C1) = IF TIME < 0.2 THEN ((3 * M * DaqB*60) / (V*p* a^2) * (Scc - C1)) ELSE IF TIME > 76.4 THEN ((3 * M * DaqB*60) / (V*p* a^2) * (Scc - C1)) -(S / V2)* k1 * C1 ELSE (3 * M * DaqB*60) / (V*p* a^2) * (Scc - C1) - (kgrow * As * (1/(V/1000)) * ((C1-Css))^b) - (knuc * (C1-Css)^q) - (S / V2)* k1 * C1

d/dt(C2) = (S / V2) * k1 * C1

d/dt(As) = IF TIME < 0.2 THEN 0 ELSE IF TIME > 76.4 THEN 0 ELSE (kgrow * As * ((C1-Css))^b) + ((V/1000) * knuc * (C1-Css)^q)

d/dt(M) = - (3 * M * DaqB*60) / (p * 1000 * a^2) * (Scc - C1)

;initial conditions

Init(C1) = 0; dissolved uM

Init(C2) = 0; dissolved uM

Init(As) = 0; solidundissolved uM

Init(M) =56.4459; solidundissolved umol

;cocrystal solubility

Scc = (Ksp * (1 + (KsA*mic) + (Ka1A / H0) + (Ka1A * Ka2A / H0^2)) * (1 + (KsB*mic) + (H0 / Ka2B) + (H0^2 / Ka1B / Ka2B)))^(1 / 2)

;drug solubility

Css = So * (1 + (KsB*mic) + (Hb / Ka2B) + (Hb^2 / (Ka1B * Ka2B)))

;parameters [SUC Blank FeSSIF]

Ksp = 2.7e4; uM^2

Ka1A = 6.17e-5

Ka2A = 2.34e-6

Ka1B = 1.15e-3

Ka2B = 3.09e-7

KsA = 9.5e-6; uM-1

KsB = 0.0144; uM-1

H0 = 2.1877e-5

Hb = 1e-5

DaqA = 9.95e-6; cm^2/s

DaqB = 3.81e-6; cm^2/s

V = 30; cm^3

V2 = 30; cm^3

a = 0.001; cm

p = 2634.40; umol/cm^3

So = 6e0; uM

mic = 0

kgrow = 4.9021e-7

knuc = 6.8473e-6

b = 1.5

q = 1.7136

k1 = 0.02058; min^-1*cm^-1

S = 43.00840343; cm^2

CHAPTER VI

Conclusions and Future Directions

The focus of this thesis was to link cocrystal thermodynamic solubility expressions to kinetic solution behavior of dissolution, supersaturation, and precipitation observed with *in vitro* dissolution experiments. Mathematical expressions were applied to simulate cocrystal dissolution, precipitation, and biphasic partitioning rates to depict cocrystal solution behavior in an absorption environment with the aim of gaining knowledge of how cocrystals influence solution concentrations responsible for *in vitro* drug absorption. Use of this knowledge can help guide experiments in the development of cocrystal therapeutics.

A mechanistic approach was developed to simulate the rotating disk dissolution of KTZ cocrystals and partitioning of drug and coformer in a biphasic dissolution experiment. Cocrystal intrinsic dissolution rates were corroborated from established theories in literature and measured mass transfer rates of drug and coformer from donor to receiver phases revealed the potential for solution interactions to alter diffusion rates of cocrystal components. The expressions simulated concentration-time profiles of drug and coformer into aqueous donor and octanol receiver compartments from cocrystal rotating disk dissolution, laying foundational work for estimating amounts of drug absorbed *in vivo* from cocrystal dissolution.

Cocrystal solubility equations were utilized to assess the propensity of precipitation of KTZ cocrystals within four intestinally relevant dissolution media (Fed State Simulated Intestinal Fluid, blank FeSSIF, Fasted State Intestinal Fluid, and Blank FaSSIF). KTZ cocrystals have been shown

to lower interfacial pH (pH_o) when dissolving in unbuffered media at intestinal pH values. This decrease in pH_o generated lower estimated interfacial solubility advantages (SA_{int}) that would mitigate the propensity for precipitation at the interface. Buffer affected the ability of the cocrystal to maintain a lower interfacial pH, as SA_{int} increased using buffer estimated pH_o values. One to two pH unit differences in interfacial pH were estimated for KTZ cocrystals between unbuffered and 100 mM buffered media which coincided with increases of SA_{int} up to 15 times, in worst cases. This suggests that buffer selection for *in vitro* experiments could be vital for obtaining the best *in vitro-in vivo* correlations (IVIVC) for cocrystal products. Further experiments would be useful to determine if interfacial precipitation could be increased due to buffer concentrations raising pH_o and SA_{int}. Calculated bulk solubility advantages (SA_{bulk}) served as theoretical limits of bulk supersaturation and were shown to correlate with the dissolution behavior of apparent intrinsic dissolution rates, maximum supersaturations, and concentration area under the curve for KTZ cocrystals in biorelevant dissolution media. These experiments, however, did not have a large enough dose to achieve saturation with respect to cocrystal and therefore SA_{bulk} is an overestimate of the supersaturation that can be generated. Being mindful of the dose, the calculated drug dose number (D_o) is a more applicable value to estimate the theoretical limit of bulk supersaturation as it was able to strongly correlate with the KTZ cocrystal dissolution behavior.

A mechanistic particle dissolution model using Higuchi-Hiestand theory was derived to simulate the dissolution rates of the KTZ cocrystals without precipitation in biorelevant experiments. Simulations using independently measured or calculated parameters were in good agreement with experimentally measured concentration-time profiles of KTZ cocrystals in FeSSIF. Blank FeSSIF contained bulk precipitation and required addition of terms for nucleation and growth to the particle dissolution theory. A set of dependent differential equations were also

derived to simulate the solution concentration-time profiles for KTZ cocrystals in blank FeSSIF and were observed to have good agreement with experimental measurements. These equations could be applied to simulate potential experimental scenarios such as adding nucleation inhibitor to improve the dissolution behavior of the cocrystal and guide experimental design. This is expected to reduce the number of experiments required to develop a cocrystal product, saving time and resources.

The lessons learned from cocrystal particle dissolution, precipitation simulations, and biphasic partitioning experiments were combined and applied to simulate a hypothetical KTZ biphasic particle dissolution experiment. These simulations gave insight to how dissolution, precipitation, and partitioning rates influence the solution concentrations of KTZ cocrystals. Sensitivity analyses of the biphasic simulations revealed decreasing the dissolution, nucleation, or growth rates were associated with decreased precipitation of the initial dose. This increased the amount of partitioning and suggests that modulating these rates may be potential strategies for optimizing cocrystal absorption advantage. The partitioning rate was also shown to influence the amount of bulk precipitation as increasing partitioning rate was associated with lower supersaturation and precipitation. This means that dissolution, precipitation, and partitioning rates play a role in the amount of drug partitioning and must be considered together when attempting to maximize the amounts absorbed. More work is needed to better understand how cocrystal components are absorbed and *in vitro* dissolution, precipitation, and absorption experiments using physical diffusion barriers such as synthetic polymer or live cell membranes could help immensely in understanding how to best optimize drug absorption from cocrystal formulations.

More knowledge is needed to better understand how dissolution and precipitation control the amount of drug absorbed from a cocrystal system. Generating and maintaining supersaturation

is key to optimizing an absorption advantage. To do that, identifying where the supersaturation is highest, either at the interface or in the bulk, could help more quickly identify strategies to target an optimal supersaturation, i.e a supersaturation threshold below which rapid drug precipitation is prevented. Future projects to investigate both interfacial and bulk supersaturation can address the questions that arise from this thesis. Interfacial precipitation was possible under the dissolution conditions studied in this thesis, however, it was assumed negligible to simplify simulations. More investigation is needed to determine the conditions under which cocrystal dissolution could be impeded by interfacial precipitation due to high SA_{int}. KTZ cocrystals have the potential to mitigate the propensity for interfacial precipitation by lowering pH_o. This ability can be hampered by the concentration of buffer that is present in the dissolution media. Therefore, experiments modulating the SA_{int} by increasing buffer concentrations could be done to determine how interfacial precipitation influences dissolution rate.

Further investigation into methods to better control bulk supersaturation is needed to optimize cocrystal absorption advantage. The use of D_o shows promise as a strategy to lower the bulk supersaturation and precipitation. Optimal supersaturation could be targeted using D_o with the goal of lowering precipitation and increasing the drug available for absorption. This ability to increase drug solution concentration while simultaneously using less drug can lower costs of manufacturing and adverse side effects.

More work is needed to refine the simulations of cocrystal dissolution and precipitation and test their ability to estimate *in vivo* drug absorption. Determining the accuracy of the biphasic simulations in predicting the amounts of precipitation and partitioning of the cocrystal components is needed as the experimental. The utility of the dissolution-precipitation simulations would be more impactful if the nucleation and growth constants (k_{nuc} and k_{grow}) could be estimated *ab initio*

prior to dissolution studies being started. Further work towards this goal could allow for cocrystal concentration-time profiles to be generated in silico to guide experimental design and cut down on wasteful benchtop experiments. In addition, simulation approach applied to other *in vitro* experimental systems such as the Gastrointestinal Simulator (GIS) or other biorelevant dissolution systems, to estimate solution concentrations along various compartments of the gastrointestinal tract could be very useful to better understand cocrystal solution kinetics and attempt to generate greater IVIVC.

The mathematical expressions for cocrystal kinetic solution behaviors in this thesis have potential for further improvement to develop and refine their ability to predict solution concentrations from cocrystal dissolution in biorelevant conditions. More advanced particle dissolution theories could be applied to account for hydrodynamic enhancement. Nucleation and growth rates for precipitation simulations could be further investigated and the ability to calculate them from classical nucleation theory would be extremely useful and allow for estimating cocrystal behavior before *in vitro* dissolution testing. Finally, applying these mathematical expressions to simulate cocrystal solution concentrations with appropriate intestinal permeability coefficients, instead of octanol mass transfer coefficients, could allow for estimations of absorption and pharmacokinetic profiles before *in vivo* testing. These approaches have potential to streamline the cocrystal development process, eliminate wasteful experiments, and save time and resources for new cocrystal therapeutics.